UNIVERSITY OF CALIFORNIA
SANTA CRUZ

LOAD MONITORING AND FAULT DETECTION ON DC MICRO GRIDS USING STFT BASED FEATURE VECTORS

A dissertation submitted in partial satisfaction of the
requirements for the degree of

DOCTOR OF PHILOSOPHY

in

ELECTRICAL ENGINEERING

by

Atif Maqsood

March 2020

The Dissertation of Atif Maqsood
is approved:

Professor Keith Corzine, Chair

Professor Leila Parsa

Professor Yu Zhang

Quentin Williams
Acting Vice Provost and Dean of Graduate Studies

Table of Contents

List of Figures

List of Tables

Abstract

Load Monitoring and fault detection on DC micro grids using STFT based feature vectors

by

Atif Maqsood

This thesis explores load monitoring on dc micro-grids specifically applied to Naval shipboard power systems. More electronic loads are being placed on Naval ships and, increasingly, more of these loads are pulsed-power in nature; drawing pulsating current from the grid. This presents a challenge for conventional fault monitoring devices as many fault currents are also pulsating in nature and can be difficult to differentiate from a desirable pulse event. Short-time Fourier transform is the technique preferred in this work for spectral analysis of the current signals. In addition to event based monitoring, another unsupervised control is being employed to continuously check the frequency content of the current to look for arcing faults caused by loose electrical connections. The objective of the dissertation is to develop a load monitoring algorithm that records the current drawn by these loads and is able to detect events and differentiate between desirable events and faults using their frequency content in run-time. The algorithm is realized on an micro-controller unit and validated on a low-voltage dc test-bed.

To Roha.

Acknowledgments

I would like to acknowledge my research advisor Dr. Keith Corzine for selecting me for this important work. His trust means a lot to me. I have learned so much by being part of his research team. I am very grateful for his patience, guidance and support throughout this work. I thank Dr. Leila Parsa and Dr. Yu Zhang for their patience and guidance as my dissertation reading committee members.

I am very grateful for all the encouragement and prayers I got from my parents, Maqsood-ul-Hassan and Samina Rana, and my sisters. I am also very grateful to all my friends in Santa Cruz and Pakistan for always helping me stay focused and providing some relief when I most needed it.

Lastly I must acknowledge LCDR Damian Oslebo, my research associate at Naval Postgraduate School, Monterey, for helping me out with every problem I've had along the way. I have learned a lot by watching him work and I appreciate him for sharing so much of his knowledge and experience with me.

Part I

Literature review

Chapter 1

Introduction

Design innovations have furthered the use of dc power in ship systems, in particular medium-voltage dc systems (MVDC) [1]. Future Naval ship power systems will be based on an MVDC architecture [2]. Benefits of the MVDC system include fewer power conversion steps (i.e., improved power density) and overall higher efficiency [3]. It is critical to the development of dc distribution that a reliable protection mechanism be in place that can detect and take action to prevent damage from any possible electrical faults on the system [4]. This section describes the challenges of load monitoring and fault detection specifically for dc microgrids. Then some of the existing work and research in this field is summarized to highlight the interest in this area.

1.1 Dissertation Synthesis

This dissertation is a compilation of the work done on the general topic of identifying loads and faults on a dc micro grid using time-frequency features. Most of the work presented here has already been published in esteemed peer reviewed conferences and journals. The outline of the

dissertation is as follows:

- Chapter 1 introduces the problem being addressed in this dissertation, in the context of naval shipboard power distribution design. The motivation for the research and the original contributions and deliverable for this project are also included in this chapter.

- Chapter 2 provides a review of the existing methods and approaches to the problems being addressed in this work. Many of these previous works in the literature provide inspiration to the solution being pursued in this project, however chapter 2 also identifies the limitation and short comings of the existing solutions. The review provided in chapter 2 is critical to understand the significance of the research contribution presented in this dissertation.

The rest of the dissertation is divided into two parts: The first part talks about load monitoring schemes designed for two specific loads.

- Chapter 3 discusses a load monitoring scheme for a fixed load that is designed to detect arcing faults in the system while differentiating it from the normal transients in the load profile.

- Chapter 4 discusses a load monitoring scheme for a coil gun load. Several unique features of the load transient profile in time-frequency domain has been identified and are used to characterize the load in real time. These features allow the load monitoring scheme to identify any unexpected transient as a shunt fault.

- The methods in Chapter 3 and 4 yield great result in both simulation and real-time DSP implementation, however these method are specific only to the load under consideration.

The second part talks about load monitoring schemes designed to work for any general dc load with finite transitional events.

- Chapter 5 introduces the proposed load monitoring and fault detection scheme. The monitoring begins with the clustering mode, during which the processor trains itself on features extracted from a normal load profile. After some time the processor can move on to classification mode where the extracted features from load profile are compared to the features recorded during the clustering mode. The details of the scheme such as fault identification methods, and parameter design are also included in the chapter.

- Chapter 6 provides an in-depth approach to applying the proposed scheme to a simulated model of a pulsed-energy mission load. The chapter includes details on the simulation model and a step-by-step guide on pre-processing methods to pick the optimal parameters for the proposed scheme.

- Chapter 7 uses the same method as chapter 7 but on data collected from four different dc loads assembled on a low voltage dc grid, instead of simulation model to account for the natural variation in load profile. Using data from real loads adds to the validity of the proposed scheme and also highlights the importance of pre-processing and parameter selection. This chapter includes discussion on performance indexes such as false positives, and false negatives, as well as the effect of parameters on general performance

metrics such as fault detection time. The solution in general yields excellent results for both normal and fault case scenarios.

- Finally chapter 8 builds upon the results and pre-processing of chapter 7 to apply the proposed scheme to four different dc loads in real time. The real time implementation produces satisfactory results despite the limitations of the processor being used.

1.2 Protection design and ship architecture

Typically the distribution of loads on a dc microgrid is separated into independent zones being fed from a dc bus [5]. For a naval architecture there is a dc bus on starboard and port side and the zones are sharing power from each bus [6]. Port and starboard are the nautical terms for left and right sides of the ship, respectively. This kind of architecture brings redundancy to the design and allows the zone to continue to have power even when one of the buses is compromised. A simplified one line diagram for such adistribution is shown in Fig. 1.1. The loads are divided into these zones based on their proximity to each other, location on the bus, and the nature of the load. Some dc loads may need to operate at a voltage different from the dc bus voltage. In such cases all loads that need to operate at a similar voltage level can be collected in one zone and a dc-dc converter will be used to interface that zone with the bus. Ac loads such as propulsion motors would need an inverter to interface with the dc bus. Another category of loads are the passive loads such as lighting and heating that can either be off or draw constant steady state power when on. While the design of dc grid architecture for naval ship is not the focus of this project, the design informs the choice of protection scheme for any given dc microgrid system.

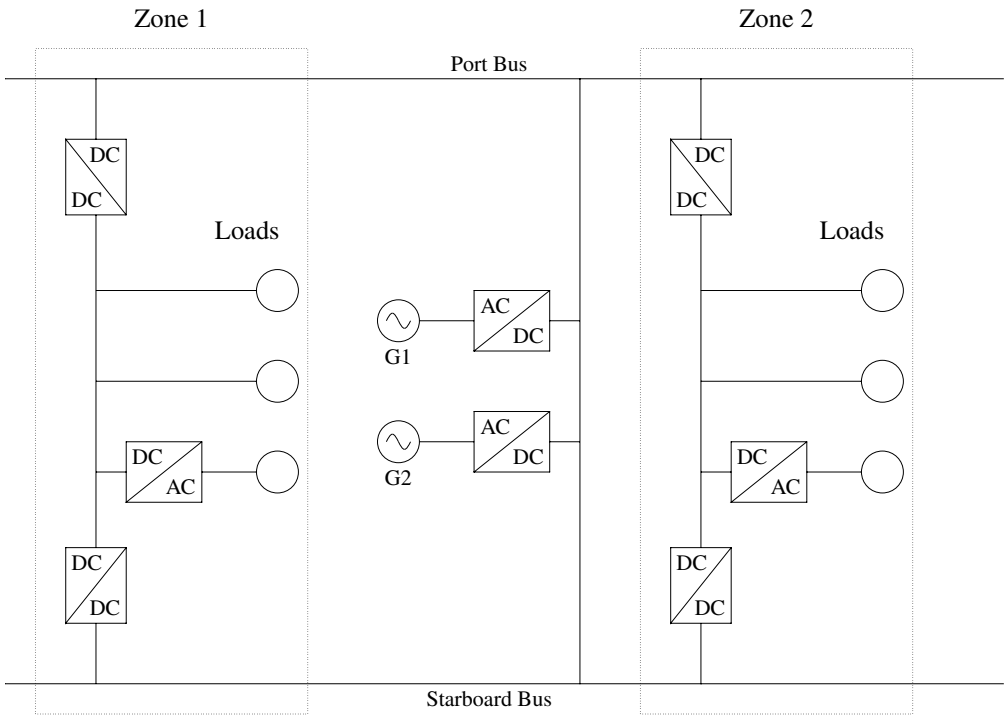

Figure 1.1: Zonal distribution system

Each electrical load zone will operate independently and can be isolated from the grid in case of a fault or maintenance. Mechanical contactors are commonly used to isolate the zones when required but for dc loads they are risky to operate while the system is still drawing current [7]. Ac currents naturally cross zero during normal operation and even during most faults. This allows the contactors or ac breakers to operate without interrupting large currents. Interrupting a large current by contactors could create arcing as the system inductance will try to sustain the current by electrical breakdown of the airgap between the contacts. The resulting sparks from the arcing can be a serious fire hazard. Therefore the preferred method of interrupting current is

through solid-state switching devices [8]. Several designs have been proposed for dc breakers based on high current, high blocking voltage thyristors [9]-[13].

Breakers based on solid-state switching devices can be placed in each dc load zone in series with the contactor. The breaker can then operate when it receives the signal from a relay unit that is programmed to detect faults through processing the zone variables such as current, temperature and voltage etc. Such a configuration is referred to a breaker based protection scheme. It provides an additional layer of protection to vital loads and can be added to a system without the need to modify the load controls. Since the solid state switch will be in the conduction path it will incur conduction losses thus reducing the efficiency of the system. An alternate to breaker-based approach is breakerless protection scheme. Most loads will have interface with the dc bus consisting of power electronic units. In a breakerless scheme the relay unit is built into the power electronic interface unit and thus avoids the need for an additional breaker unit [14]-[16]. Each of these approach has its merits and will be utilized in some way for this project. Breakers are the actuators for any protection scheme but the contribution of this project will be largely geared towards the relay unit.

1.3 Motivation and Problem Statement

Having advanced electric load monitoring on ship power system allows reliable unmanned supervision of the ship operation thus reducing costs and crew sizes [17]. It is a system that

is free of human error and also is able to pick up the changes in load condition that may be too fast or subtle to be observed manually. Due largely to the development of fast and compact microprocessors, load monitoring in some form is now an integral part of most micro grids [18].

Metering for commercial and residential buildings could be considered a very basic and most common form of load monitoring. It uses the information from instrumentation transformers to calculate the power being drawn by a load zone. Smart meters can provide useful information about power consumption to the consumer and the utility which can be utilized for load management. This form of load monitoring can not associate the change in power to individual loads inside the building so the information gained is limited. For example if a washing machine and a heater draw the same amount of steady-state power, the meter installed outside the building will not be able to identify the load responsible for the increase in power.

An advanced form of smart meters can however perform some diagnostic processing to identify the loads associated with power consumption inside the house. ”Sense” is one such commercially available product manufactured by a Massachusetts based company [19]. It is a small device that must be hooked up to the electrical panel in the house as shown in Fig. 1.2. It analyzes the steady state power profile of the power being drawn by the house and can provide information about when a certain kind of load inside the house is switched on. Sense collects the power profile when any load turns on and shares it online in real time. The profile is then classified into a specific kind of load after processing it through the online database and the information is sent back to the user. After a few weeks of training this device can identify most

kinds of household loads.

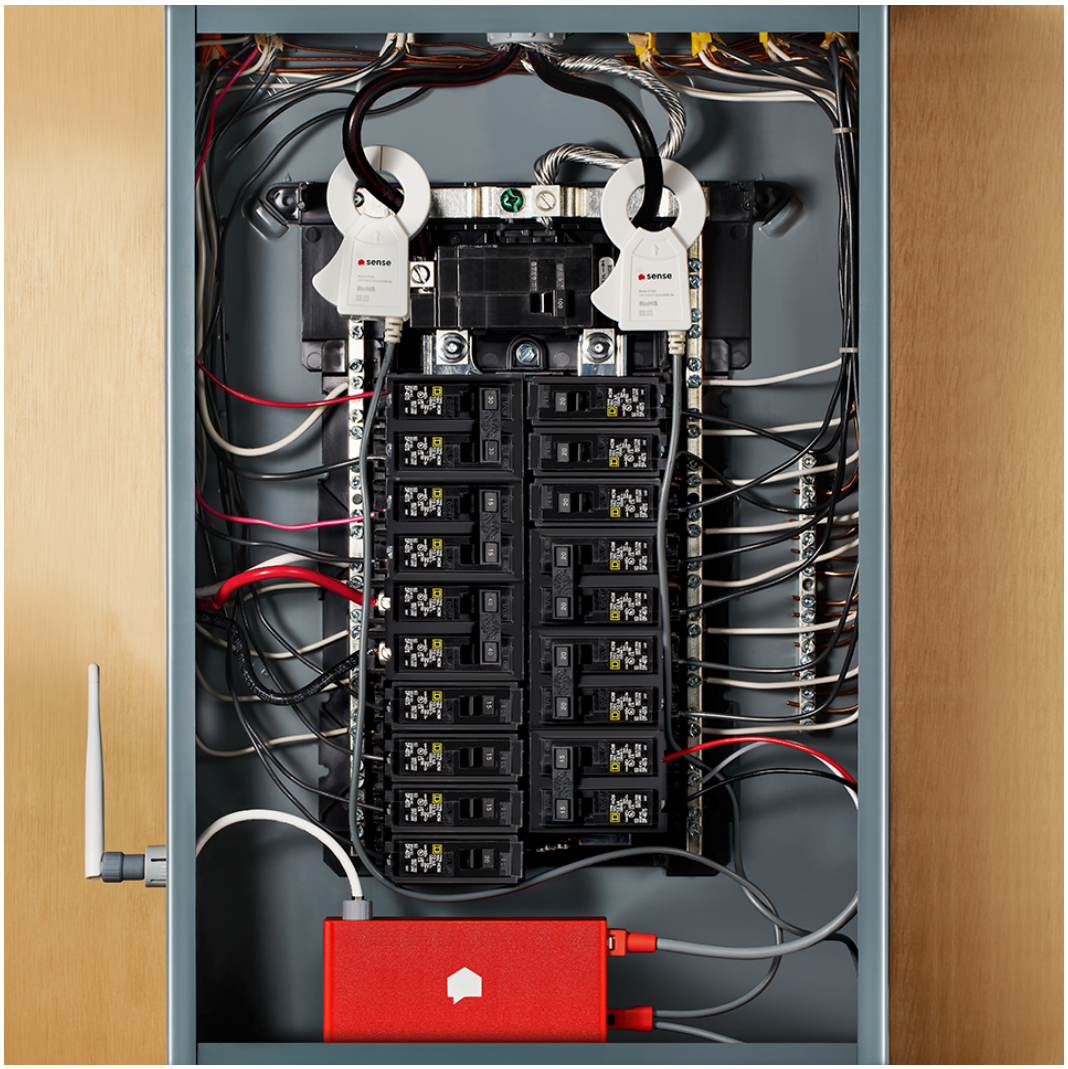

Figure 1.2: A picture of Sense hooked up at the electrical panel [19]

Sense is a state-of-the-art product for load monitoring needs of a household electrical system but there are some special requirements for a naval electric ship system which makes it

more challenging to monitor. Some of those features are listed here.

- Since dc micro grids are relatively new not many products have been developed that cater specifically to a dc distribution system and dc loads.
- For security reasons it is not ideal for the power consumption of ship loads to be shared to an online database. Navy values its privacy and any online processing could be a risk. It is therefore desirable to have all the processing performed on site.
- While sense performs sampling at a much higher rate than utility smart meters it is still not optimum for many naval loads. A real-time load monitoring should be able to estimate when a load started with an accuracy of a few milliseconds. That would require processing the transient of the power profile and not the entire cycle leading up to the steady state.
- Commercially available domestic load monitoring solutions are designed with the aim of load management and not fault detection. A load monitoring solution that could also detect faults and any irregular behaviour could be very valuable to the protection scheme and improve the reliability of the system.

This project is motivated by these unique needs of a shipboard electrical system. The original contribution of the project is to deliver a load monitoring solution that is:

- fast, i.e uses the transient behavior of the loads, to provide information to the user in real time

- compact, i.e performs all processing on site
- able to recognize a variety of faults including shunt faults and series arcing faults
- flexible, i.e can operate for a wide range of dc loads with minor adjustments to the programming variables

Chapter 2

Previous Work

The literature search for this project was divided into three categories. The first group is feature extraction. This is an important concept in load monitoring. The idea is that every load will have a repeatable and unique load profile. This is because these profiles correspond to different physical processes [20]. For example the physical process involved in a coil gun operation is charging of a capacitor at a fixed and controlled rate and then discharging the capacitor through a known and fixed resistance. The profile of a heater would correspond to a physical process of power dissipation through a resistor, the value of which may vary in discrete steps based on the heat setting. The physical process in starting a motor would involve energizing the winding inductance and so on. Based on these inherent differences in the nature of the load, the load profiles will be different in transient stages even if the steady state power are the same. Taking advantage of this phenomena some unique features can be extracted from the load profile to represent any given load. The section on feature extraction explores various features that have been used for this purpose in the load monitoring research area.

Although theoretically every incident of a given load's operation should have identical load profile it rarely is the case. There could be several reason for that:

- Sampling error: Data acquisition is critical to a load monitoring system. The most important attribute to data acquisition with regards to load monitoring is consistency rather than accuracy. However there will always be limitations when converting a continuous signal to a discrete time signal. Two exactly identical signals in continuous time could look different in discrete time if they are sampled out of sync with one another. This is illustrated in the plot of Fig. 2.1. Two identical continuous time signals look different in discrete time because of this synchronization issue. The effect is exaggerated in this figure because of the slow sampling rate but in reality if the sampling frequency is very high compared to the bandwidth of the signal the effect should not be this drastic. The data acquisition of the load monitoring system cannot be dependent on the control system for the load so the signal can start at any point with respect to the sampling instant. This is one source of variation in data collection.

- Variation in external conditions: External conditions such as ambient temperature or core temperature due to extended use could cause the load profile to look slightly different at every operation. Sometimes the degradation of the load from repeated use could also have an effect. Some loads may have energy storage elements that can have residual energy from a previous use, causing the load profile to vary every time it is operated. The load monitoring program should be robust enough to allow for these variations and not

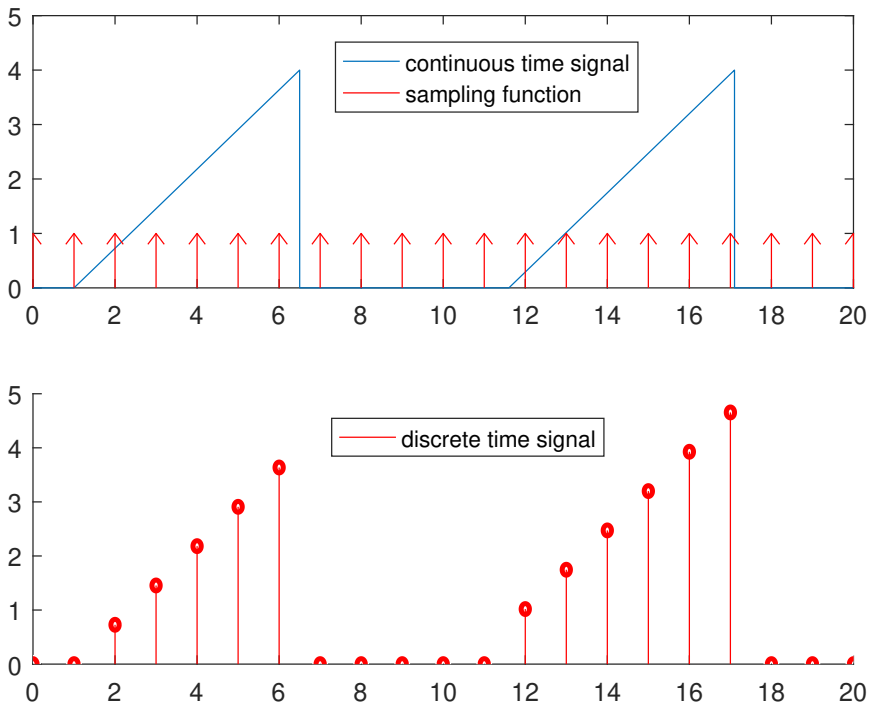

Figure 2.1: Sampling a continuous time signal

misdiagnose a load.

- White noise: The feature extraction may also be affected by white noise. This noise is random and difficult to predict and can influence the actual quantity as well as the acquired data. One source of the noise could be other loads operating in the system and that might vary every time that data is collected. Changing the connections, wire length and layout of the load could also create small variations in the collected data.

Due to all these sources of variation the collected feature set might not exactly match the expected feature set for any given load. The second section of literature research focuses on work done to classify the collected feature set accurately as feature of a given load despite the small mismatch.

Finally some recent research that has been done with focus on fault diagnosis rather than load monitoring is summarized in a third section.

2.1 Feature Extraction

Most of the research on this area is focused on ac grid and ac loads with few notable exceptions. Therefore some of the discussion here will include concepts like harmonics, reactive power and power factor that are primarily concerned with ac loads. Nevertheless the work summarized here is still relevant because the signal processing techniques to obtain these features are similar to what will eventually be utilized in this project.

Non-intrusive load monitoring (NILM) techniques have long been used in residential power systems to accurately determine energy use [21]-[23]. These techniques are typically

based on extracting transient-state features, but can also involve time-frequency analysis such as the wavelet transform [21]. A number of research publications focus on shipboard power system applications of non-intrusive load monitoring [24]-[27] where time-frequency methods are followed by load disaggregation. Load monitoring equipment has been placed on ships [26]-[27] and one valuable outcome has been the ability to determine long-term degradation of components via the load behavior. As an example, a pump that operates at an unusual frequency may indicate a problem with the pump or associated sensors. Unusual spectral components from NILM can be used as triggers to investigate running equipment to conduct early preventative maintenance, rather than corrective maintenance after equipment failure.

A comprehensive look on NILM research shows two broad categories of features exploited for load recognition; Macroscopic and Microscopic. According to [28] Macroscopic features are those extracted at lower sampling frequency, i.e less than 200 Hz, while microscopic features are extracted from data sampled at a higher rate, typically 1kHz and above. Examples of macroscopic features include changes in real and reactive powers, power factors, steady state RMS values, and the shape and duration of transient events. Common microscopic features are harmonic content of the signal, (extracted through either Fast Fourier Transform (FFT) or Short Time Fourier Transform (STFT)), Total harmonic Distortion (THD), Spectral Envelope extracted through STFT, Wavelet Transform coefficients, and high frequency shape features of the raw data.

The pioneering work in the field of NILM was done by G.W Hart in the late 80's and early 90's. The first published work [29] used the change in steady state real and reactive power as the unique identifying feature of the load. This approach worked for large loads with

ON/OFF modes and distinct power ratings as one would expect from household appliances. Low power loads or loads with variable or multi level power draw cannot be identified using this feature only.

Some works have tried to extract more macroscopic features in order to target a wider range of loads. Significant works in this category include the work by A. Cole and A. Albicki [30]-[31]. The additional feature they included was the edge count for a given power profile and the variations in real and reactive power over an extended period of time as long as 900s. In this way they were able to distinguish appliances that had more than one mode of operation and went through several steady state real and reactive power through their operation.

It was later noted that most appliances either have very low reactive power or quite distinct real power and thus could be classified based on just the changes in real power. This approach is often coupled with features related to the usage pattern of the loads [32]-[33]. The earliest work in this area was done by J.T Powers et al [34] who used the time of occurrence and frequency of occurrence over a long period as a feature of the load profile. Similarly the work by Barnaski et al [35]-[37] extract features such as duration of use, and frequency of change in power levels etc. Baranski had good success detecting appliances such as refrigerators, heaters and stoves etc that have a regular pattern of use. This method requires data storage for five to 10 days to reliably look for patterns.

The most well developed load monitoring system based on just macroscopic features is presented in [38]. The program called recognition of electrical appliances and profiling in real time (RECAP), gathers some macroscopic features from the voltage and current data into something called the appliance signature. These features include change in real power, power

factor, RMS current, peak voltage, peak current and signature length. Just like the appliance Sense introduced earlier this profiling must wait for at least one complete cycle of the load operation to construct this signature. It is however a useful and comprehensive feature extraction for ON/OFF household appliances like kettle, oven, heater etc. Very similar to this approach is another work presented in [39] which uses power factor and time to reach steady state power as additional features but it is still in the experimental stage so its effectiveness is not known.

With monitoring household appliances, fast detection has not been a primary concern so most algorithm using just macroscopic features perform adequately. In some cases, specially for certain loads, it is easier to differentiate between loads based on its harmonic content which is a microscopic feature and requires high sampling frequency. The first work to include harmonics analysis as a feature was done by Sultanem [40] in late 80s and early 90s, although he concluded that most household devices could be identified just on the basis of real and reactive power changes.

The use of high sampling frequency and microscopic features was truly developed by S.Leeb, S.Shaw and his research group at MIT. The ground breaking contribution of Leeb was to extract useful frequency features from turn on transients of various devices rather than steady state features like changes in power and RMS etc [20],[41]-[42]. In this way the work being pursued in this project most closely resembles Dr. Leeb's work but with different target applications. He employed the technique of short term fourier transforms (STFT) to calculate the spectral envelope of the signal[41]-[42]. Changes in envelope of third and fifth harmonics were monitored over time and recorded as feature of the transient. A large library of these unique transient features has been developed for a variety of common ac loads and even some

dc loads [43], [47]-[49]. Load monitoring system has been tested extensively on household and commercial ac loads and recently on ship systems too where it has showed promising results and even been able to detect deviation from normal behaviour in case of a worn out equipment [26],[43]-[45]. With Shaw's work the focus of NILM has shifted more towards diagnostics [46],[50] along with monitoring of loads but fast fault identification for dc loads has not yet been produced. Following Leeb's work many other research groups have also exploited harmonic content of the transient extracted through STFT as a unique feature of the load [51]-[54]. More details on the application of STFT will be provided in later sections.

The application of STFT imposes certain limitations on the analysis of the input waveform. The window size of data considered, number of discrete points in the data, and sampling frequency are all fixed which means that the frequency resolution and the range of frequencies analyzed are fixed too. This may limit the ability to detect features from a wide variety of loads. A more advanced harmonic analysis technique called wavelet transform is employed in more recent research that allows the program to zoom into the sampled window of data and retrieve information at various frequency resolutions. As shown by the work in [55] the wavelet transform has an advantage over the STFT when trying to extract frequency information from a transient. However the wavelet transform is complex to implement and would take more processing time unless implemented on a processor with parallel processing abilities like a multi core Digital Signal processor (DSP) or a Field Progammable gate array (FPGA). One simple example of the discrete time wavelet transform (DWT) is shown in Fig. 2.2. In this approach the input data set is passed through a series of high-pass and low-pass filters to extract coefficients corresponding to the energy in various bands of frequencies at various resolutions. Many works

recently have used DWT instead of STFT to extract time-frequency features from the input data due to easy access to high speed multi core processors [55]-[63].

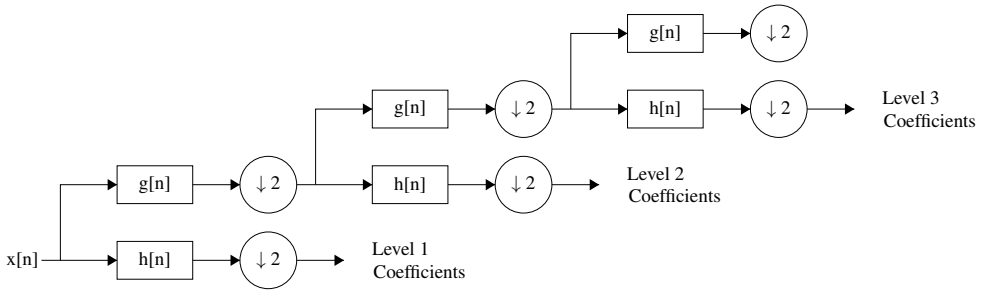

Figure 2.2: Example of a DWT

Not all microscopic features have to be frequency based like in the case of STFT and DWT. Some work has been done on saving high frequency sampled data from raw current and voltage waveform as a way to save the unique signature of every load. The most detailed work in this category is done by Lam et al in [64] where instantaneous voltage and current data is used to create features to capture the trajectory of each load. these features include direction of VI trajectory, the area enclosed by it, measure of asymmetry in the VI trajectory, its curvature and slope with reference to the mean value across different segments. Other efforts in the time domain analysis as a form of feature extraction include [65]-[69]. Even better performance is obtained by using a combination of time domain microscopic along with frequency domain features as shown in [70]-[72]. Using time domain features reduces the complexity of feature extraction process, but it is less reliable as some load transients look very similar. Furthermore frequency based features are more robust to noise and errors in data acquisition [65].

In the presence of so many features that can be used to uniquely identify a load or

a transient, the challenge is to pick the right number of features that can reliably identify a reasonable range of common profiles without making the process overly complex and resource consuming. An interesting work in combining the features to come with the most reliable monitoring system using least number of features is presented in [73].

2.2 Classification

The first part of the research effort is to extract the features that can completely represent a load profile. The second part is to then compare it to either some known load profile or a combination of known profiles to classify it into a category. Some of the methods used in literature are summarized here but this is not an exhaustive list of algorithms that can be used.

The Viterbi algorithm is a commonly used dynamic programming algorithm that recursively solves for a hidden layer of sequence of states that can best account for the observed layer of sequence of events. It has long been used in the field of speech recognition where the recorded audio signal is the observed sequence of events and a string of words would form the hidden layer. In power system signal processing a variation of Viterbi algorithm is applied in [35]-[37] where the observed load profile over a prolonged period is the observed layer. Probability distribution is derived from data stored for up to 10 days. The hidden layer is then the sequence of known states that can most closely match the observed layer. This algorithm can become very complicated when a large number of states are involved. For N states there are 2^N combinations. The algorithm in [36] performs some optimization to greatly reduce the number of probable combinations. In terms of fault recognition this approach is not ideal because it is

difficult to categorize the fault itself as a stage since the nature of fault is so unpredictable, also ideally fault detection should occur as soon as it happens but this method records data over an extended period of time involving several events.

A very similar approach is also used by [65] and [71] with good success. Instead of recording data over several load cycles [65] uses the instantaneous feature of the observed load and recursively solves for the combination of states to determine which loads are contributing to the observed waveform. Another method based on the Viterbi algorithm is the Factorial Hidden Markov Model (FHMM) which is used in several papers [74]-[76]. The important development in these papers is that they employ something called the unsupervised learning technique where the training dataset is not required to have one-to-one correspondence with the class type. Getting a training dataset from each class of load can be difficult or impractical in some applications. This leads to more complex models compared to supervised learning where the relationship between the sample of training dataset and the corresponding class is known. The method in [77] uses a unique fuzzy logic based approach which is also unsupervised and performs with 85% accuracy.

Cognitive electric power meter [78], often heralded as the next step in smart meter technology [79], performs classification based on bayes classifier. This is a probability based approach which is suitable for a electric monitoring a large number of loads over an extended period of time. Consider a feature vector **x** is observed and there are M possible classes of load denoted as ω_1,ω_2,...ω_M. The cognitive meter would require prior knowledge of probabilities of occurrence and would classify **x** as ω_i if conditional probability of ω_i given **x** is greater than conditional probability of ω_j given **x** for all $i \neq j$. In other applications such as this project the

training dataset may not be so large so to implement probability based classifier approach.

Matching each observed feature of one event to an array of stored features for all possible events can broadly be categorized as a pattern recognition approach. The most common and intuitive approach is the minimum distance classifier, specifically Euclidian distance classifier. Suppose all the extracted features for any event observed at time t can be combined into a vector X, and an array of vectors m_i contains the mean value of those features for class ω_i. For a system with M classes of loads, m_i is calculated from a pre-programmed database or historical data used for training. The unknown feature vector X is assigned to class ω_i if Euclidian distance between X and m_i is less than Euclidian distance between X and m_j for all $i \neq j$ [80].

Another simple classifier which is very commonly used is the nearest neighbor classifier. The subtle difference between nearest neighbor and minimum distance classifier is that each feature in the feature vector is analyzed independently. If the algorithm has n different features i.e X is a vector of length n then each feature is processed through a minimum distance classifier to determine the nearest feature among all classes. After all features are analyzed, the algorithm looks at which class has most features closest to the observed feature vector. Because of its simplicity and performance many papers use nearest neighbor approach in some form for their classifier algorithm [52]-[53],[81].

Neural networks form another family of classifiers which are more complex than other methods discussed here and require more processing time and training data. Despite their complexity a large number of papers use some form of neural network as their classifier [51],[71],[29],[50],[41]. The most basic form of neural network is a perceptron which can

classify a given feature vector into either one of two classes. It does this by assigning specific weights to each feature in the feature vector. These weights are calculated through a recursive method on a large training data set. A figure to represent a perceptron operation is shown in Fig. 2.3 [80]. The activation function is just a step function in this case. The output y is the assigned class which would be either 1 or 2 depending on whether the input v is positive or negative. Neural network with multiple layers or more than 2 classes is formed by series or parallel connection of several of these neuron units.

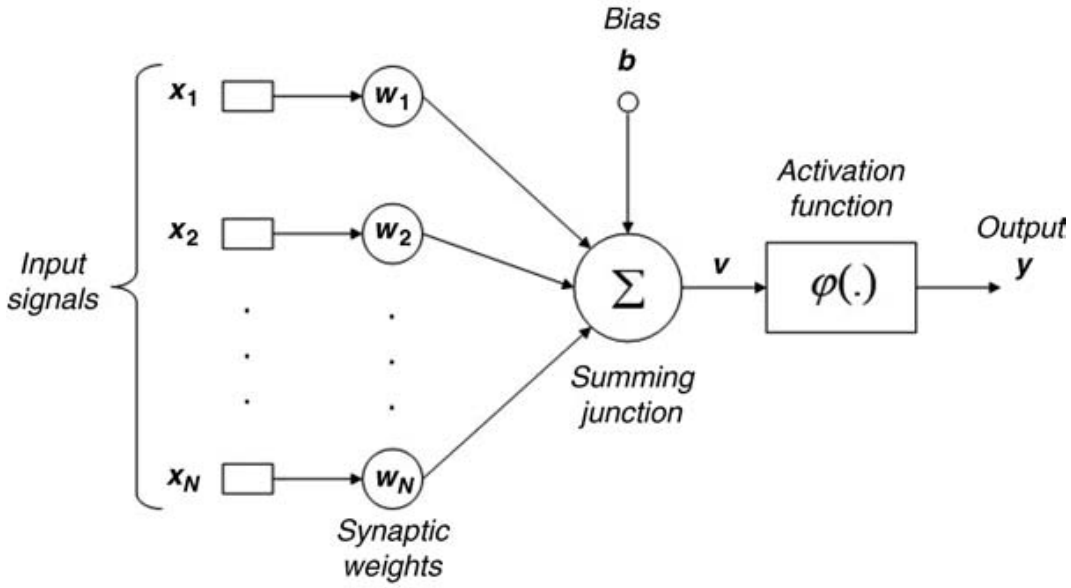

Figure 2.3: Neuron Unit for a neural network

2.3 Fault Diagnosis

Using the feature extraction and classifier tools mentioned above several recent research efforts have been made to use microscopic features of load profile to detect faults such as low

impedance shunt faults [82]-[86] or high impedance series arc faults [87]-[91].

Research effort in [82] and [85] is specially pertinent to this research because it targets dc grids in particular. The work in [82] still focuses on the faults on the ac loads attached to the dc grid while [85] discusses faults on several locations on the grid including at both ac and dc sites. The most developed work on shipboard MVDC fault detection using wavelet transforms has been presented in [85] but it still does not cover a comprehensive range of faults, and the algorithm has not been tested on hardware which would test the robustness of the program. It implements an artificial neural network and provides detailed theoretical background to its proposed method which is a useful contribution of this paper. Research in [83] provides a comparison of DWT and STFT for feature extraction with a focus on fault diagnosis. Based on various simulated ac faults [82] concludes that DWT can provide slightly more easily detectable features for a majority of faults however this conclusion is based on a neural network approach as classifier and the research does not comment on the ease of implementation as a trade off factor between STFT and DWT.

A very common form of fault in any electrical system is series arcing fault. Despite being a common fault there is very little work on modeling series arc as an electrical phenomena. The nature of the fault makes it very difficult to model as a time varying impedance as there are so many factors involved such as line inductance, air gap, contact material etc. Work in [90] provides a detailed account of modeling these series arc in time domain. Very useful work is provided in [88] based on several experiments to characterize the arc in frequency domain. STFT is used extract these frequency components in [88] and an algorithm is later presented that can detect the arc based on its frequency composition. The arc detection method is not tested

in real time on a processor and the arc current supplied through a parallel capacitor is analyzed instead of the actual current flowing through the air gap. The theory of the algorithm and the modeling work in [88] makes it very relevant to this project. Another work of significance is provided in [87] wherein wavelet transforms are used to detect series arcing fault. The work in [87] provides a theoretical algorithm but remains to to be applied in real time to a test system. Furthermore it also needs a network of capacitors which may not be practical for every kind of load but is useful for dc transmission lines.

STFT is a commonly used technique in digital signal processing. Some examples of the recent applications of STFT in power signal processing include the work in [97] where it is applied on ac waveforms. The second derivative of the second harmonic of the current signal is used for event detection and the first 8 harmonics are used to create a feature vector. Work presented in [98] also applies the STFT to ac voltage/current waveforms, however it only uses the information at the fundamental frequency as a way to ascertain voltage sags and swells resulting from fault conditions. Similarly [99] applies the STFT to ac waveforms and proposes a fault detection method based on using the average of the frequency spectrum output as an identifying feature.

STFT on dc or non periodic waveforms have also been commonly used in recent years. A novel approach is outlined in [100] where eight features are extracted from the STFT spectral output and used as feature vector to detect partial discharge from high voltage cables. A unique application of STFT for fault detection is presented in [101] where STFT is applied on vibration signals recorded in the vicinity of a bearing to monitor defects in bearing function or installation. Only some known frequencies of interest are calculated and monitored in the

entire spectrum. One of the more developed STFT based algorithm for fault detection on dc waveforms is presented in [102] and a similar idea is presented in [103]. The work in [102] presents a very detailed scheme on detection of shunt fault by monitoring the shape of the spectral output after STFT, specifically the periodic zeros that can be expected in the spectrum of a constant dc signal. While the method shows good result for a constant load application it will not be able to work for a system with pulsed load or large transients.

Part II

Specialized load monitoring and fault detection schemes

Chapter 3

A coupled-inductor dc breaker with STFT based arc detection

he Z-source breaker [92]-[94] is a recently developed type of solid-state breaker that automatically responds to faults and is closely related to the coupled-inductor dc breaker [95]-[96] that is being used in this chapter. Common undesired events that require a response in dc systems are shunt faults and series arc faults. These both have their respective characteristic change in current, yet it can be challenging to distinguish between them and the normal operation of pulsed loads such as radar or railguns. Using time frequency characteristics of load current profile for event detection and characterization has proved useful for dc applications [82]-[86], especially for series arc that can be specially difficult to detect. [87]-[91]

Categorization is determined by the use of time-frequency (Short Term Fourier Transform) analysis via digital signal processor (DSP) in this chapter. Rapid computation and a sliding window sample set is realized through an arc detection algorithm. This is fast enough to

prevent any damage to the rest of the circuit. The additional feature of analyzing the load current also opens the doors for other tasks such as detecting component and wire degradation, preventing excessive maintenance costs.

The experiment involves a low voltage dc power system, which models fixed load zones on an electric ship. Three events are introduced; a low impedance shunt fault, a series arcing fault, and a step change in current. The simulation results indicate that the detection system can properly identify the three different events using STFT, and implement the appropriate interruption.

3.1 System Description

The system being considered here is to model fixed loads on a dc electric grid such as heating and lighting. There are no solid state switches as part of the load itself as it is being operated on the grid voltage without any dc-dc conversion. Unlike the faults in ac systems, a typical shunt fault in dc systems does not have a zero crossing. If a mechanical contact is used to isolate the load during the fault, the inductance in the conduction path will create a large voltage across the contacts as they are being pulled apart. This voltage could ionize the air and force a path for conduction known as arcing. Arcing usually leads to extremely high temperatures and possibly fires. In this case, a mechanical switch may either not be able to isolate the fault or would need extensive arc extinguishing methods to do so. It is therefore proposed to use a coupled-inductor dc breaker, previously introduced in [95], as shown in Fig. 3.1.

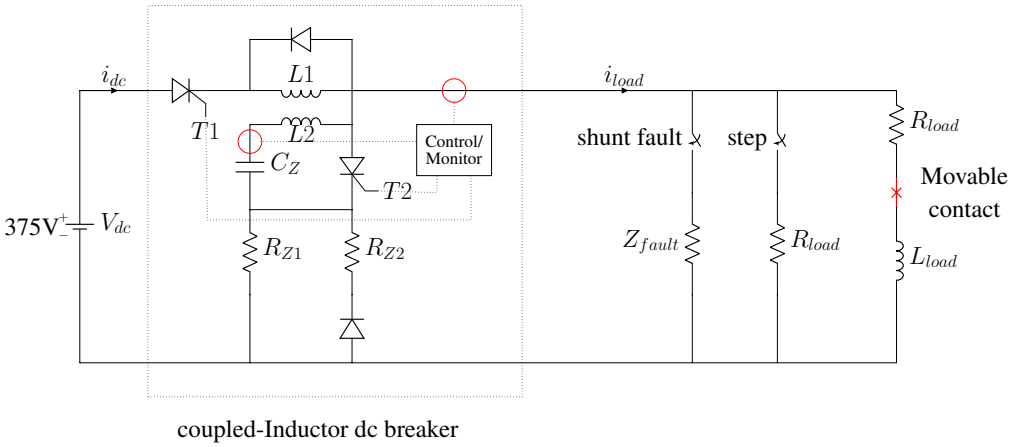

Figure 3.1: Simulated system.

3.1.1 Coupled-Inductor dc breaker

A coupled-inductor dc breaker, inserted in the system as shown in Fig.4.1, adds a solid-state switching device (i.e. a thyristor or silicon controlled rectifier (SCR) to the conduction path). This allows for a faster and safer method to isolate the load from the source in case of a fault. The design of the breaker allows it to perform this function automatically in case of a sudden increase in output current. To close the breaker a pulse must be applied to the gate of the thyristor labeled T_1. Once the current reaches steady state, the gate pulse must be removed and the breaker will now be considered armed and ready to operate. The control & monitoring block shown in Fig. 4.1 can monitor current or voltage at the output or at the capacitor C_Z to determine if steady state has been reached and accordingly provide the gate pulse to the conducting thyristor. For the system simulated in this chapter the output current is being monitored but for

other systems it may be desirable to monitor the capacitor current. A low-current LEM sensor can be added there instead of the output current which could require a large sensor due to the steady-state current.

During normal operation the load current flows through the coupled-inductor $L1$ while the capacitor C_Z is charged to input voltage. The resistor labeled R_{Z1} is the charging resistor designed to limit the inrush current while the capacitor charges. In the event of a shunt fault as shown in Fig 4.1, the transient current is supplied by the capacitor through the coupled-inductor $L2$, Z_{fault} and a parallel combination of the resistors R_{Z1} and R_{Z2}. It is desirable to design R_{Z2} to be a small resistance so the capacitor can respond quickly to a transient event.

The polarity of the coupled-inductors is such that when the capacitor injects current into $L2$ during the transient event it forces $L1$ to inject some current back into the thyristor $T1$. A design objective is to make sure that the injected current is large enough to force the current through $T1$ to reach zero in case of a fault. If the current through the thyristor reaches zero in the absence of a gate pulse it will turn off, thereby effectively opening the breaker. For a desired step change in load current, the current through T_1 will still decrease during the transient but will not reach zero if the breaker is designed accordingly. Another feature of this breaker is a manual open option. A gate pulse can be provided to the thyristor labeled $T2$ and that will provide a path for the capacitor to discharge through the inductor $L2$ leading to a similar result as a shunt fault. Further details on the design and operation of the coupled-inductor dc breaker can be found in [95]. The design parameters for the breaker used in this chapter are summarized in Table 3.1

Table 3.1: Coupled-Inductor Dc Breaker Parameters.

$L1$	$R1$	$L2$	$R2$	Lm
$51\mu H$	0.373Ω	$6\mu H$	0.128Ω	$1mH$
Rm	$N1:N2$	R_{Z1}	R_{Z2}	C_Z
1000Ω	$70:24$	100Ω	0.2Ω	$100\mu F$

3.1.2 Breaker response to transients

The system in Fig. 4.1 is simulated in MATLAB Simulink with R_{load} as 94Ω and L_{load} as $0.5mH$ to have a steady state load current of $4Adc$. For the first set of results shown in Fig. 3.2, the input and output current of the dc breaker, labeled as i_{dc} and i_{load} are plotted over a period of $0.6s$. At $t = 0.05s$ the thyristor $T1$ is triggered which allows the breaker to close and start conducting. It can be seen that there is a slight overshoot in i_{dc} which is a result of the capacitor charging current. After about $0..05s$ the current has reached a steady state value and the gate pulse from $T1$ is removed. At $t = 0.3s$ a step change in load current is requested as another unit comes online. It can be seen that the thyristor current, i_{dc} decreases but does not quite reach zero. This means that the breaker is designed to facilitate a step change that doubles the steady state current without treating it as a fault.

For the second set of results shown in Fig. 3.3 a shunt fault is simulated at $t = 0.8s$

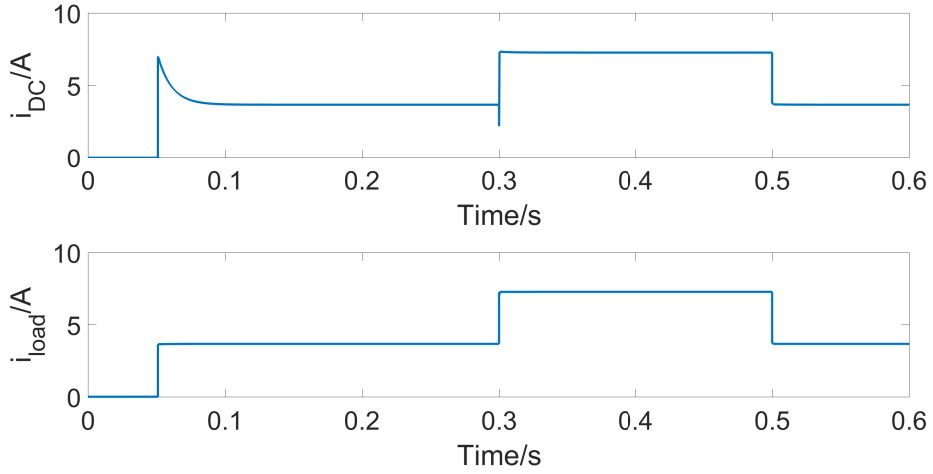

Figure 3.2: Breaker response to step change in current.

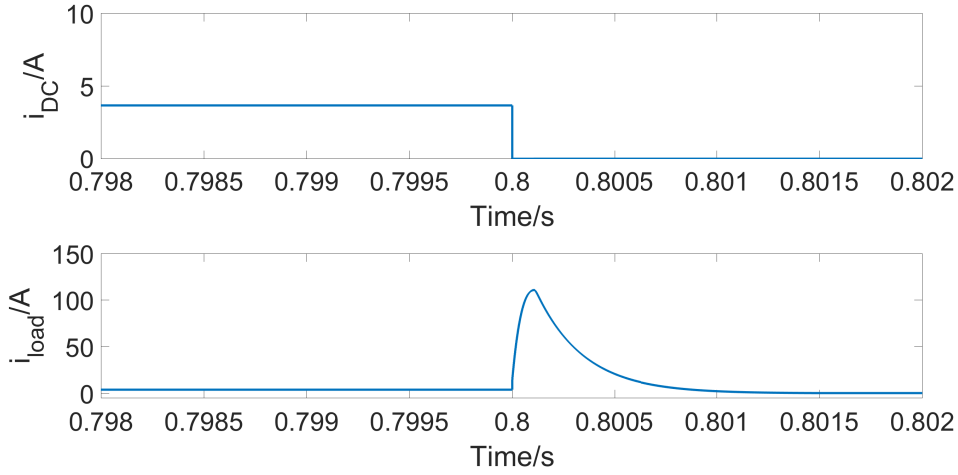

Figure 3.3: Breaker response to a shunt fault.

with Z_{fault} of 2Ω. It can be seen that the input current of the breaker falls instantly to zero so the rest of the system does not even see the fault. From the output current it can be seen that the breaker opens within $0.5ms$ seconds of the fault being created which is a very fast response.

3.2 Series Arcing Fault

The coupled-inductor dc breaker is designed to open automatically for large and sudden changes in current which is a useful feature but unfortunately does not provide comprehensive fault protection for all dc loads. A common source of faults in dc loads is a series arcing fault which may be generated due to loose electrical connections or a mechanical fault creating an air gap in the path of conduction. Such a fault will not generate a large transient in current, in fact the dc current may remain nearly the same or decrease slightly. Therefore a coupled-inductor dc breaker or any dc breaker looking only at the transients or time value of current will not be able to automatically react to this kind of fault.

3.2.1 Series Arcing Device

In order to study series arcing it is important to be able to create the arc in a low-voltage lab setup in a repeatable and controlled manner. An arcing device, shown in Fig. 3.4, is designed for this purpose. The contacts are made from copper rods machined into a conical shape. Arcing creates very high temperature so the rods are embedded into ceramic housing. Ceramic is an excellent electrical insulator and has extremely high melting point in excess of several thousand Fahrenheit. One of the contacts is fixed while the other is connected to the barrel of a micrometer screw gauge and can be moved laterally away from or towards the fixed contact. The micrometer barrel allows precise movement of the contact so the air gap can be controlled and set to a desired value. The apparatus is mounted on a high temperature resistant plastic base. The

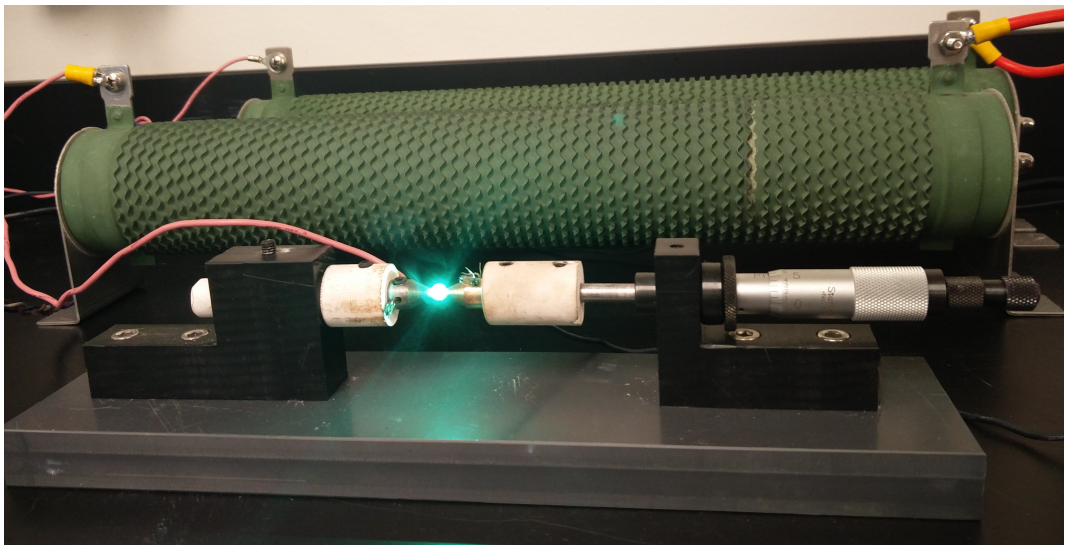

Figure 3.4: Series arcing device.

location of this arcing device within the system is marked as movable contact in Fig. 3.1.

Fig. 3.5 shows the arc current and the voltage across the contacts for an air gap of 25mil and steady state current of $4A$. R_{load} is 94Ω and L_{load} is $0.5mH$. As expected there is not a large change in load current. It only decreases to about $3.6A$ from $4A$. The contacts start moving apart around the $4s$ mark. At around $5s$ the air gap is created as indicated by the sharp change in current and voltage. It takes another $1s$ for the air gap to reach 25 mil after which the contacts do not move and the arc is sustained for rest of the period.

3.2.2 Short Time Fourier Transform

The data recorded from the arcing device is imported to MATLAB for more detailed analysis in both time and frequency domain. Some important observations can be made from the results

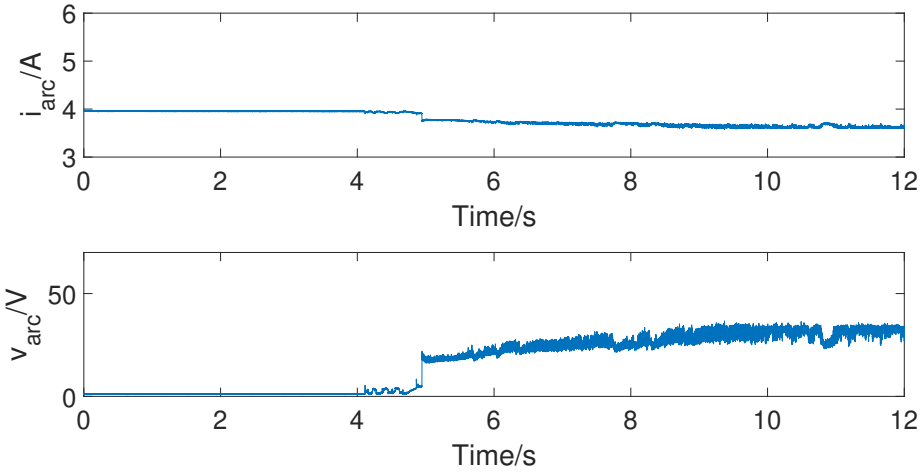

Figure 3.5: Arcing current and voltage across the contacts.

in Fig. 3.6 where the frequency content of the normal current and the sustained arc current are being compared over different range of frequencies. The first observation is that the noise introduced by the arcing in the sustained arcing current is mostly in lower frequency range i.e below a few hundred Hertz. This makes sense as the arc current is in series with a large inductance. Another observation is that the noise in frequency domain has a rather wide band distribution. It is not limited to one or two frequencies but instead shows up in a range of frequencies which is consistent with the random nature of the arcing process. During the sustained arc the temperature is always rising and the contacts are in the process of burning and the occasional sparks are produced, all leading to a very dynamic process and fluctuating noise.

Now that the frequency content of sustained arc compared to normal current is known, the options to extract this information from time domain signal can be considered. Wavelet transforms and short time Fourier transforms (STFT) both can provide information on frequency content of a signal with respect to time. Because of the simplistic nature of this prob-

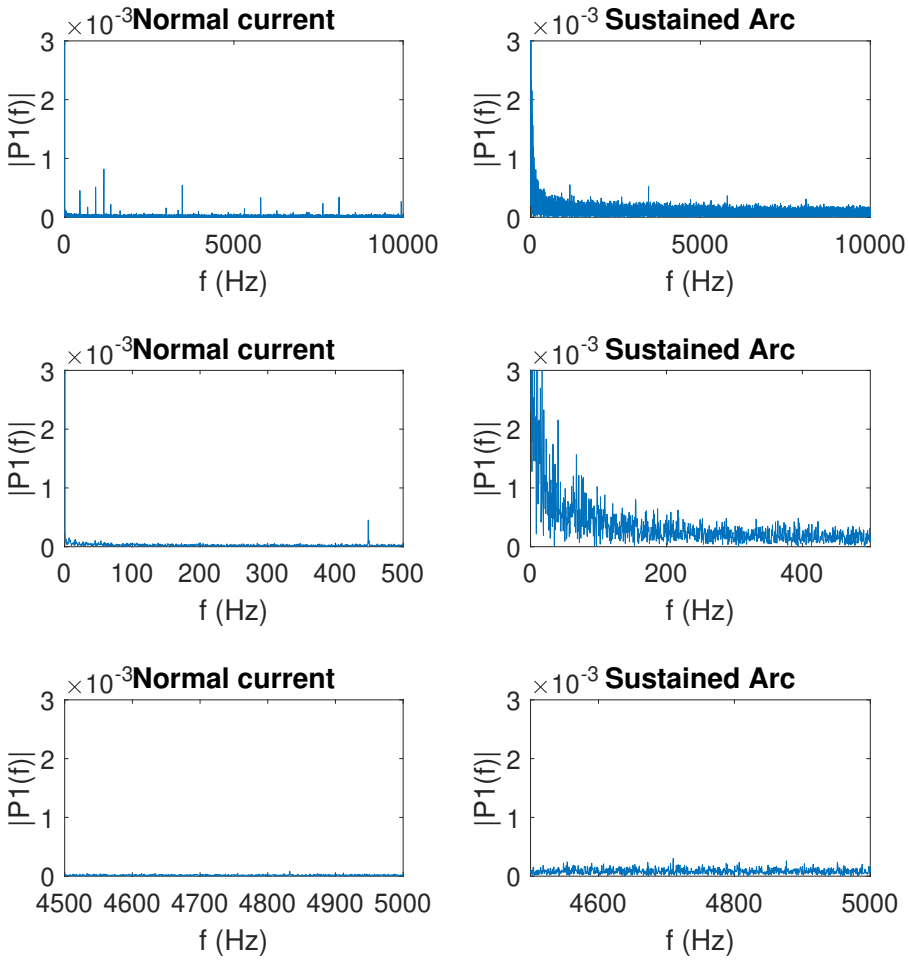

Figure 3.6: Arcing current frequency content.

lem and the ease of implementation STFT will be the preferred method in this chapter.

STFT involves taking the fourier transform of N number of discrete time domain signals sampled at frequency F_s. The result of that provides the frequency content of $N/2$ discrete frequency components within that signal equally spaced from $0\ Hz$ to $F_s/2$ Hz. One iteration

of this STFT will provide this frequency content within a time domain window of N/F_s. Next iteration can be performed by sliding this time domain window by a k multiple of sample time $1/F_s$. For this application, since the information of interest as shown in Fig. 3.6 is within 500 Hz, the sampling frequency F_s is selected to be 1 kHz. A window size of 0.25s is selected that leads to $N = 250$ and provides a frequency precision of 4 Hz. k is selected as 1 so one iteration of the STFT will be performed every 1 ms.

3.2.3 Arc detection algorithm

Fig. 3.7 shows the result of STFT implemented by MATLAB over a current signal of 20s using the parameters specified above. There is arcing present in the current from 5s to 15s as indicated by a wider spread of power in the frequency spectrum during those times. Another representation for this current profile is shown in Fig. 3.8 where the sum of the power in the frequency components from 20 to 300 Hz is calculated through STFT is plotted against time. It can be seen that a significant increase happens during the sustained arc and that is the basic parameter which will be calculated and monitored for the detection of arc. This will be denoted as P_f for the rest of the chapter.

The first condition for arc detection will be that P_f must exceed a predetermined threshold which will be denoted as T_f. However this is not a sufficient condition for arc detection. There will be scenarios where P_f will exceed T_f but there will be no arc. These scenarios include all the desirable step change or large transients in the system such as breaker closing, step change and breaker opening. The large sudden changes in time domain signal translate

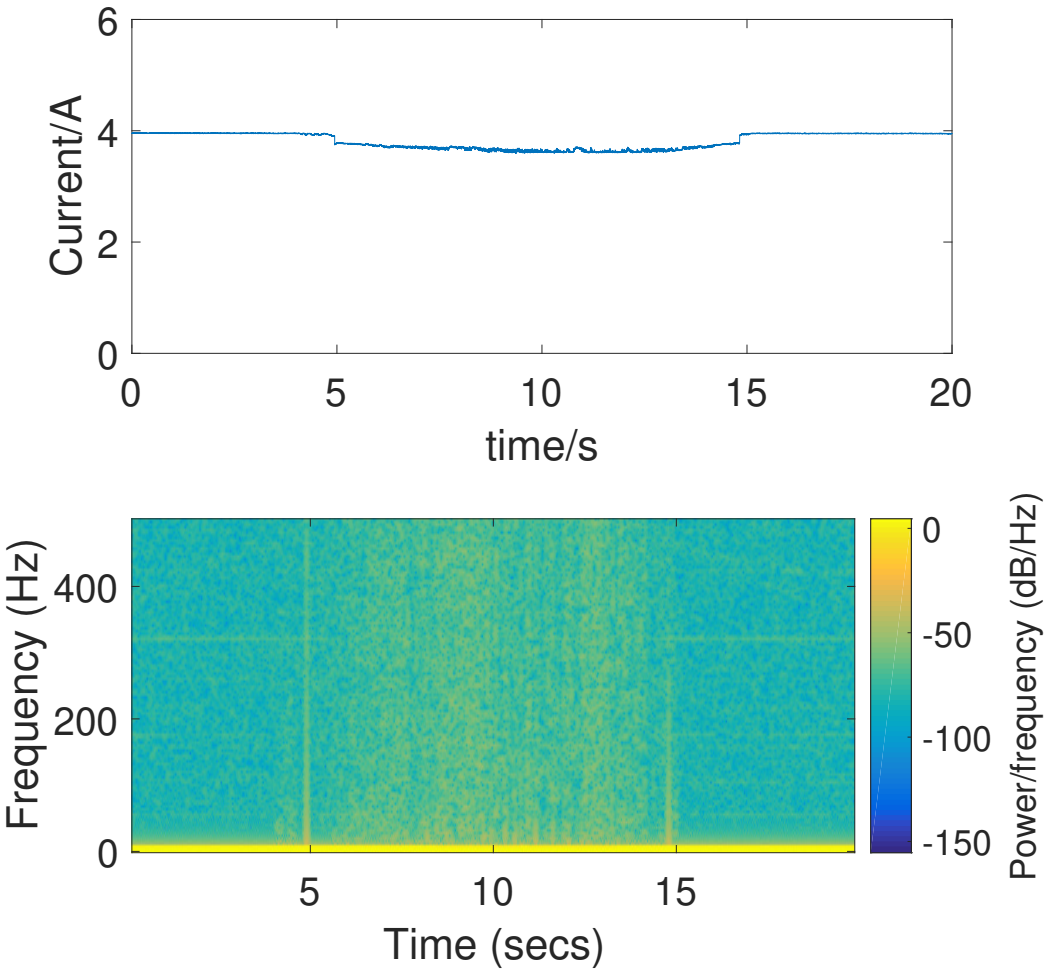

Figure 3.7: STFT results for a current profile with sustained arcing.

to wide band noise in frequency domain. Hence the monitoring must be able to identify these large transients as well.

To detect these transients, the sum of power over the very low frequency components will also be recorded. In this case these frequencies are from 0 to 10 Hz. It will be denoted as P_0. P_0 is an approximation of the dc component of the signal. If P_0 has changed by more than a threshold

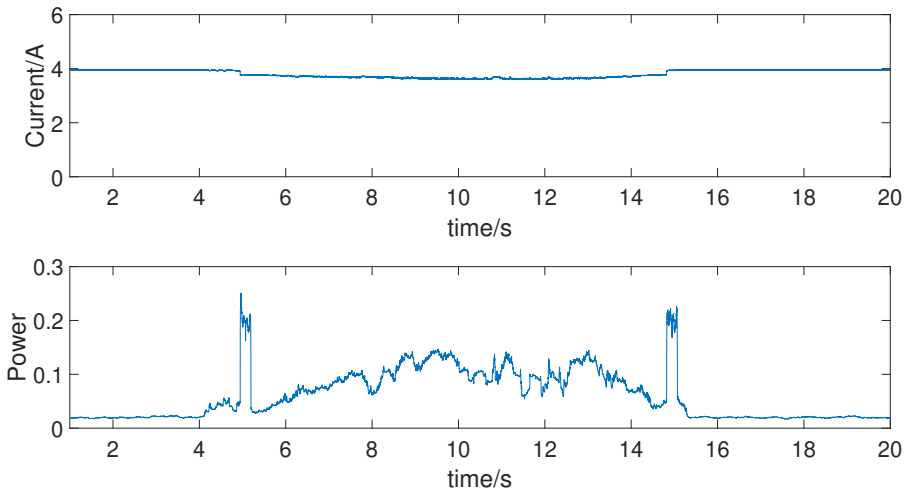

Figure 3.8: Variation in power of frequency components 20Hz to 300Hz.

value denoted by T_0 over the duration of previous 50ms then it will be considered as a large transient change and the first condition will be ignored. This algorithm is summarized through a flow chart in Fig. 3.9.

3.3 Implementing The Arc Detection Algorithm

3.3.1 Selecting the parameters

The algorithm outlined in previous section and Fig.3.9 depends on some parameters like T_0 and T_f, as well as sampling parameters like N and F_s. The choice of sampling parameters depends on the frequencies of interest and the capabilities of the microprocessor being used. Based on

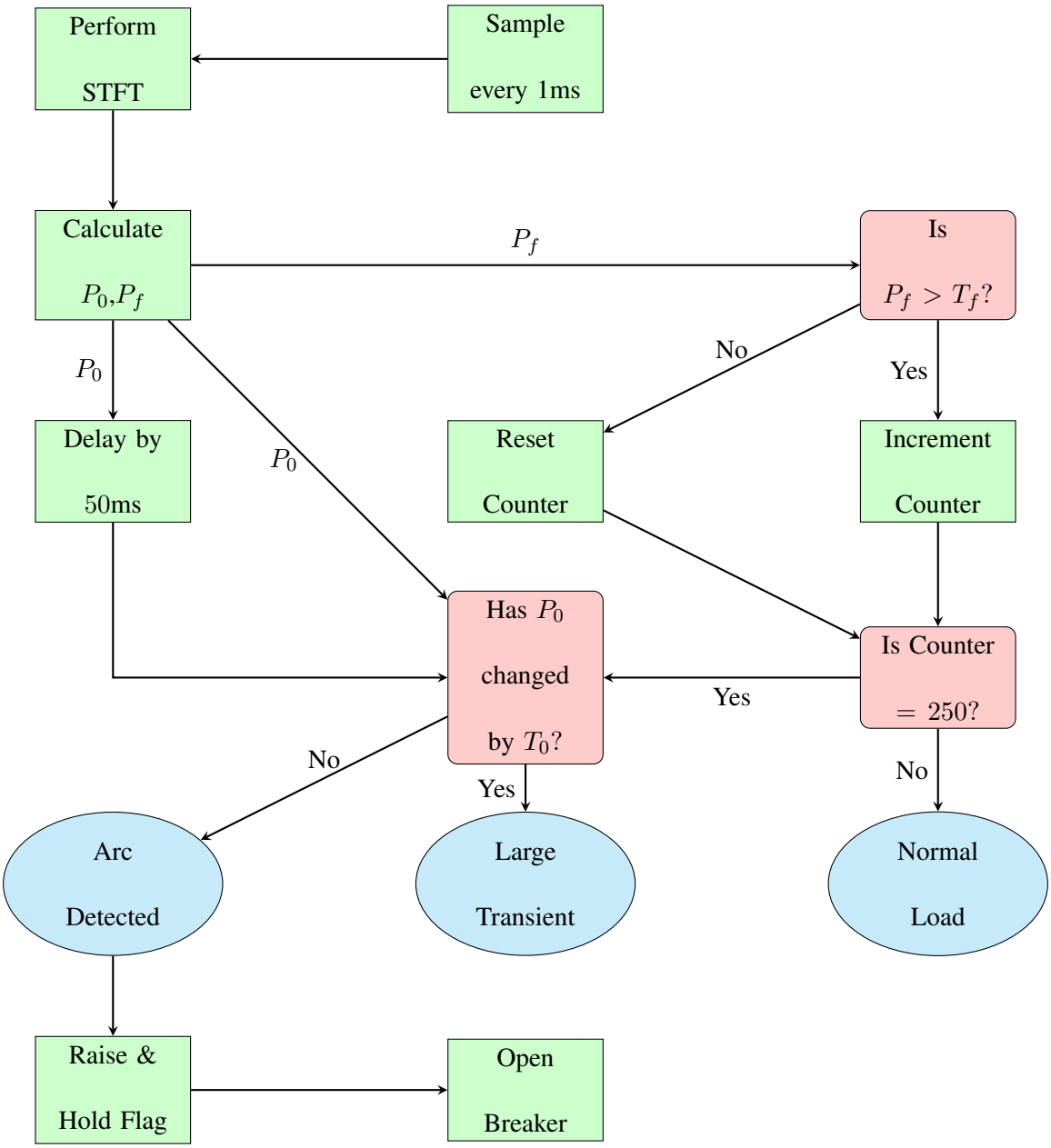

Figure 3.9: Decision process for arc detection.

the analysis of previous section, the frequencies of interest are known and the capabilities of the microprocessor will be discussed in the next subsection.

For the given sampling parameters, the choice of algorithm specific parameters depends on the system variables like V_{dc} and i_{dc}, as well as the expected fault variables like air gap of the arc, speed at which the contacts move away, the material and shape of the contacts etc. System parameters like V_{dc}, i_{dc}, R_{load} etc are known in advance so their effect on the parameters can be predetermined through analysis. If a system is expected to operate at different i_{dc} or R_{load} during the course of operation, the parameters can be updated accordingly as a function of these system variables. For example based on Fig. 3.5 a good value for T_f would be 0.03 for an i_{dc} of $4A$. The magnitude of the first element of the STFT, denoted by k_0 is equal to the i_{dc} so that information is already being calculated by the monitoring system. Instead of assigning a fixed value to parameter T_f it could be calculated as a function of k_0 as it is directly proportional to the square of k_0 as shown in 3.1. This approach will be better for a system that involves multiple loads. The effect of L_{load} on the parameters remain to be studied in further detail.

$$T_f = \frac{0.03}{4} k_0^2 \tag{3.1}$$

The fault parameters also affect the choice of parameters. With the arcing device designed for this research, air gap between contacts, is the most convenient variable to study as it can easily be controlled. Arc is sustained over various values of air gap and the current profile is recorded and shown in Fig. 3.10. The frequency content of the sustained arc at different air gaps is shown in Fig. 3.11. From the analysis similar to previous section it is observed that the

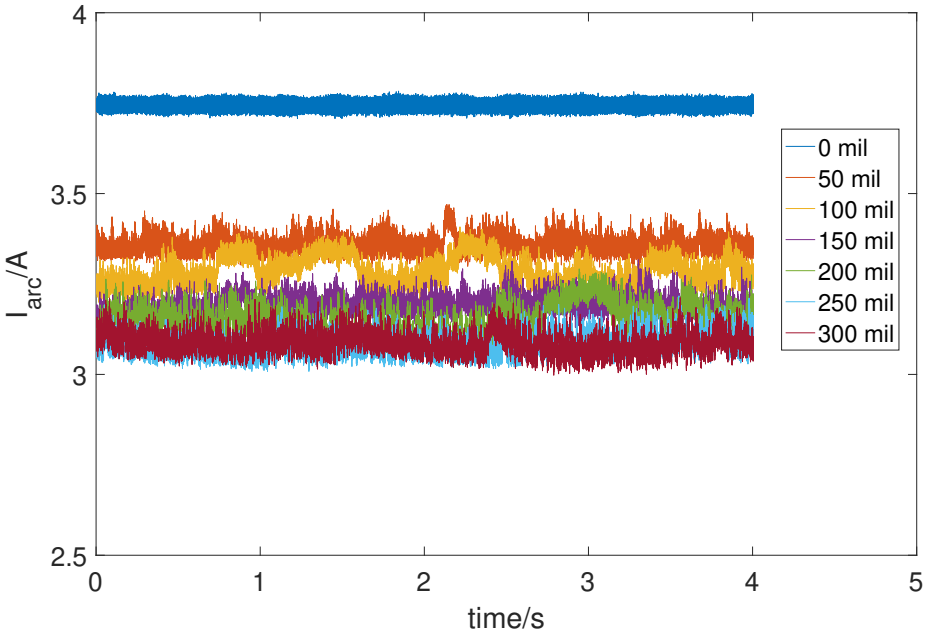

Figure 3.10: Sustained arc at different air gaps.

noise in the arcing current generally increases and eventually saturates at higher air gaps. Also higher air gaps cause a greater dip in the steady state current. This means that if the parameters are determined for a fault of air gap 25 mil, they will also detect arcs at any air gap more than as well. If more sensitivity is required then T_f can be lowered. The effect of other fault parameters such as speed of separation, contact material and shape remains to be studied further.

3.3.2 Simulated results

The current and voltage data obtained from a sustained arc at 25 mil using the arcing device, as shown in Fig.3.5, is used to calculate the arc impedance. This arc impedance is then imported

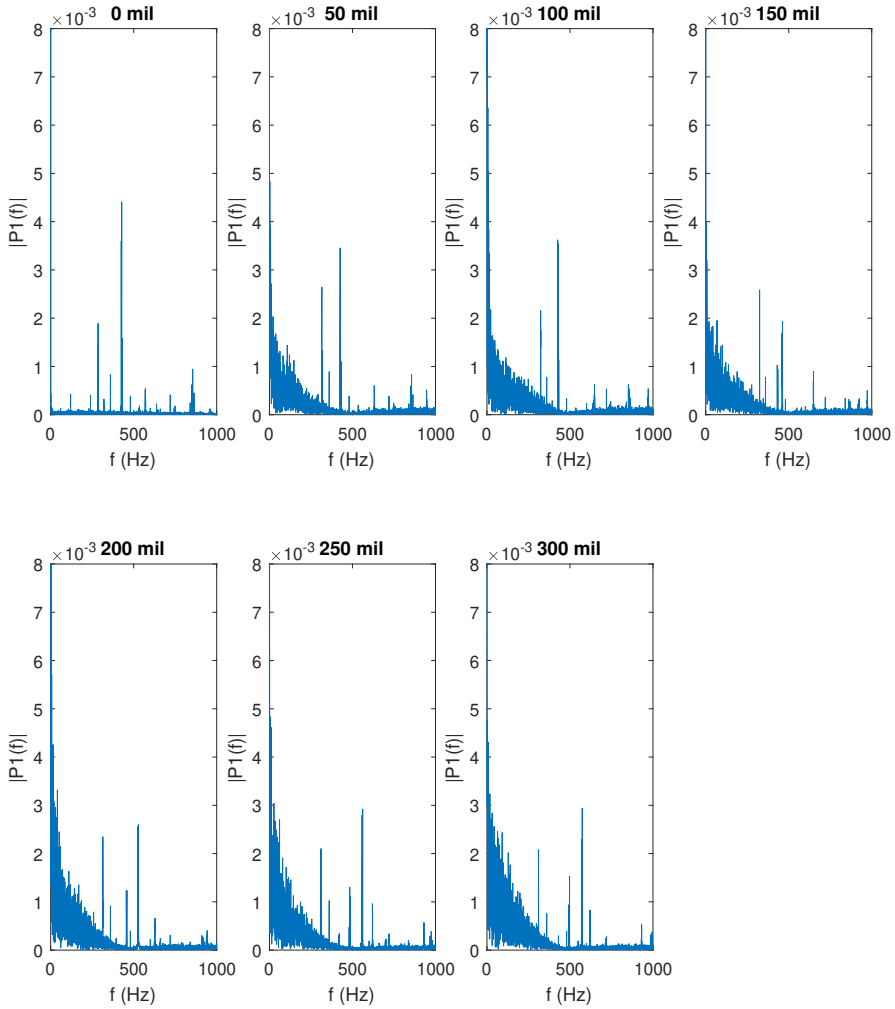

Figure 3.11: Frequency content of sustained arc at different air gaps.

into a variable resistor model in simulink to model the movable contact in the system shown in Fig. 4.1. The arc detection algorithm with Parameters shown in Table 3.2.

In the result shown in Fig.3.12, the system from Fig.4.1 is simulated along with the arc detection algorithm. The top subplot shows the current being monitored and the bottom

Table 3.2: Arc Detection Algorithm Parameters

N	F_S	T_0	T_f
250	1 kHz	0.2	0.03

subplot shows the flag for arc detection at the output of the arc detection system. This flag also drives the gate of the thyristor $T2$. The system starts with some transients and there is a step change of load from $t = 1$ to $2s$. It must be noted that no flag is raised for any of those transitions. The movable contacts begin moving around the 4 s mark and the air gap is created shortly afterwards. As soon as the noise in the signal exceeds the threshold the algorithm positively identifies the arc and raises the flag. This flag drives the thryristor $T2$ forcing the coupled-inductor dc breaker to open hence disconnecting the faulty load from the source. Once the current drops to zero the flag is also removed.

3.3.3 DSP Implementation

The monitoring device used to implement arc detection is a Texas instruments Digital signal processor f28335. It operates on a clock rate of 150 Mhz and is a good fit for the computation required in this process. Selecting the proper values for N and F_s depends largely upon the

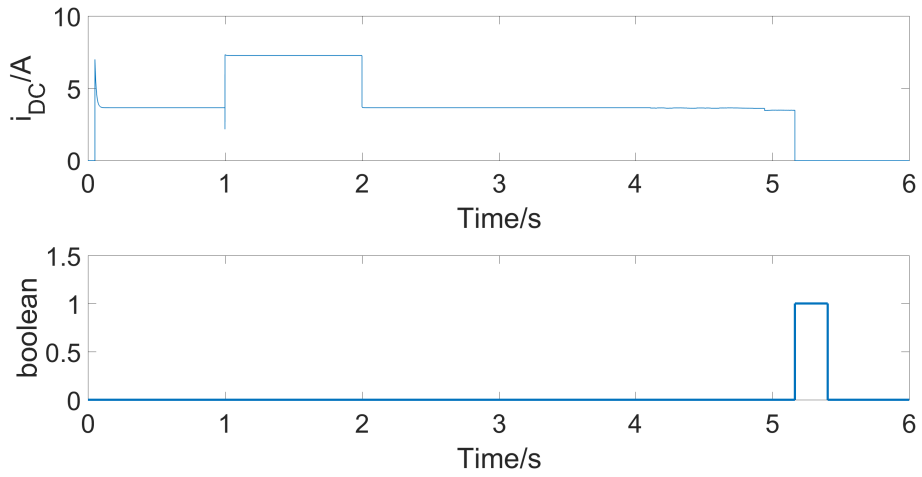

Figure 3.12: Simulation results.

computation abilities of the microprocessor. It was observed that this DSP took several milliseconds to compute FFT of a discrete sample of 250 elements. Using F_s of 1kHz it is not possible to use this DSP to calculate FFT of a new set of 250 samples every 1 ms. Therefore a faster method of STFT known as recursive Discrete Fourier Transform or recursive DFT is applied. In this method one new element is added to the window while one sample is removed from the window and the updated set of STFT is calculated as a function of these two elements. It is an efficient way to perform STFT and brings the computation time lower than 1ms so now the desired F_s of 1kHz can be used. In addition for real signals the values of the magnitude of the first $N/2$ elements of the STFT is the same as last $N/2$ elements so only the first $N/2$ are calculated which further decreases the computation time by half.

The current signal could contain power in frequencies greater than $F_s/2$ which will cause aliasing and distort the frequency content in lower frequencies. To avoid that an anti aliasing analog filter is designed to process the current data before sampling by the DSP. The cut off

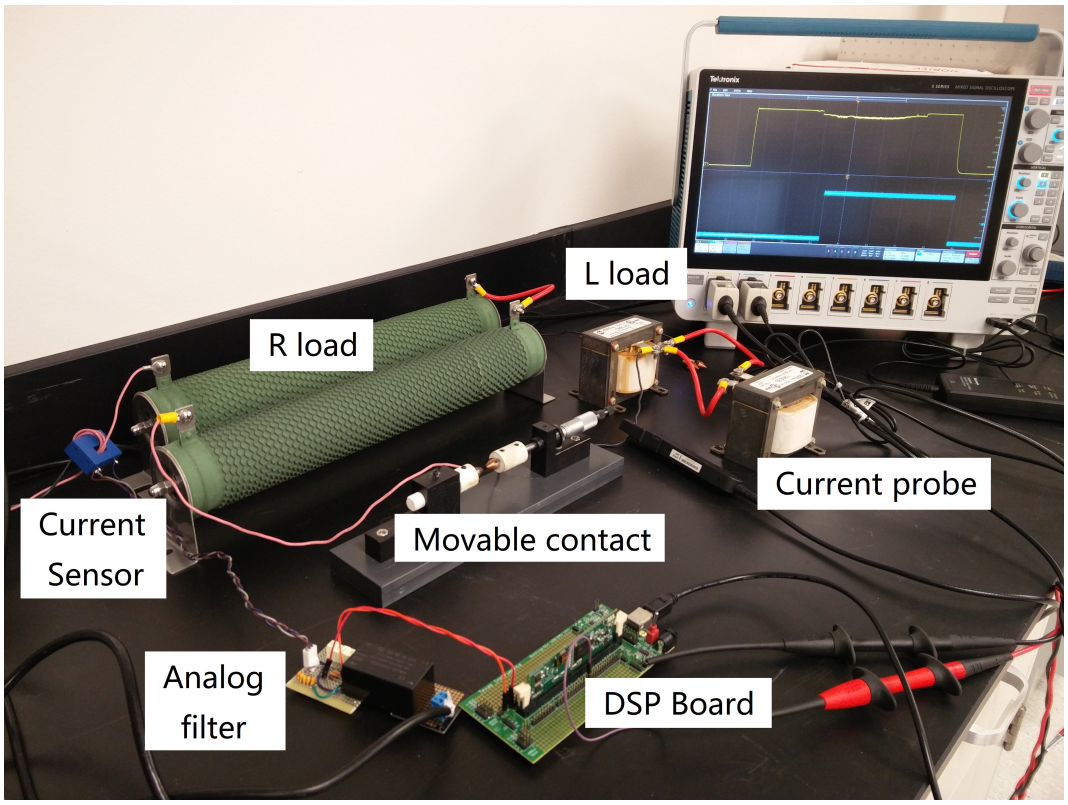

Figure 3.13: Lab setup.

frequency for the analog filter is designed to be less than 500Hz but greater than 300Hz, which is the highest frequency of interest in this application. A figure of the lab system is shown in Fig. 3.13. The setup consists of $375V_{dc}$ power supply, R_{load} of 94Ω and L_{load} of 0.5 mH. A coupled-inductor dc breaker, shown in Fig. 3.14 is being assembled and will be added in future to lab setup along with a parallel load to provide a step change in current.

A series arc is created with an air gap of 25 mil and the results are shown in Fig. 3.15. The bottom subplot is the current being monitored by the DSP and the top subplot is the output of the DSP that will serve as a flag and gate drive signal for thyristor $T2$. It can be seen that once the flag is raised, it opens the dc breaker hence isolating the load. During the experiment

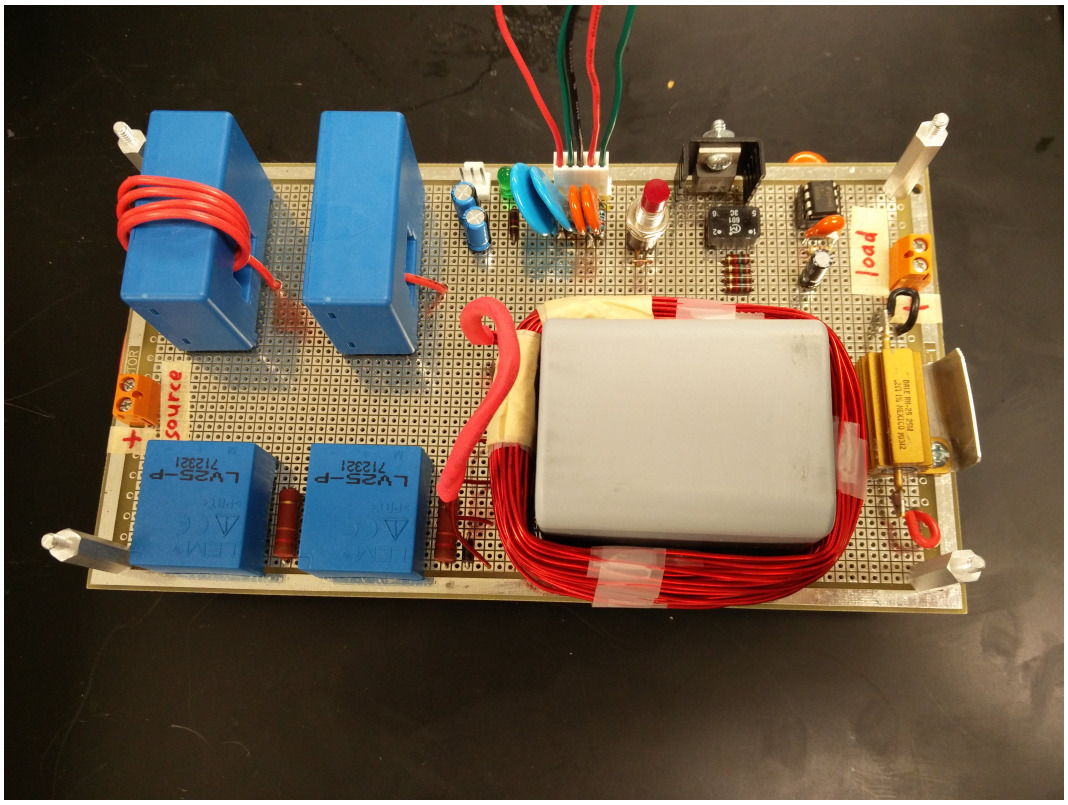

Figure 3.14: Coupled-inductor dc breaker.

it is observed that the DSP detects the noise in the current due to the contacts moving apart and allows the breaker to open before the arc is established. The flag remains raised till the system is shut down and the current drops to zero. Also it must be noted that the flag is not raised for the step change in current and the subsequent transients.

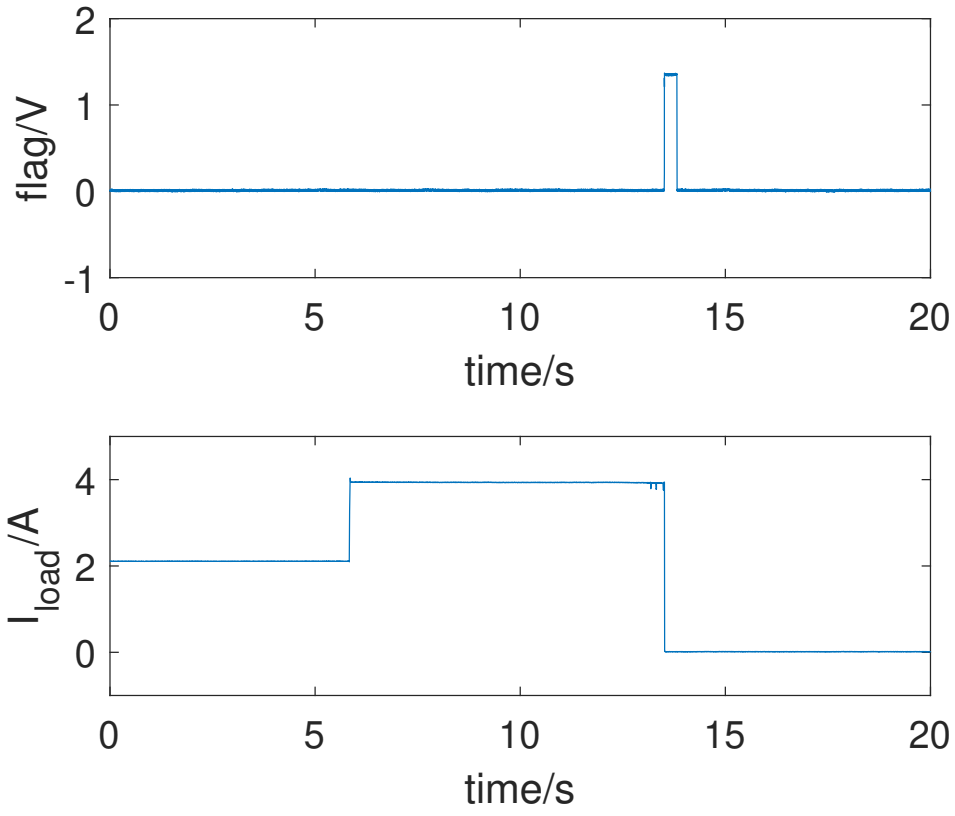

Figure 3.15: DSP implementation of arc detection.

3.4 Conclusion

This chapter proposes a comprehensive protection scheme for a dc load zone. A coupled-inductor dc breaker design is discussed and simulated to demonstrate its response to step changes in current and shunt faults. An arc detection method based on frequency content of sustained arc is proposed and implemented both on simulation and a low-voltage lab setup. A recursive DFT is used to implement a short-time Fourier transform successfully on a DSP and identify

the arc created by a series arcing device. A simulated system shows the effectiveness of the arc detection scheme with a coupled-inductor dc breaker.

Chapter 4

STFT-Based Event Detection and Classification for a coil gun load

Next generation loads, such as rail guns, laser weapon systems, air and missile defense radar, and more have pulsed waveforms that make these loads particularly demanding to the power delivery system. The pulsed waveforms of these technologies exhibit high current ramp rates in short periods of time. Contemporary DC breaker and protection systems will view a pulse load as a fault and initiate spurious fault protection actions. In this research, load monitoring techniques are explored to create a tool that can distinguish between a system fault and a typical pulsed load. The work herein focuses on the short-time Fourier transform (STFT) technique. A laboratory system is constructed which mimics a ship pulsed power zone through an electromagnetic gun. A noisy gate drive fault and a low impedance fault are introduced into the system in addition to the normal system operation. Simulation results and laboratory measurements indicate the STFT-based event classifier can correctly identify the faults.

4.1 System Description

The system being considered in this chapter is shown in Fig. 4.1. It is designed to model pulsed loads such as a rail gun on a Naval shipboard DC power system. Fig. 4.2 shows a low voltage lab setup used to generate and collect data for analysis and characterization in this chapter. In this setup a DC voltage source is connected to an electromagnetic coil gun through a controlled charging circuit. Table 4.1 shows some important design parameters for the lab setup. Keysight N8930A is used as the power supply for this setup. It is rated at 10kW (1000V / 30A), but is being used at 375V and 20A for this application. The internal impedance of the source as a function of frequency is unknown so it is lumped with the stray inductance from the DC bus and labeled as Z_S in Fig. 4.1. While Z_S is unknown, it can be estimated from the observed current profile and plays a significant role in defining the characteristic features of some events.

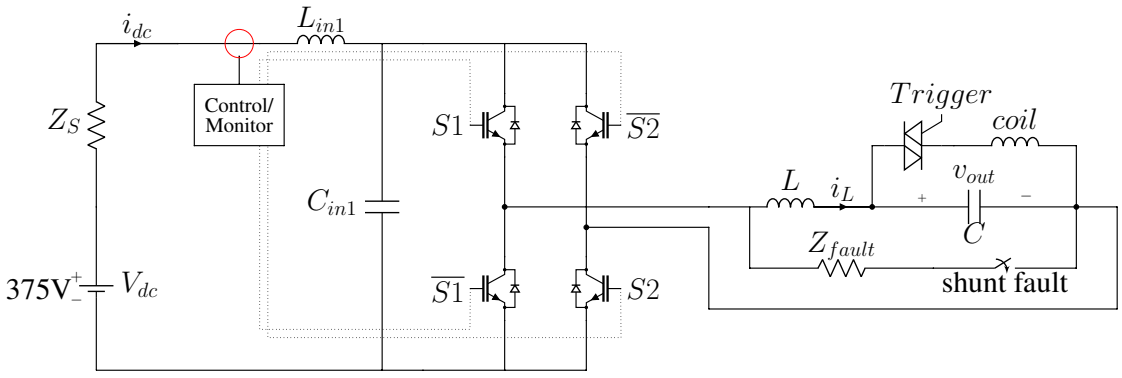

Figure 4.1: Pulsed load system.

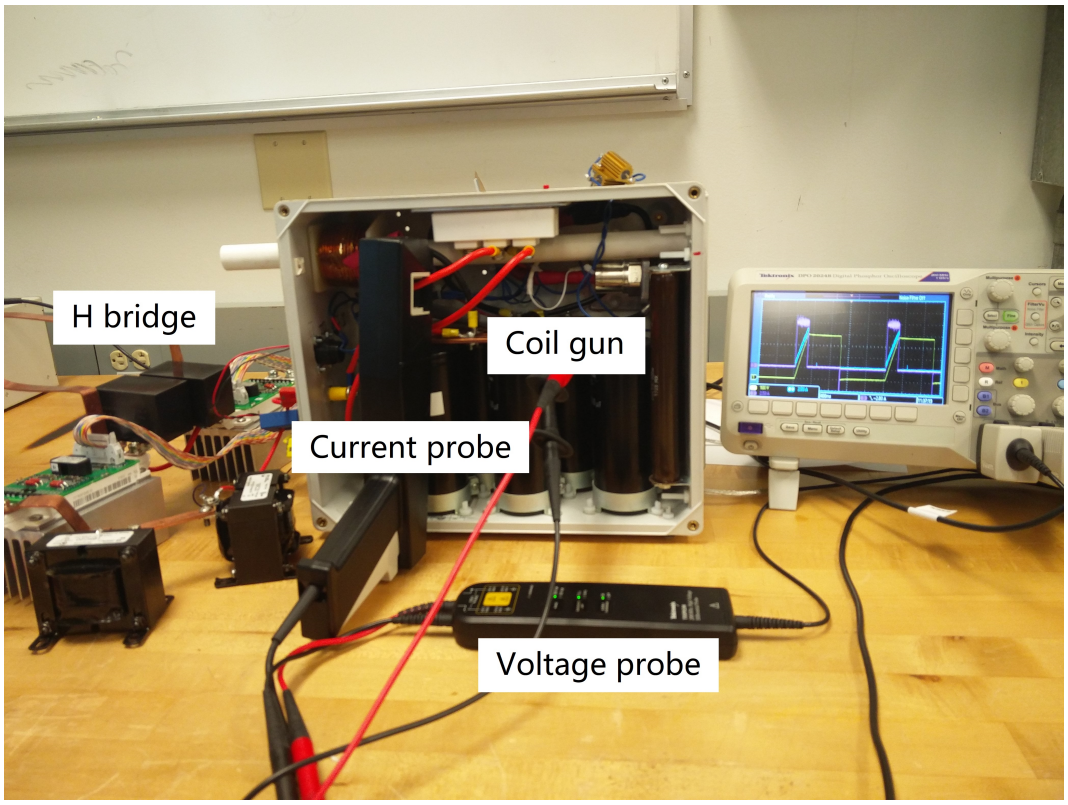

Figure 4.2: Lab setup for the pulsed load.

4.1.1 Electromagnetic coil gun and the starting circuit

The coil gun is assembled using a set of 6 electrolytic capacitors tied to a dc bus. For the gun to be ”armed”, the bus is charged up to 300V and then disconnected from the power supply. The ”firing” event occurs when the capacitors are discharged through an inductor coil wrapped around a non magnetic PVC pipe. A Silicon controlled rectifier (SCR) is used as the switch for discharge circuit because of its ability to handle large spikes of current. The SCR can be triggered manually through a push button or electronically through an interface drilled on the side of the enclosure. A projectile such as a steel bolt can be inserted into the pipe when the

Table 4.1: Coil Gun Design Parameters.

L_{in1}	C_{in1}	L	Z_{fault}	coil	C
$100\mu H$	$970\mu F$	$2mH$	15Ω	$80\mu H$	$7.05mF$

gun is armed. The large discharge current through the coil creates an electromagnetic force that would pull the magnetic projectile forward in the PVC pipe causing it to accelerate and launch out from the opposite side of the enclosure.

A starting circuit is assembled to interface between the coil gun and the DC power supply. The starting circuit charges the capacitors of the gun while maintaining a controlled charging current profile. The controlled charging current profile is later used to identify the process by the STFT-based detector. This circuit is also required in order to isolate the dc power supply from the coil gun once the gun has been armed and is ready to fire. As shown in Fig. 4.1 the starting circuit is essentially an H-bridge with the capacitor of the coil gun being its load in series with a large inductance to smooth out the charging current and make it easier to control.

At the center of the control circuit is the Texas Instrument Digital Signal Processor TI DSP 28335. It receives feedback from the current labelled i_L and the voltage labelled v_{out} in Fig. 4.1. For this particular application the DSP has been programmed to increase the charging current to the capacitors from 0 to 10A in 1ms and then continue charging at a constant 10A by adjusting the signals $S1$ and $S2$. The controller continues to charge the capacitor until v_{out} reaches 300V and at that point it shuts down all the gate signals to the H-bridge and the coil

gun is considered armed. Based on the design parameters of Table 4.1, the whole process takes around 180 ms. The DSP waits another 0.3s after the coil gun is armed before giving the trigger to the SCR that allows the capacitor to discharge and fire a loaded projectile.

Fig. 4.3 shows the load profile recorded for one instance of this operation on the lab setup. The top plot shows i_{dc} and bottom plot shows v_{out}. For the first 1 ms of charging, i_{dc} increases quite abruptly as the inductor current i_L goes from 0A to 10A during that period. Afterwards the inductor current is being controlled to stay constant so the input current i_{dc} appears to ramp up at the rate controlled by the values of coil gun capacitor C and charging inductor L. The capacitor voltage v_{out} is also ramping up at the same rate. Once v_{out} reaches 300V, i_{dc} can be seen falling sharply. During the firing event all the transistors in the H-bridge are turned off yet a small disturbance can be seen in i_{dc} at the time that v_{out} discharges to 0.

4.1.2 Faulty operations

The faults being created in the lab setup are carefully controlled so they may be easily replicated to determine the performance of the load monitoring system. Although there are several sources of electrical faults in a complex power electronic system, only two are being recreated here. The first fault type modeled is the noise on communication channels between the controller and the gate driver of the power electronics devices. Sources of this type of fault can be an unexpected bug in the programming device, a loose physical connection between electrical interfaces, or significant noise from other controlled loads on the line. Most commercial gate drivers have built in over current, over voltage and under voltage protection. These features are meant to

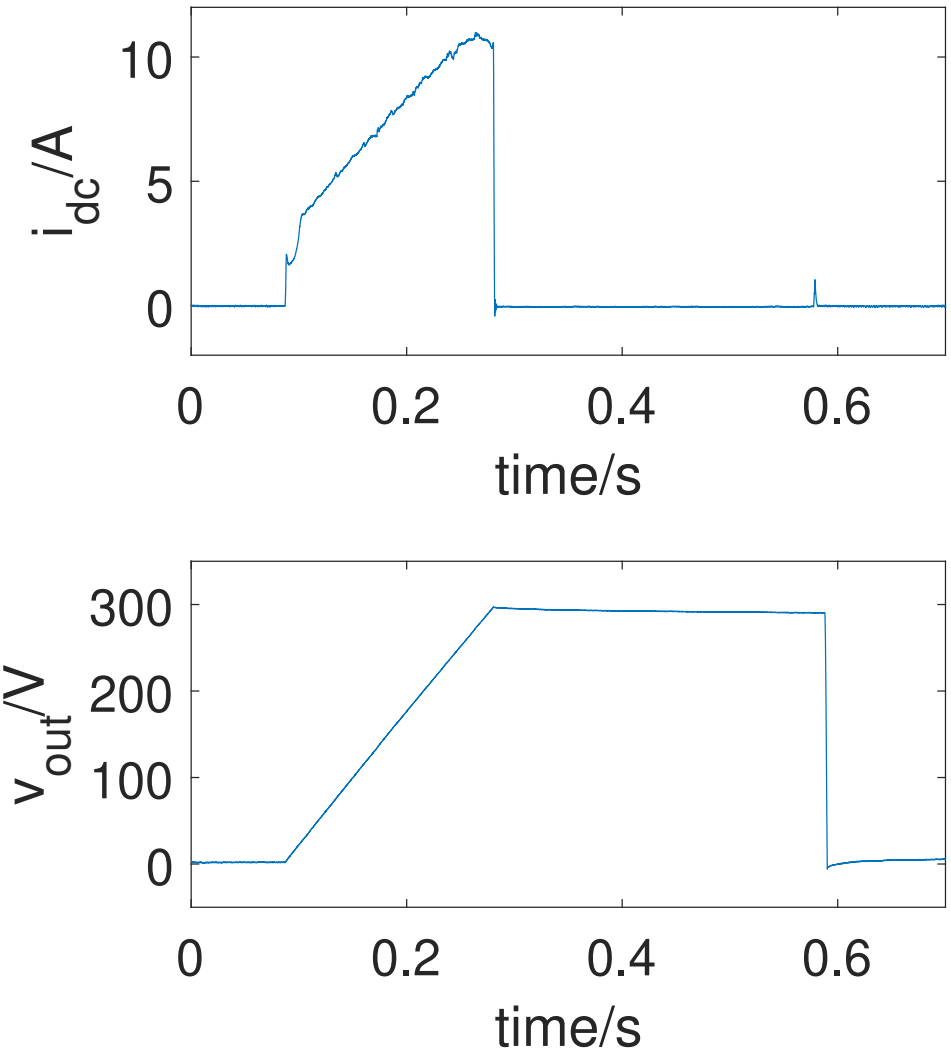

Figure 4.3: Load profile for normal operation.

protect the device from extreme operating conditions and would not react if for example some disturbance in the communication channel forces the signals to fall to zero at unexpected times. In this setup the DSP adds some random noise to the gate signal labeled as S_1 and $\overline{S}_1$ where the

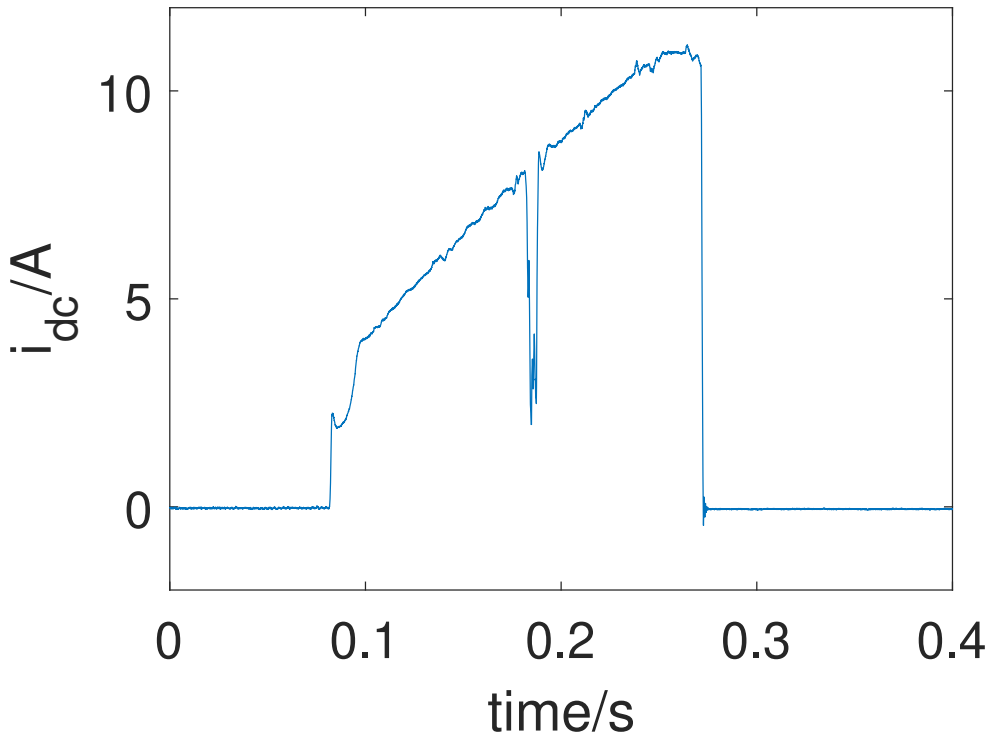

Figure 4.4: Load profile for noise on gate signal.

actual commanded signals gets intermittently overwritten by a 0 signal. This flickering noise stays for about 5 ms during a charging event. The effect of this kind of fault on i_{dc} is recorded on the lab setup and is shown in Fig. 4.4.

Another common source of fault in any electrical system is a shunt fault creating a large pulse of current. A source of this fault type is insulation breakdown and failure. Most protection relays are easily able to detect a large transient that exceeds a threshold or if the rate of change of current is too high. However this kind of detection becomes more challenging in a system where pulsed events are part of the normal operation. Further complications can happen if the fault impedance is significant and the transient current is not too much larger than the

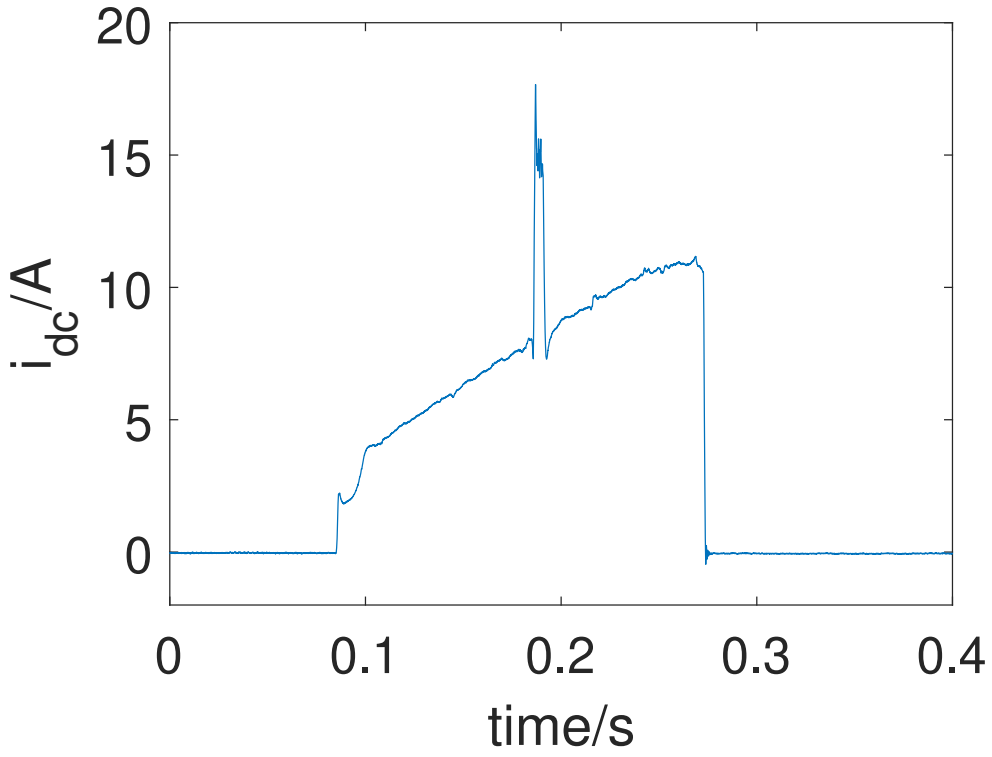

Figure 4.5: Load profile for a shunt fault.

pulsed current for normal operation. In this setup the shunt fault modeled is created in a more controlled manner. An IGBT is used as switch to add a fault impedance of 15 Ω into the system as shown in Fig. 4.1. Instead of giving a constant signal to the switch, an intermittent signal is used to mimic the flickering nature of a developing shunt fault. The fault is created for 5ms during the charging event and the current i_{dc} is recorded and shown in Fig. 4.5.

4.2 Time-Frequency Analysis

From the load profile and the system description it can be observed that this system could have faults which would be difficult to distinguish from normal operation based on an edge detection or $\frac{di}{dt}$ approach. It is therefore prudent to look at the frequency content of the load profile and use that to identify features characterizing the operation. Wavelet transforms and STFT could both be used for this purpose. Wavelet transforms provide the relative power in different frequency bands while STFT calculates the power at discrete points along the frequency spectrum with respect to time. For this application STFT would be the preferred method due to ease of implementation.

4.2.1 Selection of STFT parameters

STFT involves taking the Fourier transform of N number of discrete time domain signals sampled at frequency F_s. The result of that provides the frequency content of $N/2$ discrete frequency components within that signal equally spaced from $0\ Hz$ to $F_s/2$ Hz. One iteration of the STFT will provide this frequency content within a time domain window of N/F_s. The next iteration can be performed by sliding this time domain window by a k multiple of sample time $1/F_s$.

First it is important to determine the appropriate window size and the frequencies of interest in order to select the proper parameters N, k and F_s for this application. Consider a zoomed in view, shown in Fig. 4.6 of the falling edge of i_{dc} during one instance of normal

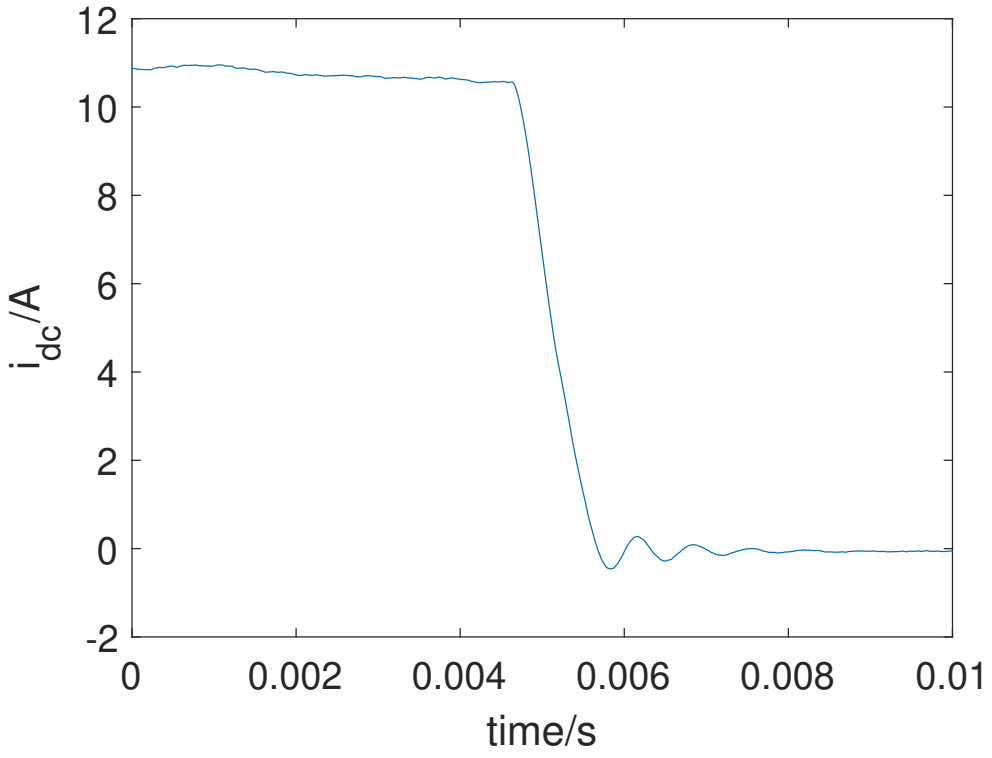

Figure 4.6: Falling edge of the load current i_{dc}.

operation. The falling time for this edge is about 1ms and is followed by ringing at around 1.5kHz frequency. The window size must therefore be greater than 1 ms to capture this transient and F_s must be greater than at least 3kHz using Nyquist principle. Also note from Fig. 4.3 that the ramp time for current is 180 ms so the window size must be significantly smaller than 180 ms so that the ramp itself does not appear like a transient. Further it must be considered that the window size should be larger enough where even a slow developing fault with rise time of several ms should be able to fit in that window and appear like a sudden change in current. A window size of 4ms was selected under the above constraints.

Several combinations of N and F_s could provide this window size. Here the con-

straint of the processing time of the microcontroller must be taken into account. Ideally a high sampling frequency would be better for detecting transients quickly and having a larger range of frequencies. For the same reason the overlap variable k is selected to be 1. In this set up the switching frequency of the power electronics devices is 25kHz so it would be desirable to have sampling frequency in the same range. However high frequency means high value of N for a given value of window size which significantly increases the processing time. A compromise is then made to have F_s as 10kHz and corresponding N to be 40. The frequency spectrum would then consists of frequencies from 0 to 5kHz at uniform intervals of 250Hz.

A load profile with fault similar to Fig. 4.5 is then run on the lab system and the current is recorded. Matlab STFT analysis with parameters selected above is performed on the data and result is shown as a spectrogram in Fig. 4.7. This data is further analyzed in the next section to determine identifying feature of this current profile based on the frequency spectrum.

4.3 Load monitoring scheme

4.3.1 Event detection

In the frequency spectrum from Fig.4.7 it can be seen that the fault as well as the other abrupt changes in current cause a significant shift of power across the frequency spectrum. On closer inspection it is noted that the effect of the fault and the falling edge of the current is significantly more well defined for higher frequencies i.e greater than 4kHz probably due to its faster rate of transition. Fig. 4.8 shows the sum of power from frequencies 3.75kHz to 4.75kHz as a function

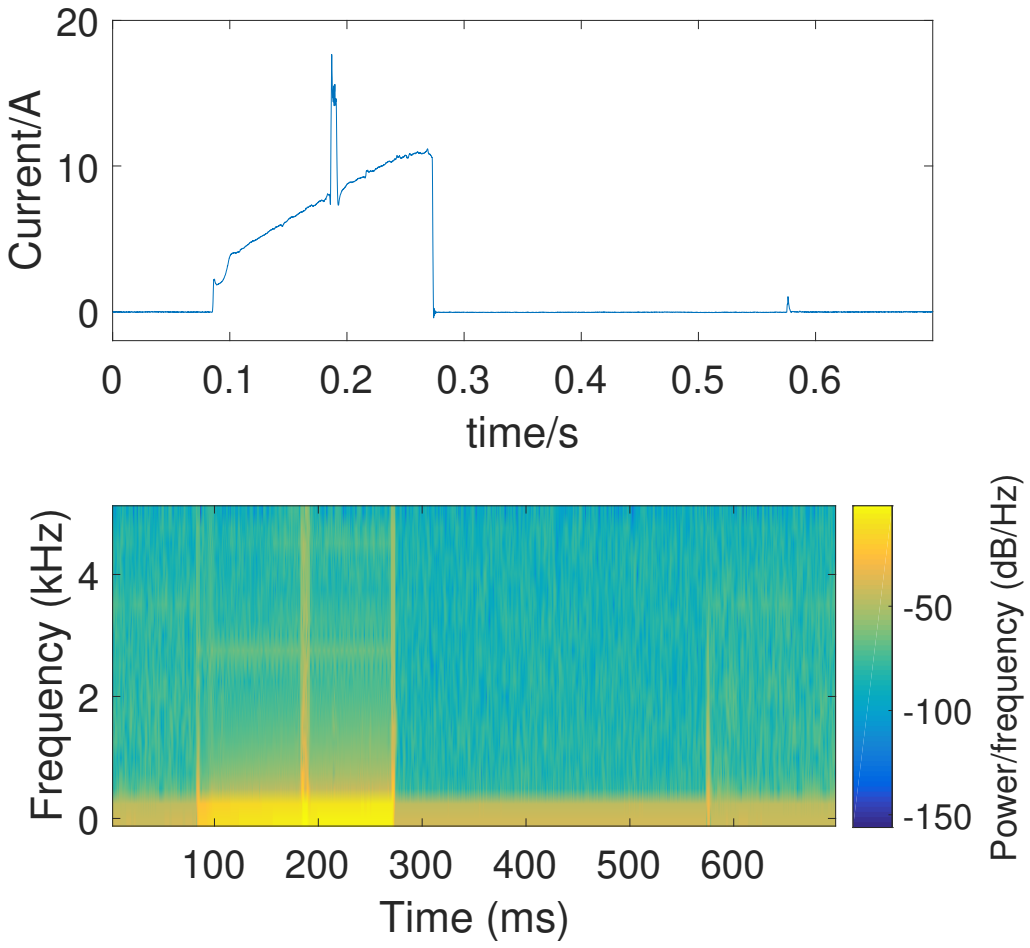

Figure 4.7: Frequency spectrum as a function of time for measured lab data.

of time calculated by Matlab for the same load profile as Fig. 4.7. In this load monitoring scheme it is not desired to consider the small abrupt change of current at the start of charging and the small disturbance in current caused by discharge of capacitor as ”events”. Power in frequency band 3.75kHz to 4.75kHz will be denoted as P_h. If P_h exceeds a threshold T_h then the disturbance will be considered as an event. Based on Fig. 4.8 0.7 is a reasonable value for

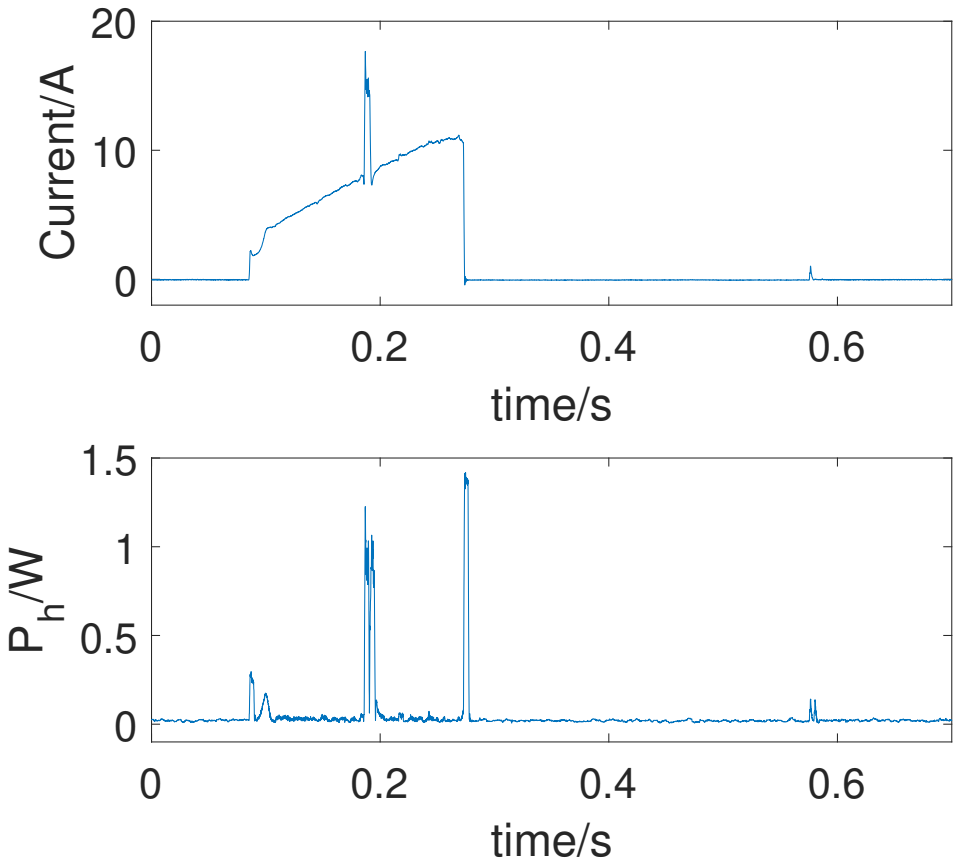

Figure 4.8: Power in higher frequency band as a function of time

T_h.

4.3.2 Steady state frequency feature

The abrupt change of current at the start of charging is not considered an event however it is important for any load monitoring in this application to know when the charging begins. As stated earlier the current is being controlled through a feedback loop on a DSP to maintain the

current within strict limits. Furthermore because the window size is small compared to the ramp rate of the current profile, the current within a sample window can be approximated to a constant. As a result a large percentage of power is in lower frequencies close to DC. This approximation cannot be made when there is no current flowing. During this period the current has low power in all frequencies so as a percentage it is not as significant. This effect can be seen in Fig. 4.7, but is more prominently shown in Fig. 4.9. Here the bottom subplot shows the percentage of power in frequencies 250Hz and below over the course of a charging operation with fault. This percentage of power will be denoted as P_l. If P_l is above a threshold T_l the current will be considered in "ramping" state. Based on Fig.4.9 value of T_l is selected as 0.88.

4.3.3 Fault identification

Faults of the nature discussed in this chapter will always be identified as an event at the time they occur due to their large transient current. However during the fault state each iteration of the fault could potentially be different depending on the duration of fault state, fault impedance, the frequency of flickering etc. A fault can occur with unique frequency characteristics that vary from other faults of the same type, and therefore a better to identify faulty behavior is to completely characterize the normal operation and identify the desirable events. Deviations from normal characterized behavior are then flagged as faults warranting further investigation.

In this setup the only desirable event is the falling edge of i_{dc}. As shown in Fig. 4.6 the falling edge is followed by resonance at 1.5kHz. This frequency is determined by the internal impedance of the source resonating with the stray inductance, L_{in1} and C_{in1}. Fig. 4.10 shows the power in frequency 1.5kHz as a percentage of power in other frequencies during

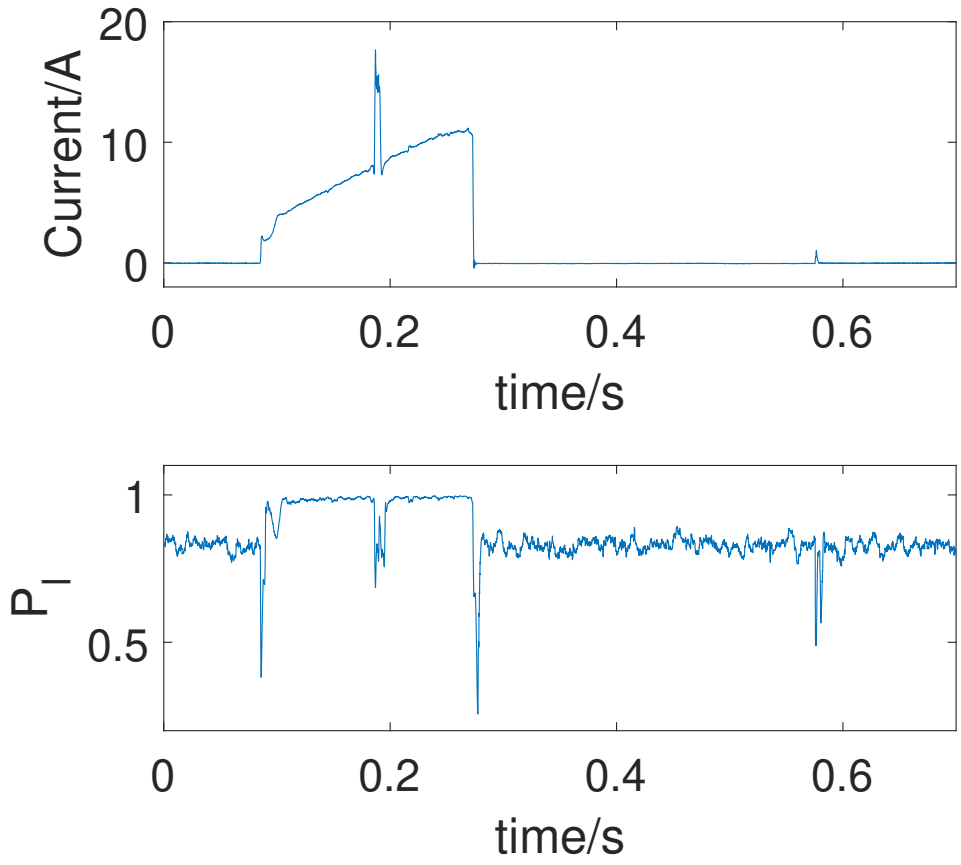

Figure 4.9: Percentage of power in low frequencies

two faulty iterations of charging current profiles. P_r will denote the percentage of power in resonance frequency of 1.5kHz, and if it exceeds the threshold value of T_r the event can be classified as a "disconnect" with confidence. From Fig. 4.10, the threshold T_r is selected as 0.03. Theoretically it is possible that a fault may also be followed by a resonance in 1.5kHz but is very unlikely keeping in mind the location and sources of faults being considered in this chapter.

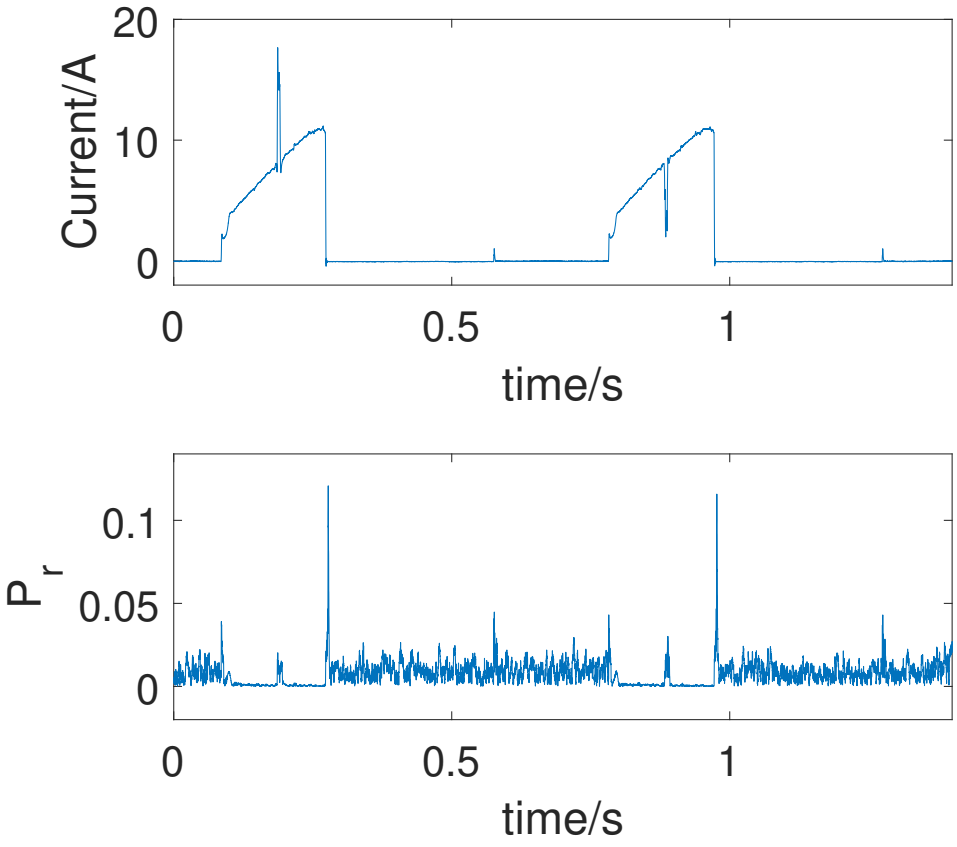

Figure 4.10: Percentage of power in resonance frequency

4.3.4 Load monitoring algorithm

A summary of the STFT scheme variables is provided in Table 4.2. Based on these parameters a flow chart describing the decisions and states involved in the proposed load monitoring scheme for this coil gun is shown in Fig.4.11. There are two internal counters C1 and C2 which get updated as a way to keep track of consistent behavior. The counters are allowed to run to certain values before any flags are raised. Keeping these values high could lead to slow response but

high reliability while keeping them too low could lead to an oversensitive system but quick response. There are also four variables; 'ramp', 'event', 'disconnect' and 'fault', defined in the previous section that are being constantly updated to provide the state of the system.

Table 4.2: Load monitoring STFT parameters

N	F_S	k	T_h	T_l	T_r
40	10 kHz	1	0.7	0.88	0.03

4.4 Implementation and Results

With the STFT parameters selected in Table 3.2, the DSP f28335 would be required to perform STFT on a new set of data every 100 μ s. This time is not enough if the inbuilt FFT function is used on a sample size of N. Therefore a faster method of STFT known as recursive Discrete Fourier Transform (recursive DFT) is applied. In this method one new element is added to the window while one sample is removed from the window and the updated set of STFT is calculated as a function of these two elements. It is an efficient way to perform STFT and brings the computation time lower than 100 μs so that the desired F_s of 10kHz can be used. In addition, for real signals the magnitude of the first $N/2$ elements of the STFT is the same as

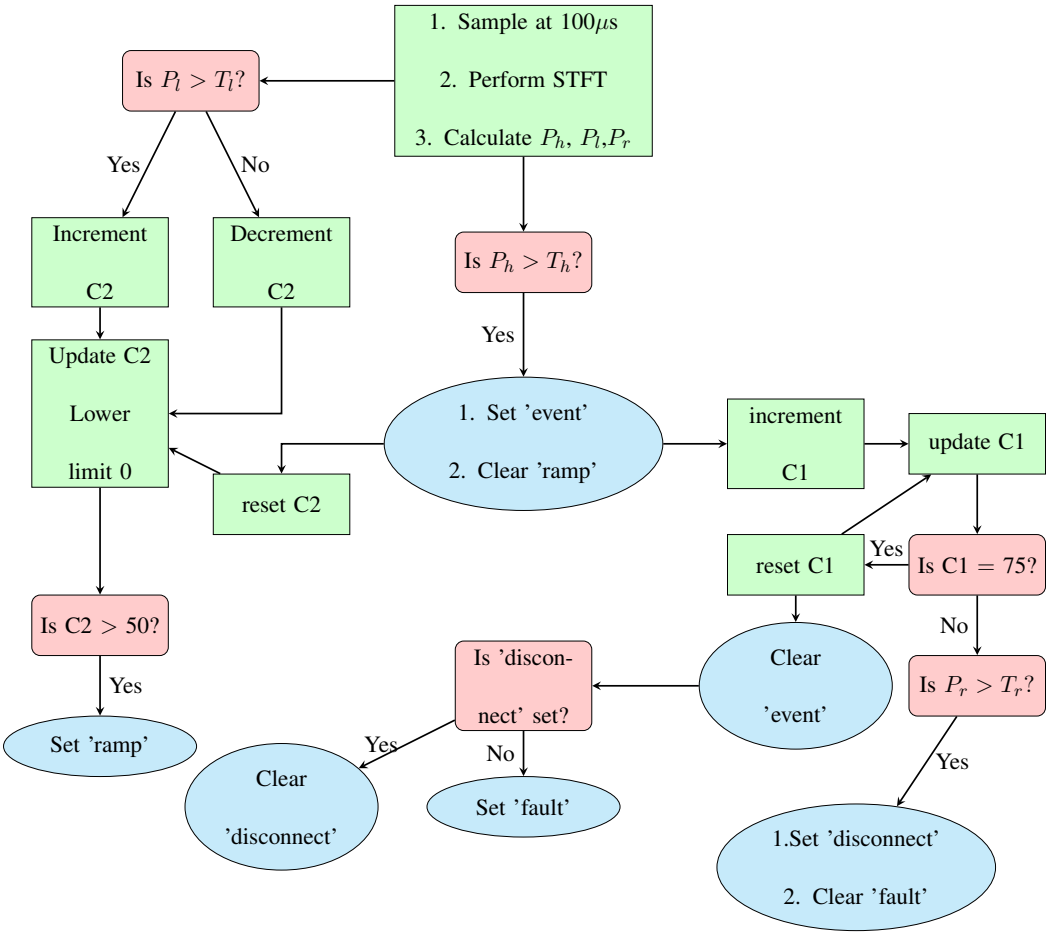

Figure 4.11: Load monitoring scheme.

last $N/2$ elements so only the first $N/2$ are calculated which further decreases the computation time by half.

The current signal can contain power in frequencies greater than $F_s/2$ which will cause aliasing and distort the frequency content in lower frequencies. An anti-aliasing analog filter is designed to process the current data before sampling by the DSP. The cut off frequency for the analog filter was designed to 5000Hz. The coil gun is operated 20 times in a row to collect a larger data set on which to test the algorithm performance. The DSP is programmed using the embedded coder support package on Matlab Simulink. The measured data is imported to Simulink as well and downsampled to match the designed F_s.

The top subplot in Fig. 4.12 shows the output of the LEM sensor recording i_{dc} after the anti-aliasing filter. The output voltage is in the range 0-3 V which is the operating limit of DSP. There are 20 iterations of the operation, where the coil gun is fired after every 0.7 s. The 6th and 12th iteration of the operation contains a shunt fault and noisy gate signal fault respectively. All four state variables obtained as boolean outputs from the DSP program are also shown in Fig. 4.12. It can be seen that the program is monitoring the load correctly. The ramp output is high every time during charging except during fault conditions. The program is able to detect every time the charging circuit disconnect the coil gun from the DC supply. It is interesting to note the rising and falling edge of each fault is identified as a separate event. This is because the duration of fault is greater than the window size. Each event that is not a disconnect is identified as fault.

Finally the program is tested on-site with the experimental setup in real time. As shown in Fig. 4.13, three firing operations are programmed. The first one is normal followed by two

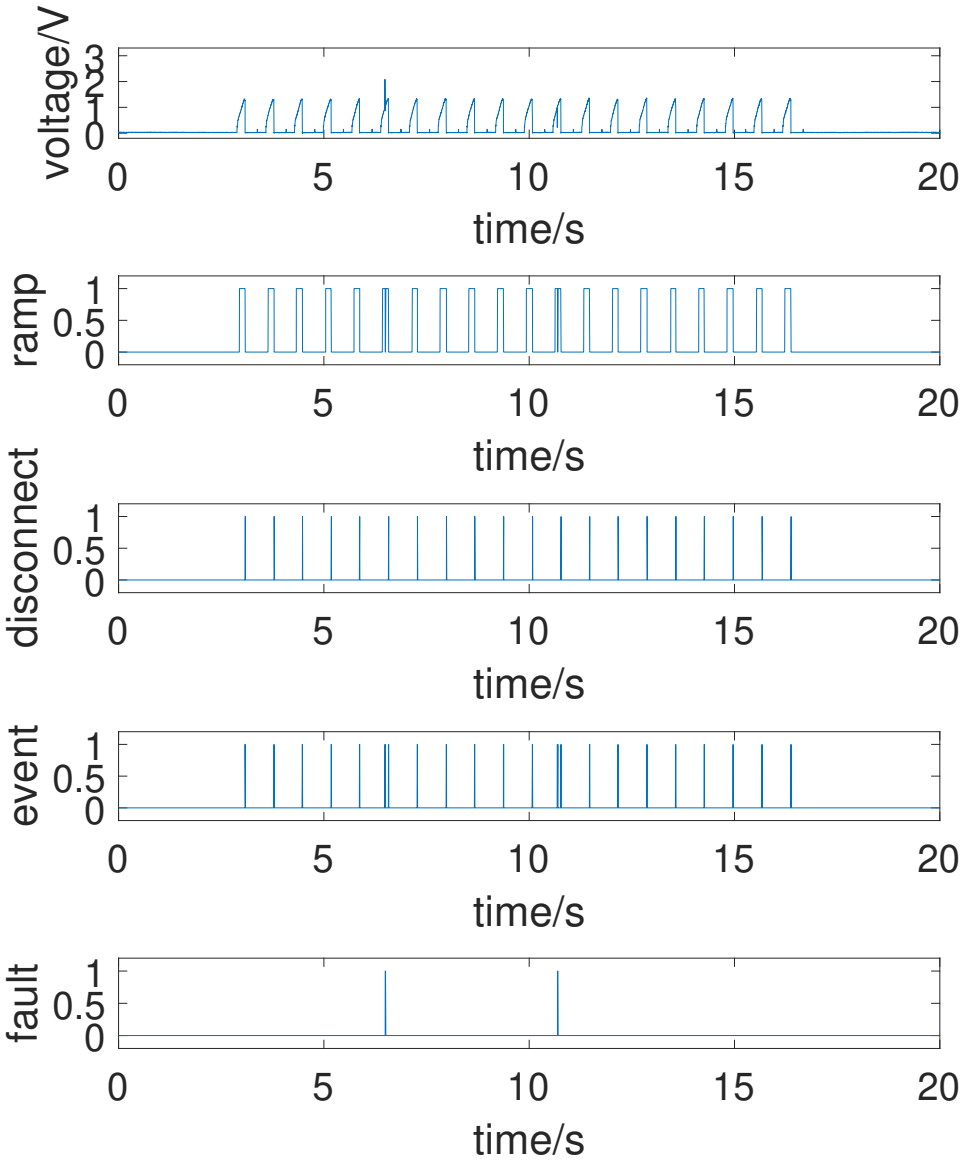

Figure 4.12: Result of the load monitoring program.

faulty operations. The top three subplots show system variables and the bottom four are the flags raised by the DSP. It can be seen that with the thresholds from Table 3.2 programmed into the DSP, it is able to detect both the fault events.

4.5 Conclusion

A low voltage electromagnetic coil gun was assembled to model pulsed load on an electric ship. Normal operation of the charging and discharging of the coil gun was presented along with some common scenarios of faults. Faults are created in this setup in a controlled and repeatable manner. A load monitoring scheme was proposed that relies not just on the instant values or rate of change of current but the frequency content of the load profile. The load monitoring scheme was very specific to the system being tested. Measured data from an actual system was analyzed to identify key features that can be used for characterization. Eventually the scheme was programmed on a DSP providing NILM and tested successfully on multiple iterations of the load profile with faults and desirable transient events correctly identified.

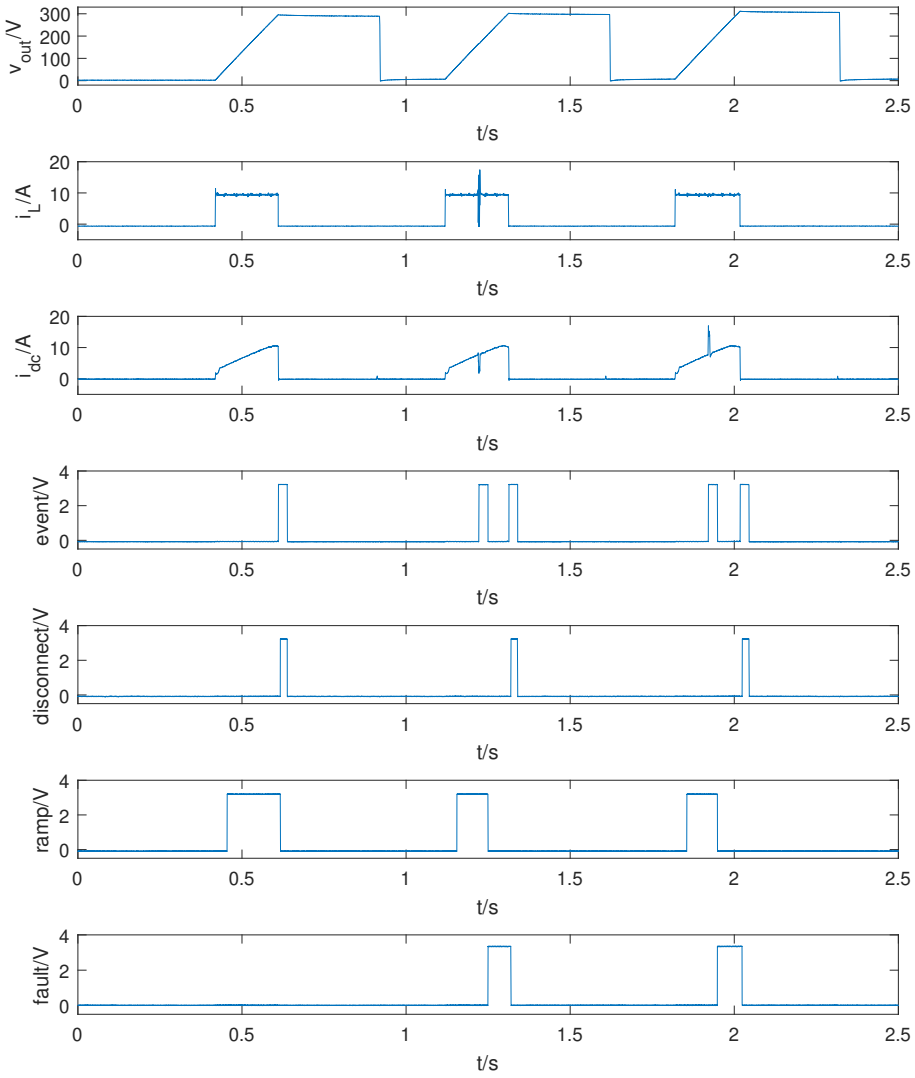

Figure 4.13: Result from the experimental setup.

Part III

Proposed load monitoring and fault detection scheme for general dc pulsed load

Chapter 5

STFT Cluster Analysis for Dc Pulsed Load Monitoring and Fault Detection on Naval Shipboard Power Systems

5.1 Theoretical background

The crux of the load monitoring scheme relies on the concept of the Fourier transform, i.e any signal in time domain can be represented by an unique combination of signals in frequency domain. If the the underlying physical process for creating the time domain signal does not vary significantly over multiple cycles of operation then the frequency domain signal would also stay the same, hence providing a means for identifying and characterizing that particular time domain signal.

The Fourier transform is an invaluable theoretical concept applicable on continuous time signals of infinite length. Most signals encountered in real life, including the load profile

of dc loads considered herein, are discrete time signals of finite length. Applying a discrete fourier transform (DFT) on an entire time signal would provide its frequency information but to see how the frequency information changes over time it is desirable to apply DFT on small windows of the original signal. This technique of extracting discrete frequency information in real time is known as short-time Fourier transform (STFT) and can be mathematically expressed as:

$$X[k] = \sum_{n=0}^{N-1} W[n]x[n]e^{\frac{-j2\pi nk}{N}} \tag{5.1}$$

In (5.1), $W[n]$ is the windowing function that is non zero only for $n = 0$ to $n = N-1$. $x[n]$ is the discrete time signal and $X[k]$ is the k^{th} harmonic of the resulting STFT. For window function of length N, the allowed values of k are $k = 0$ to $k = N - 1$. It can be seen that each instance of applying STFT yields an array of complex numbers of length N. The next instance of STFT can be applied by shifting the window function by an integer multiple of sample time. Let F_s denote the sampling frequency then consider a case where window function is shifted by N samples. In this case there is no overlap between data in successive windows and STFT is applied every $\frac{N}{F_s}$ seconds. However for highest precision in time, it is ideal that window only be shifted by 1 sample, there would be maximum overlap between data in successive windows but STFT would be performed every $\frac{1}{F_s}$ seconds.

Applying STFT every $\frac{1}{F_s}$ seconds can be computationally excessive for real time calculation. If the windowing function $W[n]$ is selected to be a rectangular function then equation (5.1) can be further simplified using a tool known as recursive DFT. With a rectangular win-

dowing function equation (5.1) can be written as:

$$X_n[k] = \sum_{l=n}^{n-(N-1)} x[l] e^{\frac{-j2\pi(n-l)k}{N}} \tag{5.2}$$

In (5.2) $X_n[k]$ is the k^{th} harmonic of the n^{th} window. In the previous window, the same harmonic would have been calculated as:

$$X_{n-1}[k] = \sum_{l=n-1}^{n-1-(N-1)} x[l] e^{\frac{-j2\pi(n-1-l)k}{N}} \tag{5.3}$$

Multiplying both sides of (5.3) with $e^{\frac{j2\pi k}{N}}$:

$$e^{\frac{j2\pi k}{N}} X_{n-1}[k] = \sum_{l=n-1}^{n-1-(N-1)} x[l] e^{\frac{-j2\pi(n-l)k}{N}} \tag{5.4}$$

The summation term in (5.4) can be rearranged to be similar to (5.2). Consequently, a substitution can be made which leads to a recursive expression for $X_n[k]$.

$$\begin{aligned} e^{\frac{j2\pi k}{N}} X_{n-1}[k] = & \sum_{l=n}^{n-(N-1)} x[l] e^{\frac{-j2\pi(n-l)k}{N}} \\ & + e^{\frac{j2\pi k}{N}} (x[n-1-(N-1)] - x[n]) \end{aligned} \tag{5.5}$$

$$e^{\frac{j2\pi k}{N}} X_{n-1}[k] = X_n[k] + e^{\frac{j2\pi k}{N}} (x[n-N] - x[n]) \tag{5.6}$$

$$X_n[k] = e^{\frac{j2\pi k}{N}} (X_{n-1}[k] - x[n-N] + x[n]) \tag{5.7}$$

Equation (5.7) reduces $X_n[k]$ to be a function of only its previous value, the new data point entering the window, $x[n]$, and the last data point leaving the window, $x[n-N]$. Equation (5.7) requires initialization for $X_0[k]$ and that can be provided as $X_0[k] = 0 \; \forall k$, which is valid if the system is starting from rest.

5.2 Feature Extraction

After every time step $\frac{1}{F_s}$, (5.7) can be used to calculate an array of length N. Each element in that array is a complex number but only the magnitude is of interest in a dc system where only the current profile is being analyzed. In the magnitude array at the n^{th} time step, the value at $k = 0$ denotes the average dc value of the data in the window. Therefore $||X_n[0]|| - ||X_{n-N}[0]||$ can indicate if the current is generally increasing or decreasing. This direction information is one of the extracted features.

In the magnitude array, $||X_n[k]||$, the values from $k = 1$ to $k = \frac{N}{2}$ correspond to frequency components from $\frac{F_s}{N}$ to $\frac{F_s}{2}$. Based on the Nyquist theorem, only the values for $k = 1$ to $k = \frac{N}{2}$ are useful and stored as features. The dc average or $||X_n[0]||$ is not stored as a feature because the load monitoring should be able to identify a transient feature regardless of the base dc value.

5.3 Event Detection

While the features are calculated every $\frac{1}{F_s}$ seconds, they only need to be stored or categorized every time an event happens. Each operating cycle may contain multiple events depending how the user chooses to define some important parameters such as event threshold and window size. A typical time domain method to detect an event would involve calculating $\frac{di}{dt}$ at every time step and setting a threshold based on that. However this method would be difficult for transients which are much slower than the sampling frequency. In this scheme a time-frequency method is

preferred which involves looking at the spectrogram of a normal operating cycle of the load and identifying surge points in a particular harmonic region. Thresholds can be predefined based on that and used to trigger an event flag.

It must be noted that using time-frequency methods allow event detection to be controlled by selecting an appropriate window size. Slower developing transients may not look like an event with a small window size and by selecting a small window size several events can be defined within a single transient. A window size is equal to $\frac{N}{F_s}$ seconds so for a fixed sampling frequency, a smaller N would mean fewer features to characterize the event however if N is too large that would make the computation process long and inefficient. Selecting these parameters is the most critical part of the pre processing involved in this load monitoring scheme. An accurate simulation model or data previously collected could help the engineer examine the load profile and make informed decisions based on the limitations of the processor and the expected current waveform.

5.4 Clustering Mode

There are two modes of operation in the scheme, a clustering mode followed by a classification mode. Every time an event is detected, an array of features is extracted from the raw data. During clustering mode the extracted features are stored in a cluster based on a predefined event-sequence-array (ESA). ESA contains the labels of the respective events in the order they are expected to happen. It is expected that the engineer knows the sequence in which the event will be happening during the clustering mode and that there will be no fault events happening

during that time. The processor must be provided ESA before clustering can begin.

ESA will also be used to declare the memory size allocated to data storage. The length of ESA will determine the total number of events while number of unique labels in ESA determines the first dimension of clustered data. Within each dimension or label there will be a matrix of data stored that can be thought of as a 2D cluster. Each row in that matrix corresponds to an instance of event with that label and the columns contain the value of each of the $\frac{N}{2}$ features including a number to represent the direction feature.

At the end of the clustering mode, marked by the last event in ESA, the processor will calculate the minimum value, maximum value, mean and standard deviation of each column in the cluster data. Using these metrics the processor should be able to characterize each feature for each labeled event.A flow diagram that summarizes the process of clustering mode is shown in Fig. 5.1.

5.5 Classification Mode

Theoretically each time an event happens the feature array extracted should be identical. However in real system it is almost never observed. There are several factors including small synchronization errors, sampling errors, gaussian noise, instrumentation errors, changes in temperature and component degradation that may contribute to small variations in each observed feature vector even if it is for the same event. When an event happens during the classification mode, the task of the processor is to find the closest match between the observed feature vector

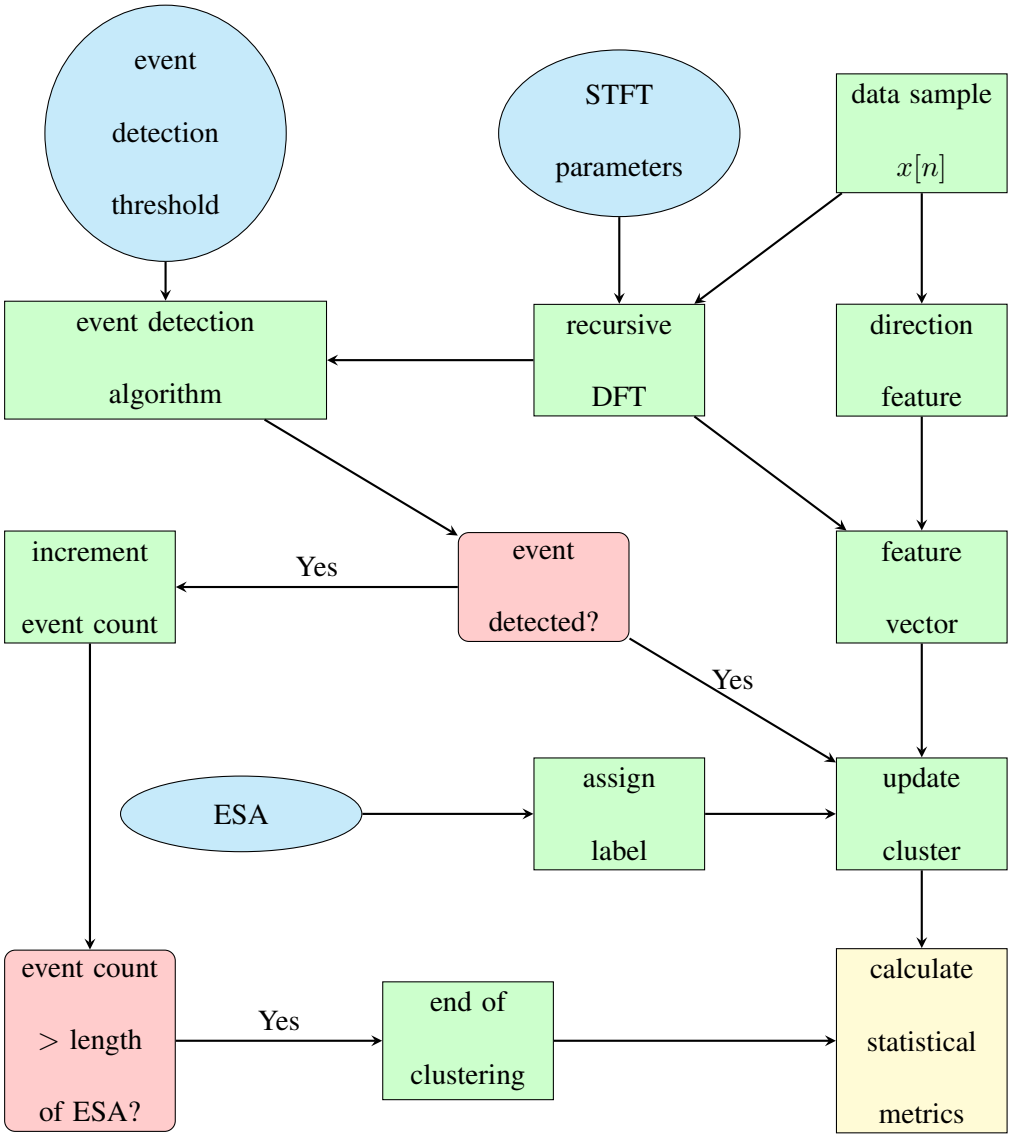

Figure 5.1: Clustering mode flow diagram

and the feature stored in clusters during the clustering mode.

A typical nearest neighbor approach would calculate the distance from mean for each feature in the cluster and the observed feature. This approach would work but is inefficient for cases where there is little or no overlap between values of features from different event labels. A more efficient way to perform classification is proposed in this scheme as a two-level approach. The first level is to populate a boolean match matrix. If the observed feature value is no more than a fraction of standard deviation outside the observed minimum and maximum of the value of the same feature for a given event label it is considered a true for match. This match matrix can be quickly populated without calculating the actual distance from the mean of the clusters. If there is one event with number of matches at least 25% more than the second closest event, the observed event is labeled as that event.

In case there are more than one events with number of matches within 25% of each other then the second level can be employed to determine the label. In this level the distance from mean is calculated, in terms of standard deviations, only for the observed features that do not match the corresponding recorded feature within an event label cluster. The event with the minimum distance is then assigned to be the label for observed event.

5.6 Event Based Fault Detection

A shunt fault on the load profile is likely to create a surge or disturbance that can trigger an event. The approach outlined above would label each event to its closest match however the desired outcome in this case would be for the event to be labeled as a fault. It is not possible

to train the algorithm on faults because each shunt fault would look different and is difficult to predict the possible fault impedance. Furthermore training on fault could cause lasting damage to sensitive equipment.

The event classification mode is slightly modified to accommodate for shunt fault detection. It is expected that even if the $\frac{di}{dt}$ or peak surge value of the fault transient is similar to the normal events it's frequency content will be different. A condition is added to the match matrix approach that if the observed event fails to match with any event cluster on more than $\frac{N}{2} - J$ features then it will be labeled as a fault. The choice of J is determined by the confidence on the recorded cluster and the desired sensitivity of the system. A small value of J may lead to any event that deviates slightly from those recorded during clustering mode to be identified as fault. A large J on other hand may lead to faults being misidentified as one of the events so it is a design choice for the programmer.

5.7 Series Arcing Fault Detection

Unlike shunt arcing fault, the series arcing fault is unlikely to trigger an event unless the event threshold is really low. What makes a series arcing fault a challenge to detect is that the average value of sustained arc current is often the same or slightly less than normal current. Event based detection will not identify arcing fault or a high impedance shunt fault. However, unlike shunt faults, the effect of arcing on the dc current can be predicted and identified using time-frequency characteristics.

Figure 5.2 shows the arc generation device used in the lab to generate and record

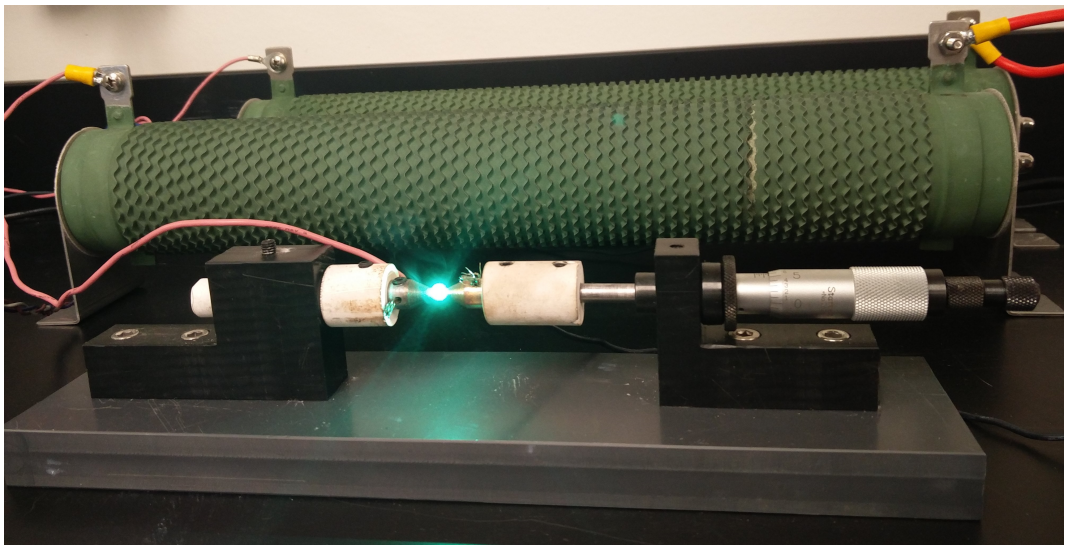

Figure 5.2: Series arc generation device.

sustained arcing current for analysis. The analysis was done using several different air gaps ranging from 50 mil to 400 mil, several line inductance values from 0.5mH to 4mH, and at several dc values of current up to 7 A. The fast Fourier transform (FFT) of a typical sustained arcing current compared to normal current is shown in Fig. 5.3. The most significant feature seen here is the additional power in the arcing current in the range from 20Hz to about 100Hz.

The series arcing detection scheme takes advantage of this characteristic behaviour of the sustained arcing current. During clustering mode the sum of the values of features $||X_n[k]||$ for k corresponding to frequencies under 100Hz is saved; except during transients. Let this new feature denoted as X_l calculated at every time step of $\frac{1}{F_s}$ seconds. During the classification mode if the absolute value of $||X_{n-N}[0]|| - ||X_n[0]||$ is less than a threshold while X_l exceeds its average value from clustering mode by 500% then the algorithm will raise a flag to indicate series arcing fault. Additionally this method would also help to identify 60Hz noise interference

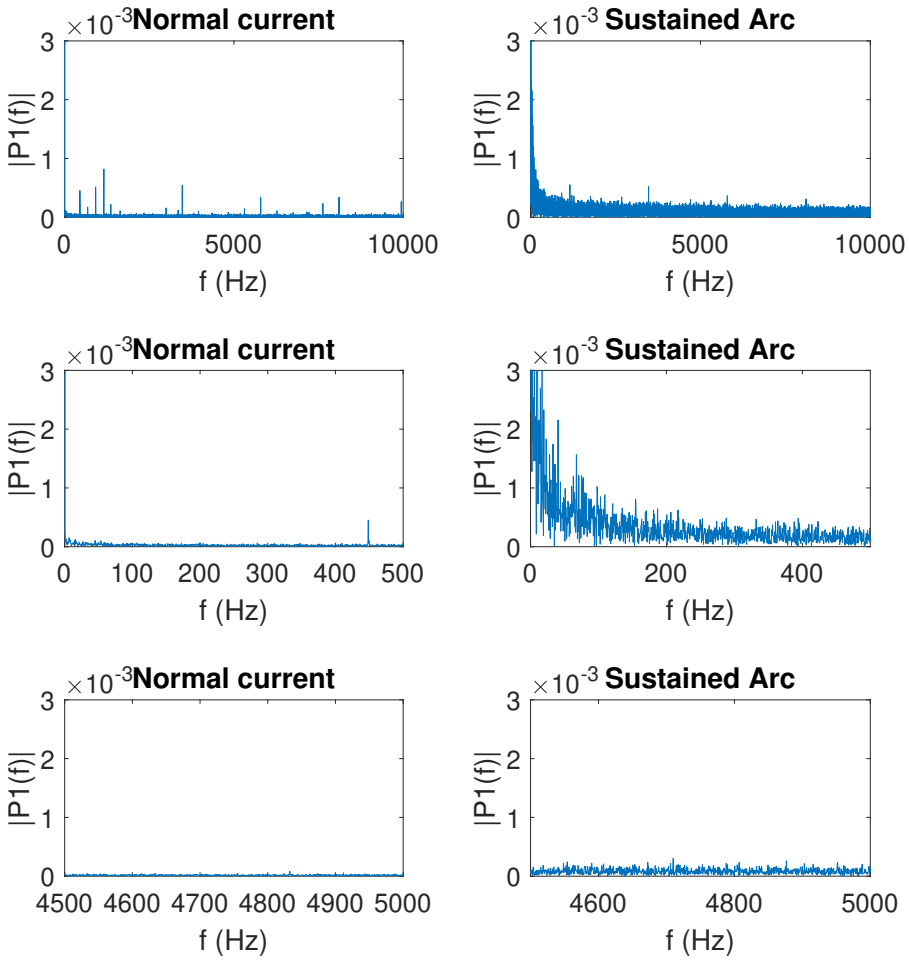

Figure 5.3: FFT analysis of current under normal operation and series arcing

from ac sources. The process of fault detection combined with classification mode of load monitoring is illustrated through a flow diagram in Fig. 5.4.

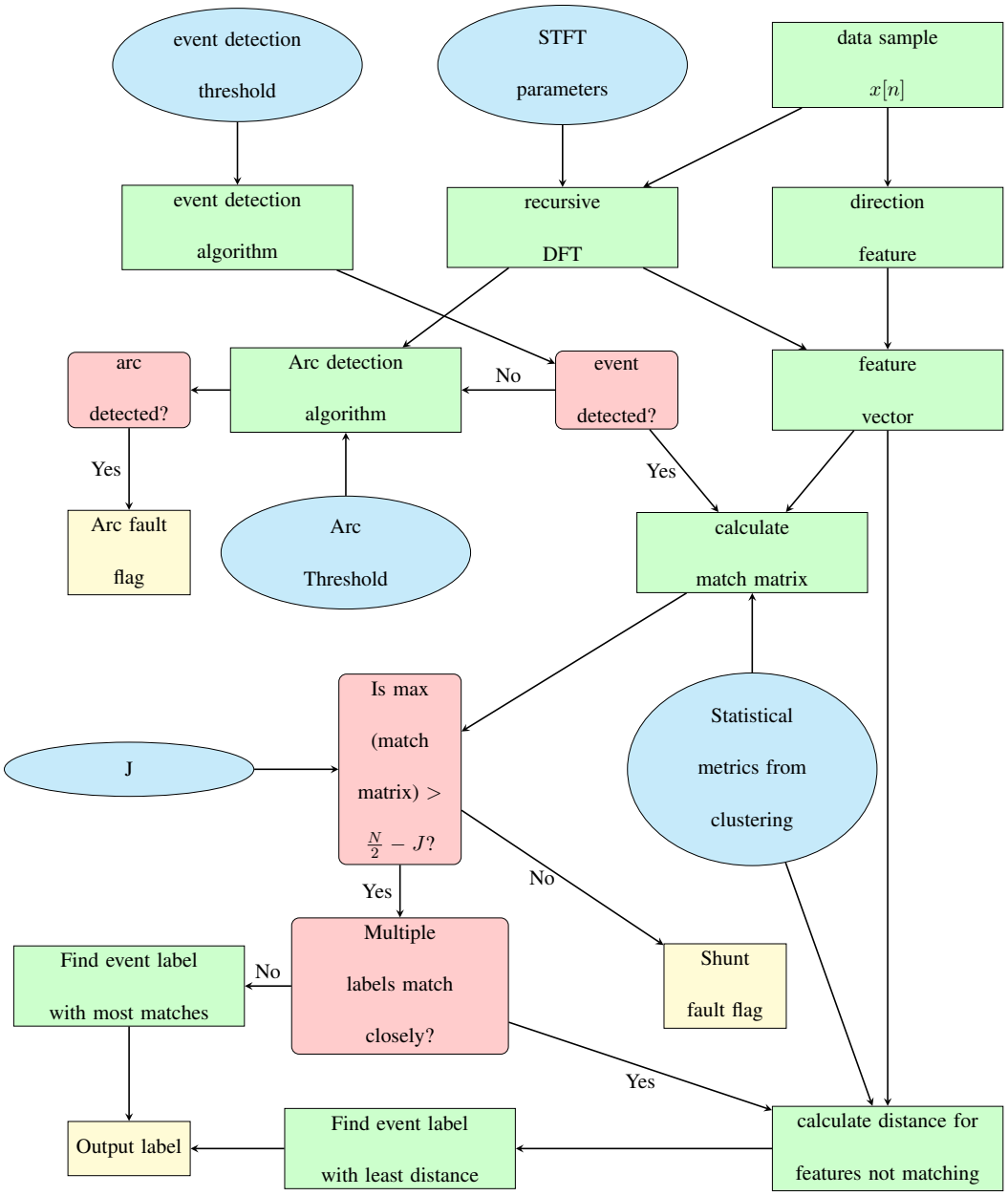

Figure 5.4: Classification mode flow diagram

Chapter 6

STFT Based Load Monitoring and Fault Detection for a Naval Pulsed-Energy Mission Load

6.1 Pulsed-Energy Mission Load Description

6.1.1 Physical and Electrical Operation

In this chapter a simulation model is compiled to represent a prototype PEML. A realistic model lends great merit to the eventual demonstration of the load monitoring scheme and provides more accurate idea of how effectively it would perform in real time. Pulsed operation is defined as rapid power demand over a short period of time. This paper describes a conceptual PEML that is emblematic of the loads listed in the Naval Power and Energy Systems Technology Development Roadmap [104]. The selected PEML requires steady delivery of 3.1 MA over a

short pulse window of 6 ms. Table 6.1 outlines the PEML energy requirements.

Table 6.1: Key PEML Parameters

Primary energy	Bus voltage	Steady state current	Pulse width	Turn-on slew rate	Turn-off slew rate
$40MJ$	$18kV$	$3.1MA$	$6ms$	$6MA/ms$	$-4.2MA/ms$

Table 6.2: Configuration parameters for capacitor rack [**?**]

R	E_{rack}	C	L	t_{peak}	I_{max}
$0.5m\Omega$	$6.3MJ$	$26mF$	$4.6\mu H$	$540\mu s$	$1.35MA$

6.1.2 Capacitor Bank Pulsed Power Supply Operation

From Table 6.1 it can be seen that a power source capable of delivering 40MJ of energy would suffice for this simulation. An ideal voltage source could be used but will not accurately depict the transients that may be observed during operation of the rail gun in a real system. Other options for the power supply model include supercapacitors, inductor coil banks, Homopolar dc generators, flywheels, etc. [105]. The implementation selected for this chapter is a capacitor bank based pulsed power supply (PPS), due to ease of implementation and power efficient design [105]. Work published in [105] has already shown the design for a capacitor rack PPS. The configuration parameters from [105] are used to calculate trigger times listed in Table 6.3 and have been recreated for the simulation model used in this chapter.

Table 6.3: Trigger timing for capacitor rack PPS after fire command issued

1	2	3	4	5
$0.0ms$	$0.0ms$	$0.0ms$	$1.45ms$	$2.25ms$
6	7	8	9	10
$2.9ms$	$3.35ms$	$3.7ms$	$4.0ms$	$4.35ms$

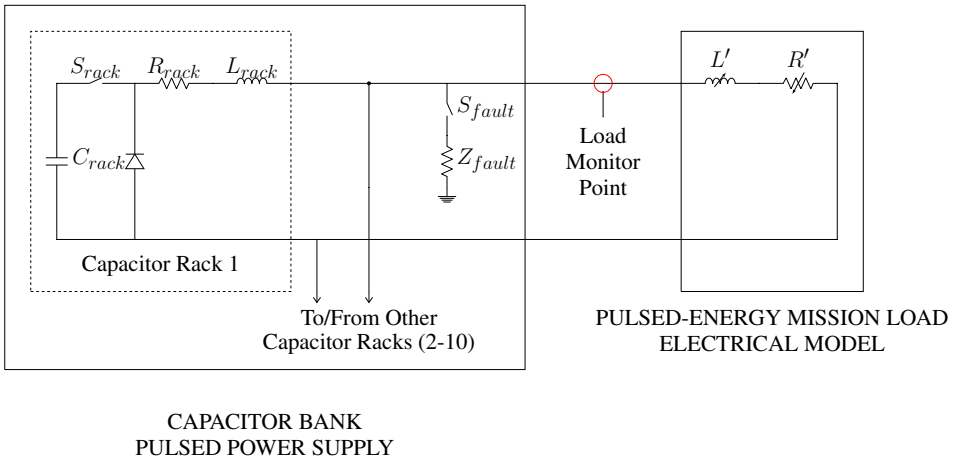

Figure 6.1: PEML pulsed-power supply and electrical model

A system diagram for the simulation is shown in Fig. 6.1. The PEML model can be represented by a resistance and inductance gradient R' and L'. For this implementation R' was set at a constant value of $1.7\mu\Omega$ plus a ramp of $0.82\Omega/s$ and L' was set to a constant value of $0.135\mu H$ plus a ramp of $0.5mH/s$. The load monitoring point is selected to be at the interface of the load with the PPS. The current pulse collected at that point will be used for training and testing the load monitoring scheme in the next section. Only one capacitor rack is shown in the figure but the simulation model consists of 10 such racks in parallel supplying power to the load model. The parameters for the capacitor rack are shown in Table 6.2 and in Fig. 6.1 R_{rack} and $Lrack$ represent the lumped resistance and capacitance of each capacitor bank. A diode has been added across the capacitor to prevent back flow of power and voltage oscillations. The location for a possible shunt fault is also illustrated.

In a typical sequence of operation all the capacitors, C_{rack}, in the PPS are charged to the rated voltage of the PEML which is 18kV in this case. When the pulse is about to fire, the switch to the racks labeled S_{rack} is closed for the first three capacitor racks allowing the load to draw enough current to start its operation. This determines the characteristics of the rising edge of the pulsed current observed at the load monitoring point. Once the current begins rising, it is desired to keep the current constant so the load can operate at a consistent power. To achieve that the rest of the capacitors banks are switched on at regular intervals to maintain a regulated flow of current.

This sequence is listed in Table 6.3 in terms of the time from the launch of the pulse. Initially the first three capacitor banks are switched and the fourth bank is brought on after 1.45ms. In about 4.35ms, all the capacitor banks have been switched on. This sequence of

switching has also been designed in [105] for smooth operation of a notional pulsed power load.

6.2 Simulation Results

The load monitoring and fault detection scheme presented in the previous chapter can be applied to any pulsed load if the parameters are designed correctly. The focus and contribution of this work is to apply the scheme to a specific case of PEML supplied by a capacitor rack PPS.

6.2.1 Pre-processing and parameter selection

A typical load current profile for PEML for one cycle is shown in Fig. 6.2. It can be observed that the rising and falling time for pulse is about 0.5ms while the entire pulse duration is about 5.5ms. An ideal window size must therefore be more than 0.5ms to capture the entire rise and fall transient but less than 5.5 ms so that the entire pulse does not look like one transient. Based on this observation a window size of 2ms is selected.

Several combinations of F_S and N may be used to satisfy the requirement of 2ms window size. For this experiment, a sampling frequency of 20 kHz and N equal to 40 is selected. This allows the algorithm to work with 20 features to uniquely identify each transient. Also the system would have latency of $50\mu s$ which is low enough for dc fault protection. Picking a higher F_S would mean the micro controller will have to do calculations involving more features in smaller amount of time which might be difficult for typical digital signal processors.

Using the parameters selected above, it is possible to perform the STFT for a typical load cycle. The transients show a surge for almost all frequency components. Any of those can

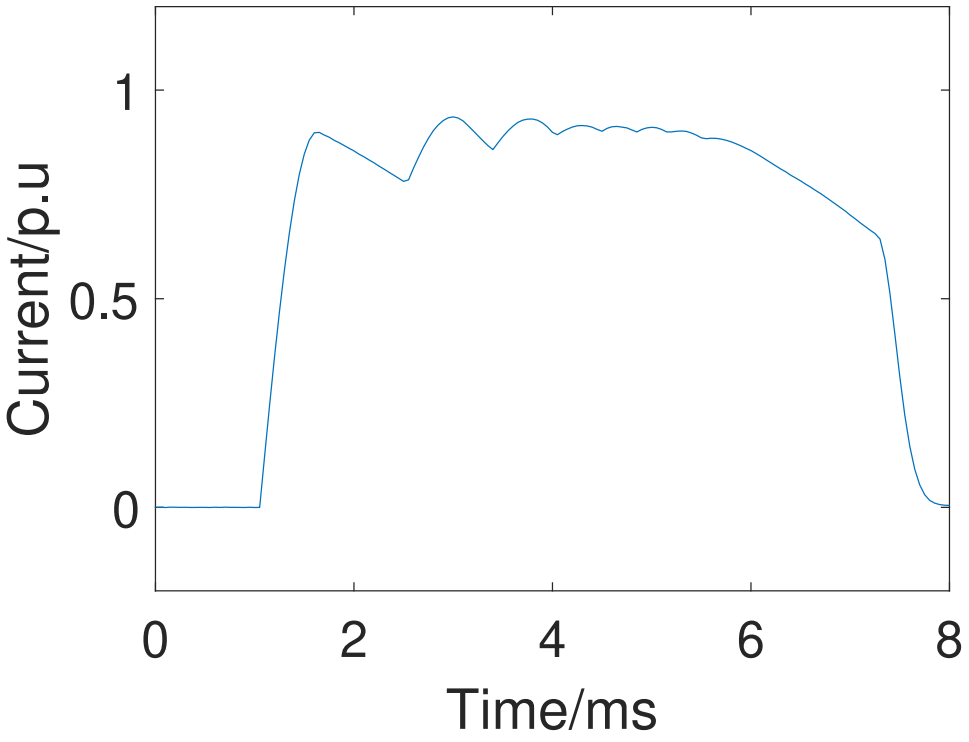

Figure 6.2: A typical load cycle

be used for event detection. This choice is dictated by the number of distinct events desired per load cycle. Looking at the load profile of Fig. 6.2 it is decided that 4 events might be sufficient to describe this cycle, 2 each for the rising and falling transients. Therefore k=2 is selected as the frequency component for event detection since it has 4 surge points for each load cycle. Fig. 6.3 shows the variation in Xn[2] over time for one load cycle. Based on Fig. 6.3, event threshold is selected as 0.1 p.u.

6.2.2 Simulation Results and Accuracy Metrics

The normal operation of the PEML has been described in detail. To test the fault detection algorithm some faults need to be simulated to represent some actual faults that may occur on the system. There are three different kinds of faults being considered here, each of which is expected to either create a disturbance large enough to trigger an event or occur during the normal events. The three faults being simulated are as follows:

- A supply shunt fault can be simulated as shown in Fig. 6.1. It results in a sudden dip in the load current and could result in overheating of the supply.

- A capacitor bank switch failure can be simulated by selecting one of the S_{rack} at random and keeping it on. This would result in an irregular load current and may compromise the operation of the PEML. Consequently the capacitors fire in a wrong sequence affecting the load profile.

- Sensor failure has been simulated by changing the rail gradient drastically during simulation. This changes the slope of the profile.

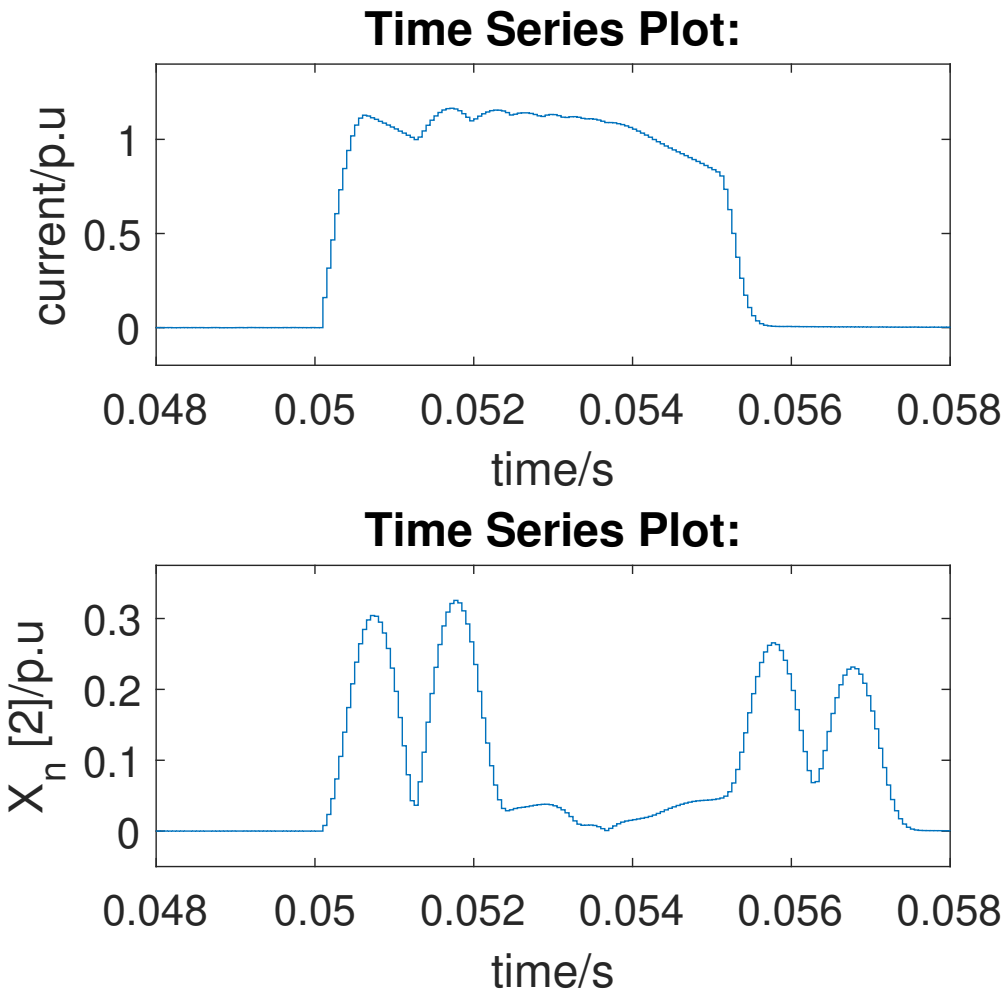

Figure 6.3: Time-frequency curve for k=2 (one load cycle).

The test data for this experiment consists of a total 190 cycles of load profile from PEML simulation. Of these cycles, 100 are from normal operation while the other 90 are collected while one of the faults is simulated on the system. Each fault is simulated 30 times. To measure the performance of the fault detection algorithm the following metrics have been defined:

- A false positive (FP) refers to the percentage of normal load cycle that are flagged as a fault.
- A false negative (FN) refers to the percentage of load cycles with fault that are not detected or misdiagnosed as a normal event.

There are four distinct events in each normal load cycle which can be labeled event 1, 2, 3 and 4. The size of the training data or the length of ESA can be selected based on how much variation can be expected during normal operation of the load. If all the load cycles are exactly identical then theoretically only one cycle of load profile can be enough to train the algorithm however that would be a poor representation of a realistic system. In this simulation, a variation of 1% is added to all the simulation parameters at each iteration of the load cycle. Furthermore there is Gaussian noise with mean of 1kA added to the current measurements. A long ESA would result in more reliable classification but it would be inefficient and inconvenient. The accuracy metrics defined above have been used in this experiment to study the effect of ESA length for the simulated system.

Another parameter that effects these accuracy metrics is the feature match variable J defined in the section above. For the same test data of 190 cycles the accuracy metrics are

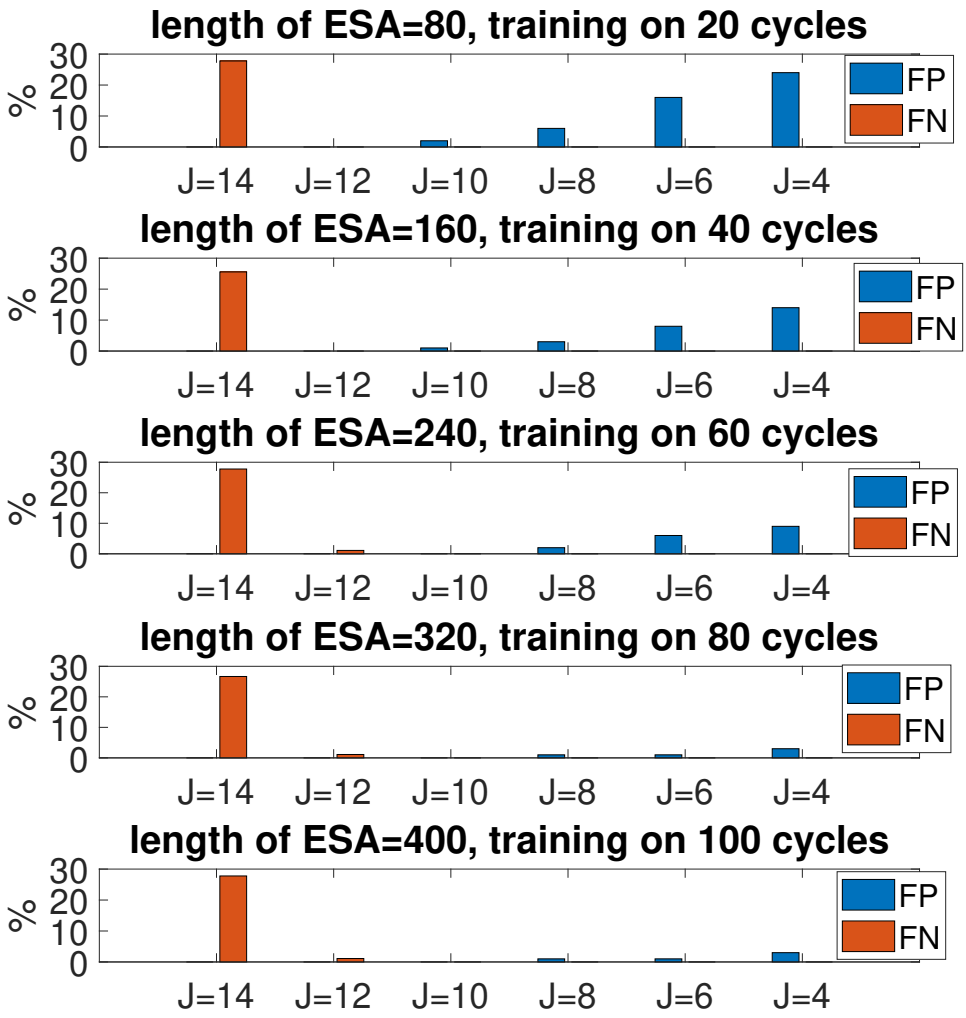

Figure 6.4: Simulation performance over a range of parameters

presented in Fig. 6.4 for six values of J and five values for length of ESA. It can be seen that training for 100 cycles does not offer any noticeable advantage over 80 cycles as accuracy metrics begin to saturate. In general J equal to 10 and 12 offer the most accurate results. False negatives increase rapidly at J equal to 14 so it is safer to keep J equal to 10 for the additional margin. A summary of the parameters is listed in Table 6.4.

Table 6.4: Parameters for load monitoring.

F_S	N	Event Threshold	J	Length of ESA	Events per cycle
$20kHz$	40	0.1 p.u.	10	320	4

Based on the parameters listed in Table 6.4, the load monitoring algorithm is run for the load current of an PEML. Two cycles of load current during testing phase are shown in Fig. 6.5. The first cycle is without faults so the event labels provided by the output are 1, 2, 3, and 4. A shunt fault is created during the second cycle causing the load current to dip sharply towards the lower half of the cycle. The change is so subtle that it can be barely perceived by visually in time domain. However this time-frequency based fault detection method is able to detect that abnormality in the current profile and the subsequent event labels at the output are -1 indicating a fault.

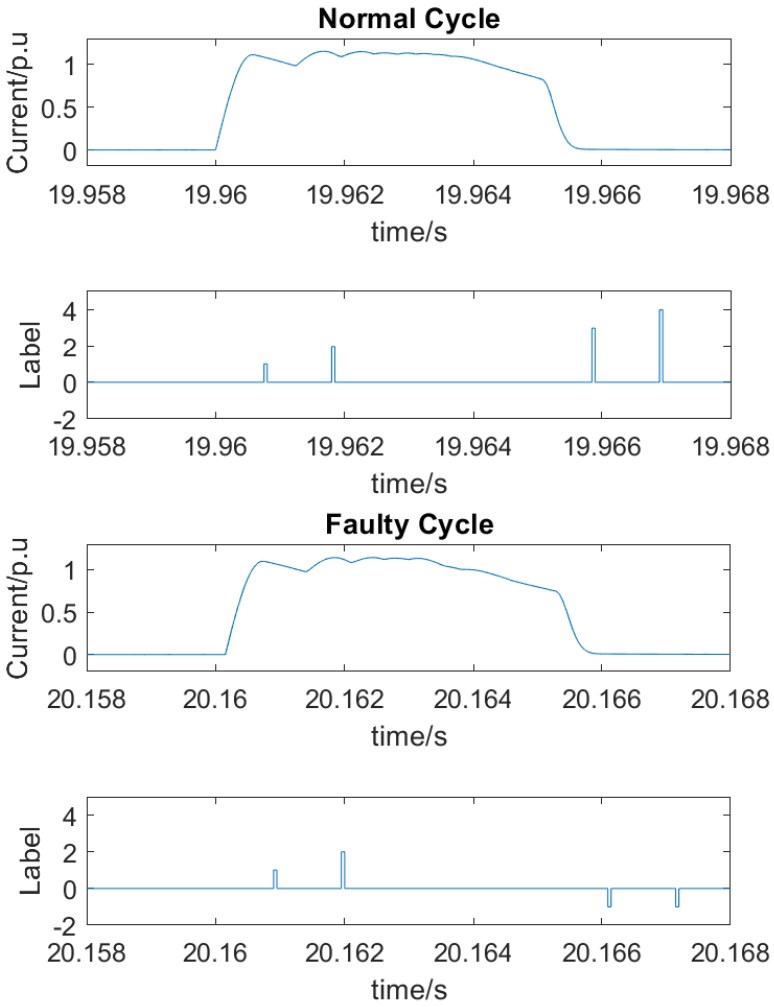

Figure 6.5: Proposed algorithm performance

6.3 Conclusion

Pulsed-energy mission loads on dc distribution systems are going to be a vital part of the next generation of Naval warships. A simulation model is presented herein that has been modified to add imperfections, random variations, and measurement noise as well as fault scenarios. A load monitoring and fault protection algorithm designed specifically for dc pulsed loads could provide tremendous value to future Naval vehicles. In this chapter a proposed algorithm is described in detail for a specific load and supply configuration. The application has demonstrated the effectiveness of the algorithm for event classification and to flag various kinds of faults that are likely to occur in a real system. The algorithm has been tuned to provide zero false positives or false negatives for a large set of data collected from a realistic simulation.

Chapter 7

Load Monitoring and Fault Detection on Data Collected from Dc Pulsed Loads

7.1 LVDC Grid and Load Configuration

Figure 7.1 shows the schematic for the low-voltage dc grid and the four loads attached to it through auctioneering diodes. Each load is designed to model loads that would be commonly found in a naval shipboard system. Figure 7.1 also shows the proposed locations for faults and load monitoring tools. Table 7.1 lists some important circuit parameters for the system in Fig. 7.1.

7.1.1 Load 1: Coilgun Load Description

Load 1 is a pulsed power load designed to emulate a rail gun or laser loads on a naval shipboard system. The capacitor C is connected to the dc grid through an H-bridge charging circuit. A TI 28335 DSP is monitoring the current I_L and capacitor voltage V_{out}. Each operation cycle of this

Table 7.1: System design parameters.

Load 1 parameters		
$V_{dc} = 375V$	$L_{in1} = 100\mu H$	$C_{in1} = 970\mu F$
$L = 2mH$	$V_{out} = 300V\,DC\ max$	$C_{out} = 7mF$
$coil = 80\mu H$	$Z_{fault} = 15\Omega$	$L_{load} = 4mH$
Load 2 parameters		
$L_{in2} = 100\mu H$	$N1 : N2 = 70 : 24$	$L_{N1} = 51\mu H$
$L_{N2} = 6\mu H$	$C_Z = 100\mu F$	$R_Z = 100\Omega$
$R_{load} = 470\Omega$	$L_{load} = 1mH$	$R_{step} = 470\Omega$
Load 3 parameters		
$L_{in3} = 1mH$	$C_{in3} = 2\mu F$	$L_{out3} = 460\mu H$
$C_{out3} = 1.7mF$	$V_{out3} = 150V$	$R_{brake} = 100\Omega$
PMSM = TI HVPMSMMTR		
Load 4 parameters		
$L_{in4} = 1mH$	$C_{in4} = 2\mu F$	$L_{out4} = 460\mu H$
$C_{out4} = 20\mu F$	$V_{out4} = 125V$	

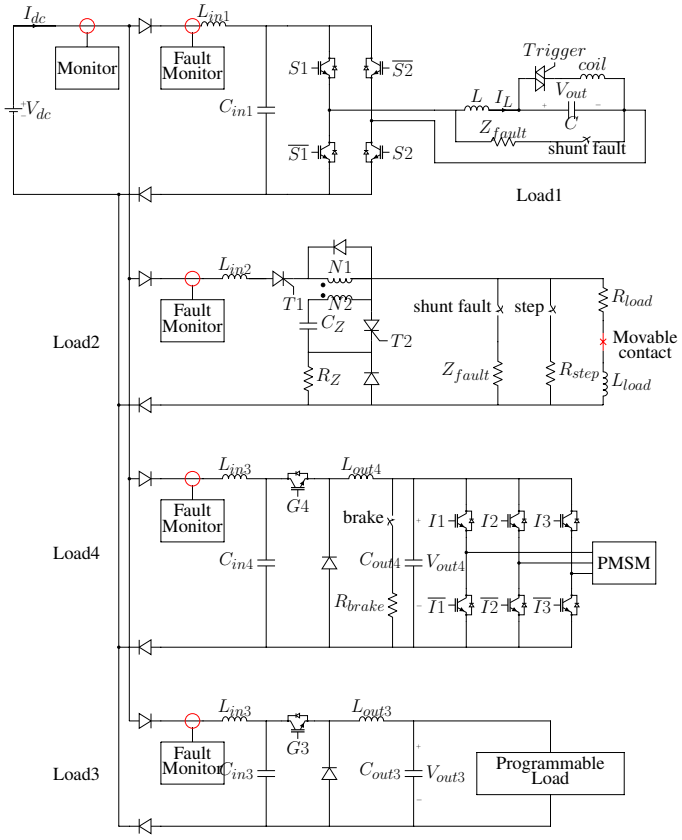

Figure 7.1: Laboratory system diagram.

load consists of the DSP switching the H-bridge to charge C at constant rate of $I_L = 10A$ till V_{out} reaches 300V. At that point the charging circuit is disconnected. After holding the charge for further 0.3 seconds, the DSP triggers the SCR to allow C to discharge through the $coil$, creating the required surge for the coil gun to launch the projectile. The lab setup for this load is shown in Fig. 7.2. Further details on the normal operations and faults on this load are presented in chapter 3.

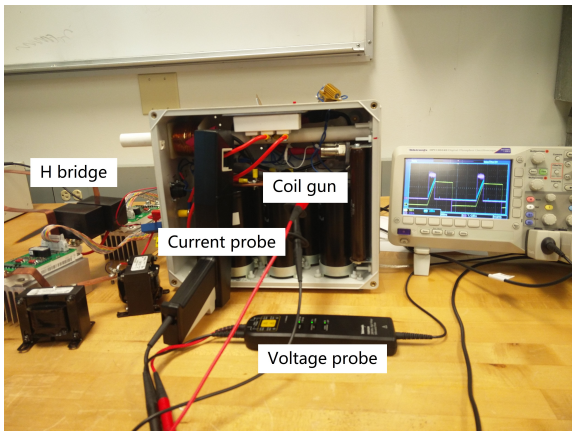

Figure 7.2: Laboratory photograph of pulsed power load.

7.1.2 Load 2: Fixed Load Description

Load 2 is designed to emulate multiple fixed power hotel loads on a naval shipboard system such as heating or lighting equipment. A typical operating cycle for this load consists of 10 second periods where only the base load is powered during the first 7 seconds and for the other 3 seconds a step load is added to the base load. Mechanical relays are operated through an arduino board to switch the current. This load is designed to operate on the dc bus voltage so does not require a power electronic interface to the grid. However it is connected to the dc grid using recently developed coupled inductor dc circuit breaker that allows automatic and immediate isolation of the load in case of a shunt fault. This breaker is unable to react automatically to series arcing fault but the proposed load monitoring scheme will be able to detect any such faults. Figure 7.3 shows the lab setup for Load 2 and the series arc generator for creating arcing faults.

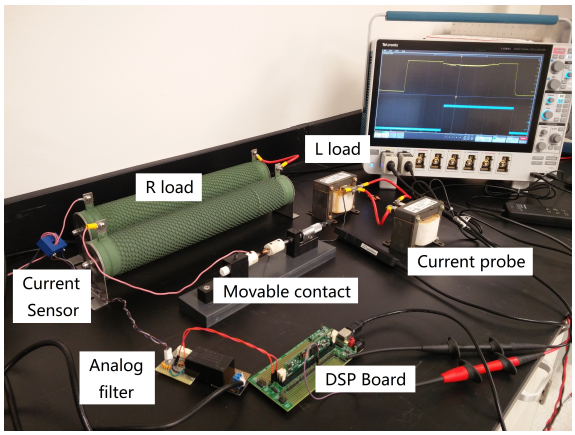

Figure 7.3: Laboratory photograph of a fixed load.

7.1.3 Load 3: Radar Load Description

Load 3 is a Chroma electronic dc load that has been programmed to emulate a radar load on a naval shipboard system. The typical cycle consists of an alternating negative and positive surge of current super imposed on a dc value at 1 second intervals. The programmable load being used is rated for maximum 150 volts while the dc bus voltage is 350 V so a Gallium Nitrate (GaN) buck converter is used as an interface.

7.1.4 Load 4: Motor Load Description

Load 4 is meant to emulate propulsion loads on a naval shipboard system. A typical 70 second operating cycle would consist of a 16 second acceleration stage where motor is accelerated linearly from rest to 1500rpm, followed by 24 second at top speed; deceleration takes another 15 seconds followed by 5 seconds of rest. A flywheel is designed to mount on the shaft of the motor so it pulls 1 A of peak current during acceleration. A buck converter is used to interface

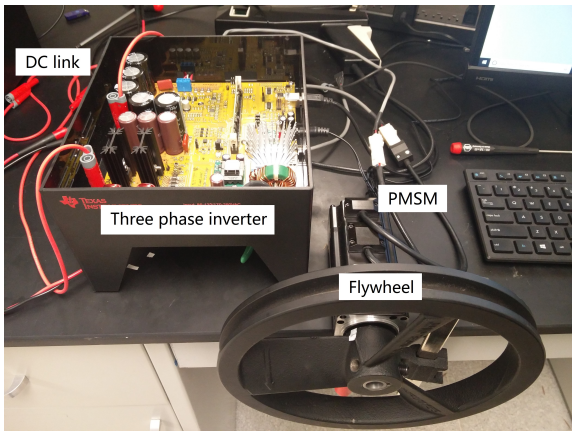

Figure 7.4: Laboratory photograph of PMSM load.

the motor drive to the dc grid and can also be used to isolate the load in case of a fault. The lab setup is shown in Fig. 7.4.

7.2 Results and Discussion

The proposed load monitoring scheme can be applied to any pulsed load with some amount of pre-processing, as long as the events to be classified are present during the clustering mode. This section provide some details on the parameter selection for 5 unique cases of pulsed load, and presents the results.

7.2.1 Load 1: Coilgun Load

Fig. 7.6 shows the load current for Load 1 during a normal operating cycle. The zoomed in box shows the three windows that have been selected as labeled events. This selection is unique to the window size of 4ms and event threshold of 0.4 on $X_n[1]$. When the H-bridge in load 1 gets disconnected the current takes about 1ms to drop to zero. the window size is therefore selected

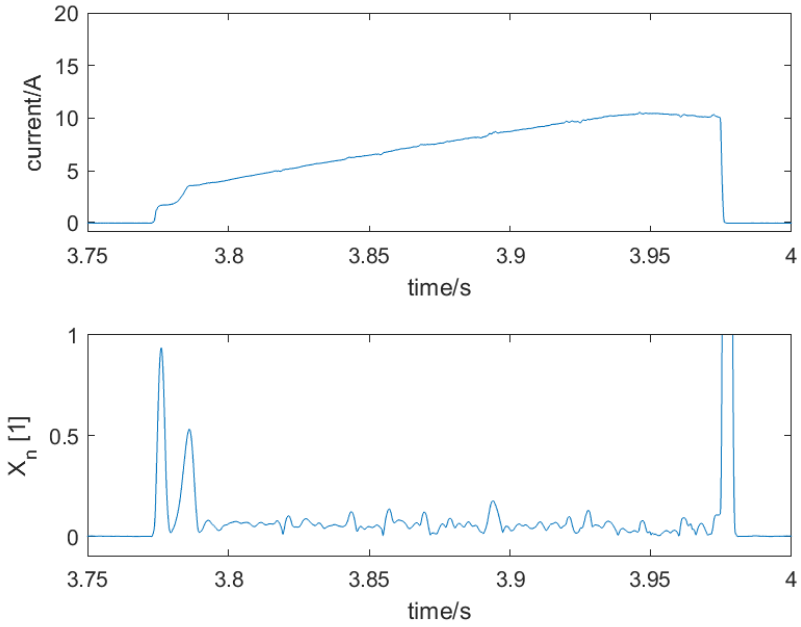

Figure 7.5: load current for load 1 and $X_n[1]$ over time

to be greater than 1ms to completely capture that transient. Additionally the event labeled 1 and 2 are only about 10ms apart so a window size of less than 10ms is selected to keep those two events in separate windows. Selecting 4ms window size at 10kHz sampling frequency allows N to be 40 which means there are 20 features available to characterize the events. This particular choice of N and F_s is compatible with the processing speed of most TI DSPs and 20 features are enough for each event to be uniquely identified. During pre-processing, $X_n[1]$ over time for one load cycle showed three distinct surges as shown in Fig.7.5. The event detection threshold of 0.4 is selected based on that result and the desire to have exactly 3 events during each normal cycle.

Experimental data for all results in this section is sampled at 10kHz using Tektronix

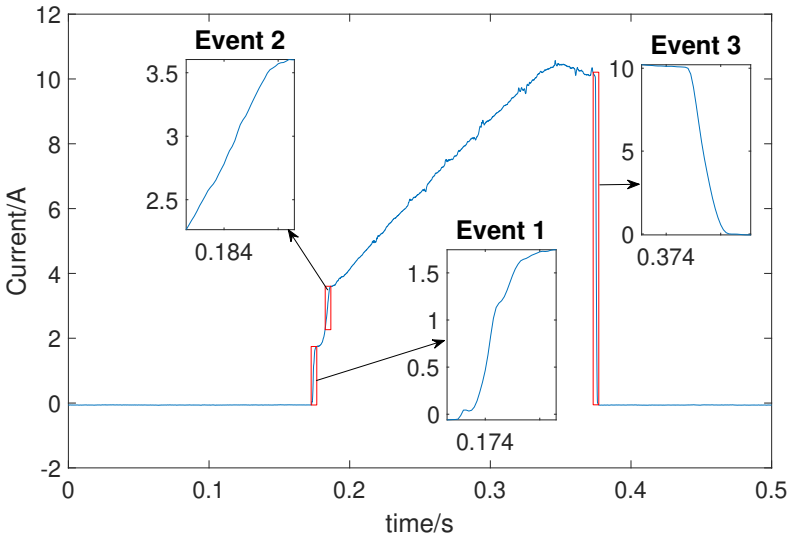

Figure 7.6: load current for load 1 and event windows

current probes of bandwidth 200Mhz. The data is saved into .mat files and fed in discrete time steps corresponding to $\frac{1}{F_s}$ to a matlab simulink program that executes the proposed load monitoring scheme. Details of the data, parameters for load monitoring scheme, and result metrics are provided for all experiments in Tables. 7.2, 7.3, and 7.4 at the end of this section.

Two kinds of shunt faults are created in Load 1. The first is through creating a shunt fault across the load of H-bridge as shown in Fig. 7.1 which results in a positive surge of current. The second is through creating a disturbance in the gate signal going to switch labeled S1 which results in a negative surge of current. Each incident of fault creates a unique disturbance because the duration and the timing of fault are randomly decided. The metrics to determine accuracy of the proposed scheme includes percentage of false positives, i.e mistaking a normal event for fault, and percentage of false negatives, i.e misdiagnosis of a fault as a normal event. The sensitivity of the algorithm depends largely on the choice of parameter J as shown in Fig. 7.7.

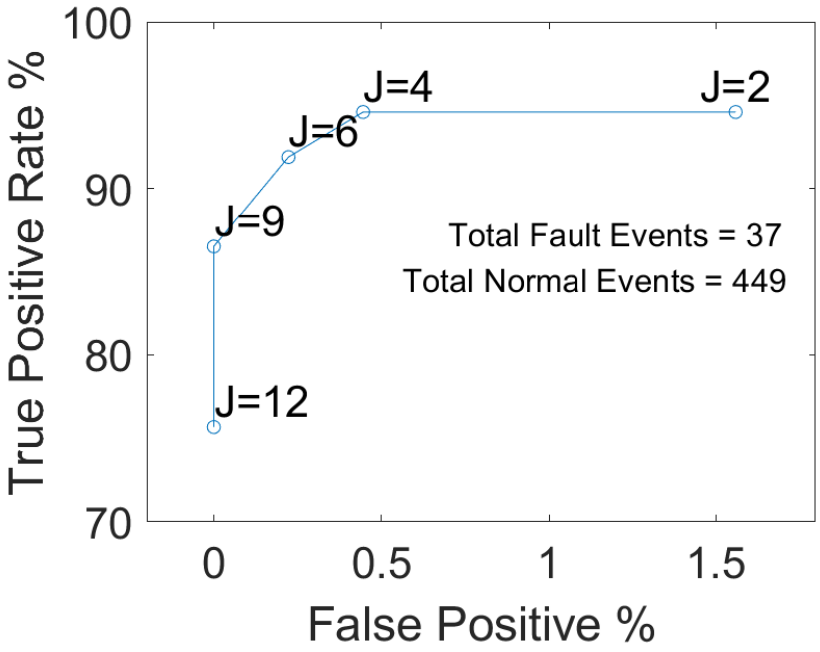

Figure 7.7: Receiver operating characteristics with respect to parameter J

$J = 4$ has been selected for this experiment based on Fig. 7.7. Fig. 7.8 shows the response of the load monitoring scheme to the data during classification mode. In this period all events are correctly labelled and the fault is correctly identified and labeled as -1.

7.2.2 Load 2: Fixed Load

Load 2 has two significant transient events. A rising transient when the step load is added to the system and a falling transient event when the relay opens to disconnect the step load. The transients last for about 1ms so a window of 4ms can be used to completely capture it. All other parameters are also kept the same as load 1. The window of labeled events are shown in Fig. 7.9.

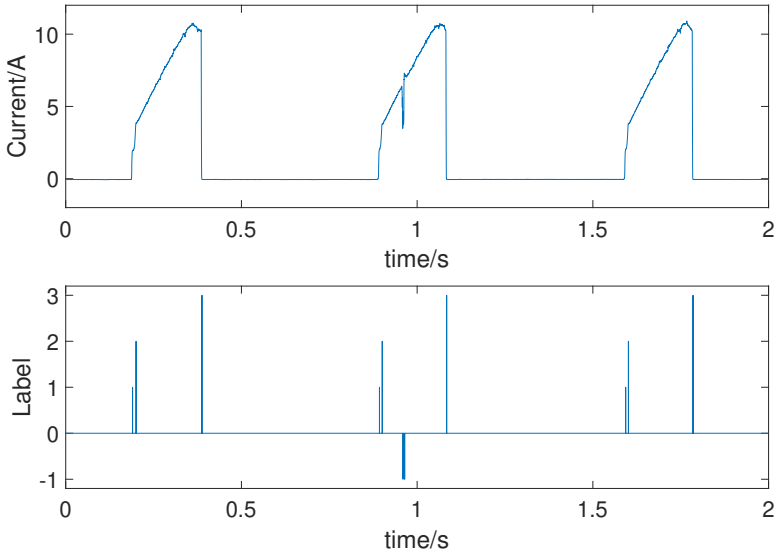

Figure 7.8: Applying load monitoring scheme to data collected from load 1

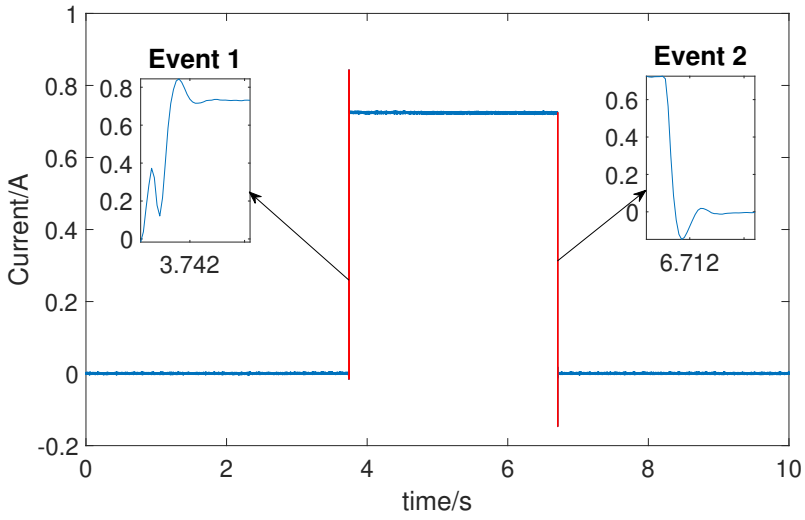

Figure 7.9: load current for load 2 and event windows

The shunt fault for this load is automatically disconnected by the coupled inductor breaker and is never seen in the load profile. However series arc has been included in the load

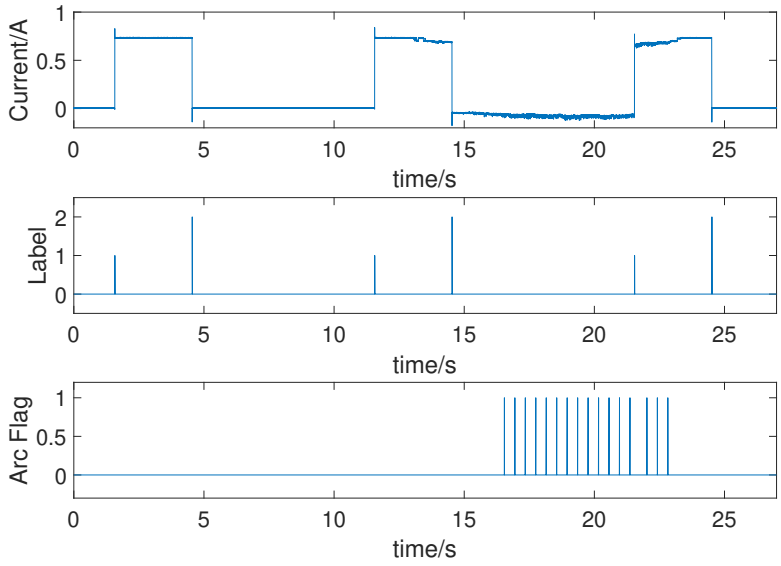

Figure 7.10: Applying load monitoring scheme to data collected from load 2

profile on a number of occasions. The location where the series arc is introduced can be seen in Fig. 7.1. Fig. 7.10 shows a small period containing arcing fault during classification mode. The top plot shows the data, the center plot shows the two events being correctly identified and the bottom plot shows the arcing flag being raised in response to the disturbance in current. Table. 7.2 shows more details on the data and the overall response of the scheme to this load.

7.2.3 Load 1 and 2 in parallel

Since all the parameters in load 1 and load 2 load monitoring scheme are the same they can essentially be monitored from a single point that carries the sum of the current going to both loads. In this experiment current collected from both loads is summed up and fed to a single simulation. Only difference from previous instance is that the events of load 2 are now labeled as

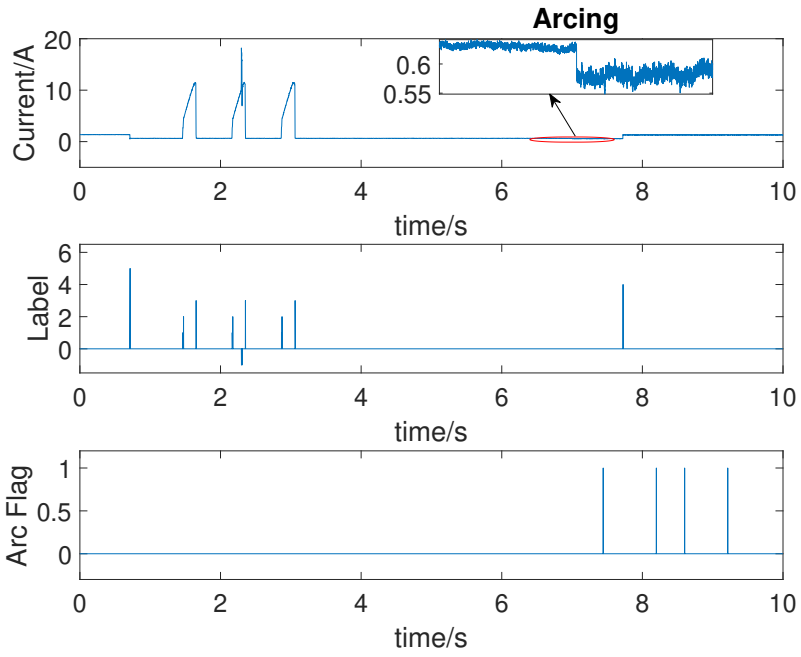

Figure 7.11: Applying load monitoring scheme to data collected from load 1 and load 2 operating in parallel

'4' and '5' in ESA so not be confused with event labeled '1' and '2' from load 1. A small section of results from classification mode is shown in Fig. 7.11 where all the events are correctly identified, and the shunt fault as well as arcing fault is flagged. Since load 1 and load 2 are operating independently, it is possible that the two events may occur during the same window in which case it will not be correctly identified. That is one limitation of the current scheme but this probability can be significantly reduced by selecting a small window or by adding some communication method between loads and the monitoring device. More details on the data, accuracy metrics and overall performance is shown in Table. 7.3.

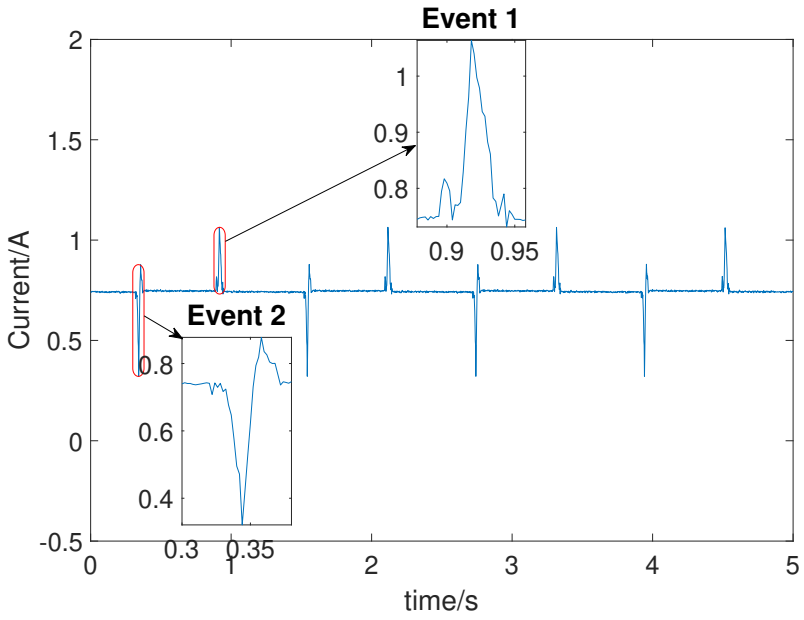

Figure 7.12: load current for load 3 and event windows

7.2.4 Load 3: Radar Load

Load 3 contains two surges of current in each operating cycle and each of them could be labeled as an event. The transients of this load are much slower than Load 1 or Load 2 so a larger window will be required to capture it. This large window of 80ms is achieved by reducing F_s to 500Hz. An effect of larger window is that the disturbance in time frequency domain looks smaller so the threshold of $X_n[1]$ is reduced to 0.06 for event detection. The resulting windows for the two labeled events is shown in Fig. 7.12.

A small amount of 60Hz interference is added to the load profile during classification mode to verify the series arc detection algorithm. Fig. 7.13 shows a small period of time from classification made where the events are correctly identified and labeled and also flags are raised

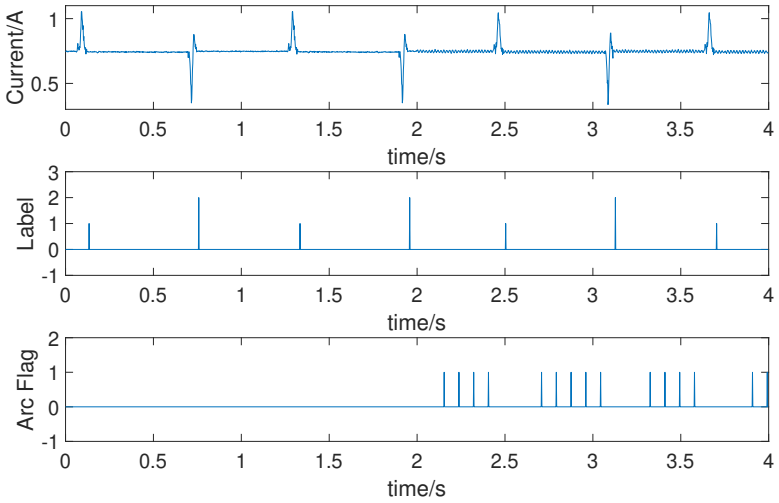

Figure 7.13: Applying load monitoring scheme to data collected from load 3

for presence of noise. More details on the data and the overall performance of algorithm for this load is presented in Tables. 7.3 and 7.4.

7.2.5 Load 4: Motor Load

Finally the load monitoring scheme is tested on profile of load 4. Load 4 has slower transients than the other loads due to high inertia of the motor. Window size of several seconds is required in this case. By selecting $F_s = 10$Hz and $N = 80$, a window size of 8s can be achieved. By selecting an event detection threshold of 0.15, two events can be created in each load cycle. The resulting windows of events are shown in Fig. 7.14 where label 1 corresponds to the motor starting to accelerate and label 2 corresponds to when the motor begins to decelerate.

Several normal load cycles are collected for the clustering mode of the scheme but some faulty profiles are also collected to verify the event based fault detection of the program.

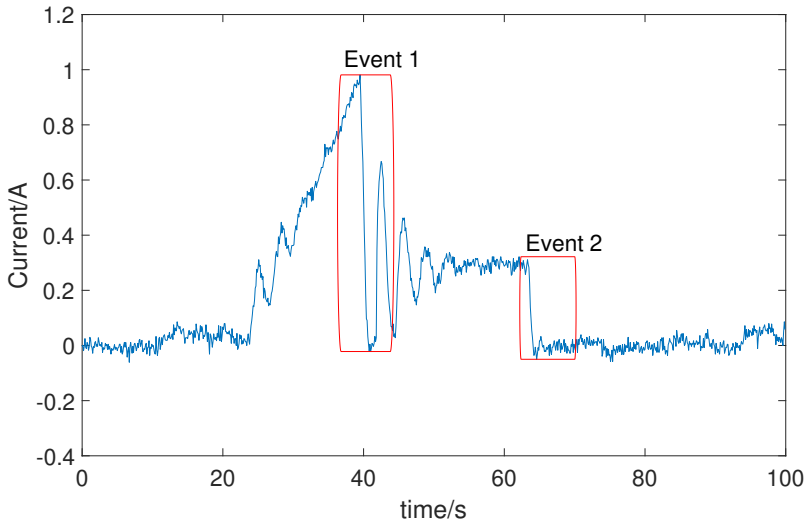

Figure 7.14: load current for load 4 and event windows

Faulty profiles are created by adding physical restraints to the flywheel of the motor during either acceleration or deceleration stage, causing the load to draw a surge of current. Each instance of fault creates a unique profile because the restraint is applied at random times and for variable duration. Figure 7.15 shows the response of the scheme for a section of time during classification mode. It can be seen that the scheme identifies and labels the events correctly and also raises a flag i.e label '-1' for the fault. More details on the data and the overall performance of the scheme is presented in Table. 7.4.

7.2.6 Performance metrics

The importance of pre-processing the load profile cannot be over emphasized as it is the first step towards selecting some critical parameters for the proposed load monitoring and fault detection scheme. This subsection briefly discusses the impact of these parameters on some common

Table 7.2: Summary of Results

Load 1 results & parameters	
F_s , Window size , Length of ESA	10kHz , 4ms , 300
J , Arc Threshold , Event Threshold	4 , 0.05 , 0.4
Event 1 appearances , % correct labeled	149 , 99.33%
Event 2 appearances , % correct labeled	149 , 99.33%
Event 3 appearances , % correct labeled	150 , 100%
Load 1 Event based fault detection	
Normal events , Faulty events	449 , 37
False Positive , False Negative	0.45%, 5.41%
Load 2 results & parameters	
Parameters same as Load 1 , Length of ESA = 400	
Event 1 appearances , % correct labeled	263 , 99.62%
Event 2 appearances , % correct labeled	263 , 98.86%
Load 2 arcing based fault detection	
Normal load cycles , Faulty load cycles	263 , 35
False Positive , False Negative	0% , 11.43%

Table 7.3: Summary of Results

Load 1 and Load 2 parallel results & parameters	
Parameters same as Load 1 , Length of ESA = 340	
Event 1 appearances , % correct labeled	155 , 99.35%
Event 2 appearances , % correct labeled	155 , 98.06%
Event 3 appearances , % correct labeled	156 , 99.36%
Event 4 appearances , % correct labeled	52 , 96.15%
Event 5 appearances , % correct labeled	52 , 90.38%
Load 1 and Load 2 parallel Event based fault detection	
Normal events , Faulty events	570 , 42
False Positive , False Negative	1.23% , 19.05%
Load 1 and Load 2 parallel arcing based fault detection	
Normal load cycles , Faulty load cycles	50 , 20
False Positive , False Negative	0% , 0%
Load 3 results & parameters	
F_s , Window size , Length of ESA	500Hz , 80ms , 200
J , Arc Threshold , Event Threshold	4 , 0.012 , 0.06
Event 1 appearances , % correct labeled	125 , 100%
Event 2 appearances , % correct labeled	125 , 100%

Table 7.4: Summary of Results

Load 3 Arcing based fault detection	
Normal load cycles , Faulty load cycles	250 , 333
False Positive , False Negative	0% , 0%
Load 4 results & parameters	
F_s , Window size , Length of ESA	10Hz , 8s , 100
J , Arc Threshold , Event Threshold	4 , 0.1 , 0.155
Event 1 appearances , % correct labeled	161 , 95.65%
Event 2 appearances , % correct labeled	164 , 98.78%
Load 4 Event based fault detection	
Normal events , Faulty events	325 , 68
False Positive , False Negative	1.54% , 10.29%

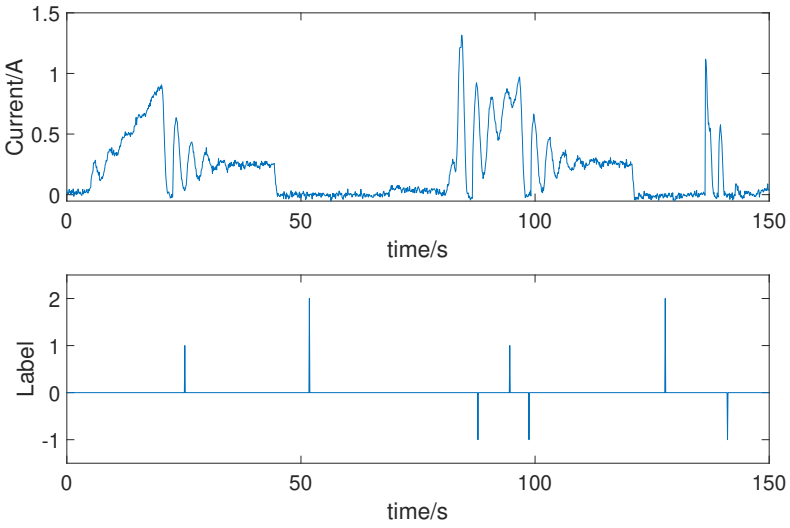

Figure 7.15: Applying load monitoring scheme to data collected from load 4

performance metrics.

7.2.6.1 Minimum fault size detectable

For event based fault detection, the minimum fault size detectable is directly related to the choice of event threshold. An example of picking event threshold is presented for load 1. Since the threshold is defined on the output of the STFT, it is in effect a limitation on the minimum detectable ramp rate of the fault. Based on equation (5.7) a threshold of x would theoretically allow the detection of any fault with ramp rate greater than $\frac{x*F_s}{N}$. This however does not mean that faults with low frequency components will go undetected. The series arcing fault algorithm can still detect faults that have power greater than the arcing threshold for non zero frequencies under 100Hz even if they do not trigger an event detection. There remains a range of faults that could escape both these methods but the thresholds can be defined to effectively minimize that

possibility.

7.2.6.2 Robustness against noise

It may be tempting to select very low arcing and event thresholds to have a broad range for detectable faults however it may lead to more false positives. Due to high cost of interference and system reboot, false positives are particularly troublesome in Naval applications. The parameter J can be tuned for a possible trade off between sensitivity and robustness as shown for Load 1. Similarly length of ESA can also effect robustness of the scheme. Training for longer period can ensure that the algorithm is more familiar with the events. In case there is less noise present during clustering mode but an abnormal amount of noise is present during classification it will be flagged as shown in case of Load 3. Adequate robustness is demonstrated by the proposed scheme as it has been tested using data collected from the hardware system with natural variations rather than idealized simulated systems.

7.2.6.3 Detection time

Another important metric particularly for dc systems is the detection time for faults. As discussed in the theory section, the application of recursive DFT allows the algorithm to provide a label for the observed event within one sampling time period. This means that theoretically the detection time cannot be more than $\frac{1}{F_s}$. Whether this can be achieved depends on the micro controller and programming tool being used during real time application. One limitation of combining load monitoring and fault detection is that it limits the fault detection time based on the transient time of the load profile. For example comparing load 1 and load 4 reveals that load

1 with high sampling frequency will have fast detection time of $100\mu s$ whereas load 4 will have slower detection time of $0.1s$. To achieve faster detection time while keeping the same window size, the sampling frequency F_s must be decreased and N must be increased. This is a trade off between computational burden and detection time that is inherent with STFT based algorithms.

7.3 Conclusion

Pulsed power loads are expected to be common place on the future medium voltage dc Naval shipboard system. They present unique load monitoring challenges and complicate fault detection methods. This paper presents a simple load monitoring and comprehensive fault detection solution that characterizes pulsed power loads based on the frequency content of its transients. The load classification uses simple cluster analysis methods and can begin classifying after a brief clustering mode. Setting a few parameters in the initialization phase can allow it the flexibility to work for a wide range of dc loads. The proposed scheme has been shown to work with an accuracy of over 90% for a variety of dc loads assembled on a low-voltage dc grid. Due to the high cost of disruption, and the observation that each incident of fault creates several events, the preference in the design has been to keep false positives low at the cost of higher false negatives. Both shunt faults and series arcing faults have been successfully identified using large sets of data collected from experimental setup.

Chapter 8

Real Time DSP Implementation of the Load Monitoring and Fault Detection Scheme

8.1 Challenges of real-time DSP implementation

The Texas Instrument (TI) DSP 28335 pictured in Fig.8.1 is being used as the processing unit for the real time implementation of the scheme outlined in Chapter 5. This is the same DSP that was previously used for real-time implementation of schemes presented in Chapter 3 and Chapter 4. The loads being tested are the same as those described in chapter 7 so the pre-processing required for parameter selection has already been presented.

Chapter 7 looked at the implementation of the proposed scheme on data collected from four different loads assembled on a low voltage dc grid. As mentioned in chapter 7, the data was processed on MatlabR2019 Simulink software. It stands to reason that the collected data can be replaced with an analog to digital converter (ADC) interface and the proposed

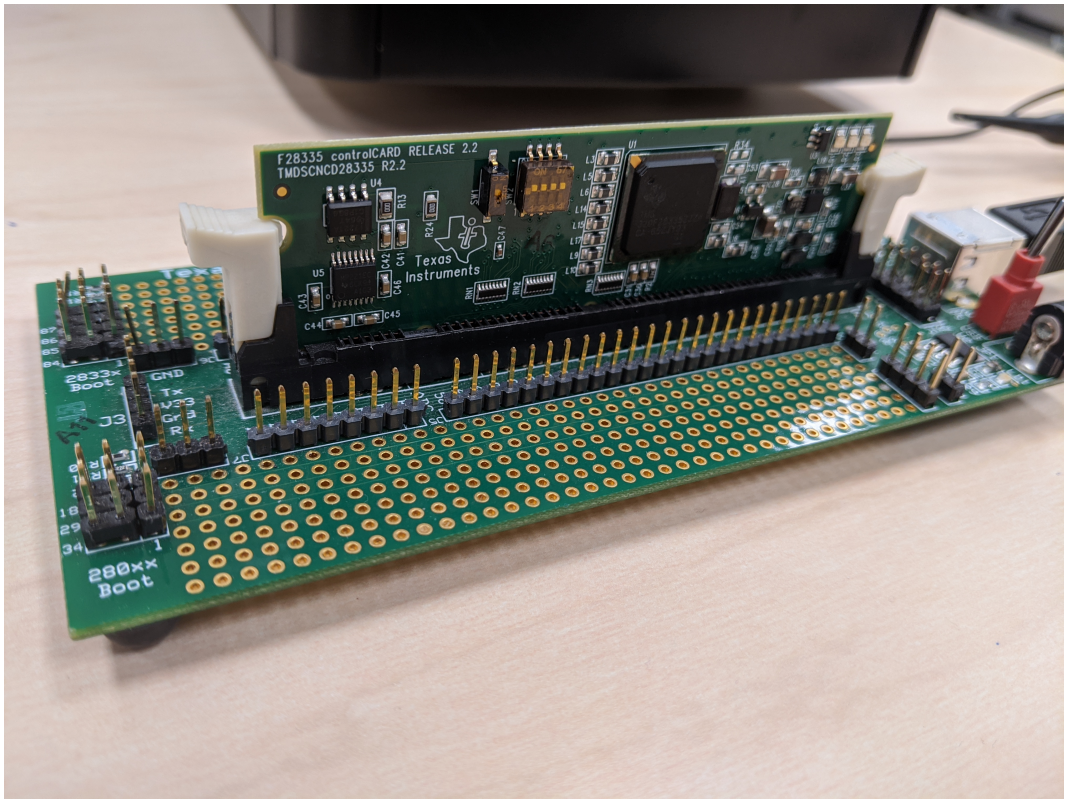

Figure 8.1: Texas Instrument DSP 28335 control card with docking station

scheme can be applied in real-time without any adjustment. The motivation for using a DSP instead of a Simulink running on a Intel core 7 processor is to demonstrate the possibility that the monitoring can be performed on a remote or isolated unit. It also makes for a portable setup where using the resources of a larger processor would be an over kill. Using a TI DSP is the preferred choice because of its easy interface with simulink software. The simulink program can be compiled into an out file that loads directly to the DSP. For a low voltage lab setup it makes more practical sense to implement the monitoring on a low cost compact processor such as the TI DSP 28335.

There are several challenges associated with translating the proposed scheme from a computer down to a single core DSP with processor speed of 150 MHz. Due to the limitations of the DSP, the following adjustments have been made to the algorithm:

- The scheme is designed such that the processor must complete one iteration of STFT calculation and compute all the clustering information in case of event detection in $\frac{1}{F_s}$ seconds. The amount of processing to be done also depends on N , i.e the number of data points in one window and on number of designated unique events in the load cycle. The highest value of sampling frequency, F_s selected in the pre-processing stage during chapter 7 was $10kHz$ for load 1 and load 2. However it was observed that the DSP was unable to process at that speed. Therefore for both these cases the sampling frequency was lowered to $5kHz$. In order to keep the window size the same as in chapter 7, the number N was also lowered to half its original value. The rest of the parameters were kept the same. Lowering the sampling frequency results in a lower fault detection time

however the new fault detection time of $200\mu s$ is still within acceptable limits for this application.

- Another adjustment based on processing speed of the DSP is the exclusion of standard deviation calculation during classifying mode. Theoretically having standard deviation as a measure of variation in features is a useful tool for identification. However it takes a bulk of processing time without adding any significant impact in this application. While the original scheme calculates the distance of observed features from the mean of the recorded features as a fraction of a standard deviation, the modified scheme calculates only the absolute distance between observed features and the mean of the recorded features.

- It has been demonstrated that a large training period helps to reduce false positives and false negatives during classifying mode. The TI DSP however has limited memory space and cannot allow long event sequence arrays (ESA). Furthermore there are practical constraints for running the loads for a long duration such as overheating and mechanical stress. Therefore the ESA used in this chapter are shorter than those in chapter 7.

- The model of TI DSP being used does not have analog output channels so a different digital output is dedicated in each load scenario for a unique event label. A flag is raised at the designated GPIO corresponsing to the event number instead of an analog output as in chapter 7

- The load monitoring algorithm receives only one analog signal for current which needs to be sampled for arc detection as well as the event based detection. The arc detection

algorithm operates at the fixed sampling frequency of $1kHz$. The same analog signal is sent to two DSP units operating at different sampling frequency. One implements the arc detection algorithm while the other performs the event based detection. Since the two algorithms do not need to be synchronized and can operate independently, two single core DSPs are used used instead of one multi core DSP.

8.2 Load 1: Coilgun Load

The parameters shown in Table. 8.1 are selected after careful pre-processing of the load profile for the coilgun load. Eight cycles of the normal load profile are used to create a database in run-time during clustering mode. Figure 8.2 shows the result for one normal load cycle of the coil gun during classifying mode. Every time an event is detected a flag is raised at a designated GPIO of the DSP. This event flag is shown in the second subplot of the Fig. 8.2. As expected, the event flag is raised three times. The width of the event flag is programmed to be equal to half the window size so it can be seen the observed events do not overlap in their window. The third, fourth and fifth subplots show the voltage at GPIOs designated to event 1, event 2 and event 3 respectively. These events are the same as defined in Chapter 7. It can be seen that the events detected are properly classified to their respective labels and that there are no false positives.

Table 8.1: Parameters for Monitoring Load 1

F_S	N	Event Threshold	J	Length of ESA	Events per cycle
$5kHz$	20	$0.4A$	6	24	3

In subsequent event cycles during the same classifying mode, certain faults are introduced in the load profile. The response of the DSP to these faulty load profiles is shown for four separate instances in Figs. 8.3, 8.4, 8.5, and 8.6. For Fig. 8.3 there is no flag raised for the first event detected because that event is still in the clustering mode. The significance of the fault depicted in Fig. 8.3 is that the peak of the fault current never exceeded the maximum current of the normal load profile. A threshold based fault detection would not work for such a scenario. Figure 8.4 indicates that the algorithm is able to catch a fault with negative polarity as well. Generally most fault schemes are designed to catch an increase in current because shunt faults commonly cause the current to rise. However this algorithm can catch any deviation in current regardless of polarity.

The faulty cycle presented in Fig. 8.6 is a unique case where the negative transient of fault current looks identical to the event label 3. It can be seen that the algorithm misidentifies that fault to be event 3. Incidentally the subsequent transients from the fault triggers a second event detection which is flagged as fault eventually.

8.3 Load 2: Fixed Load

The sampling frequency for the fixed load current profile also had to be reduced for the same reasons as with load 1. However, the window size has been kept same. The parameters are listed in Table 8.2. Eight normal load cycles are used to train the processor during the clustering mode. The challenging part for this load profile is that both the events are identical in most of their time-frequency features, the only clearly unique feature is the polarity. Despite that

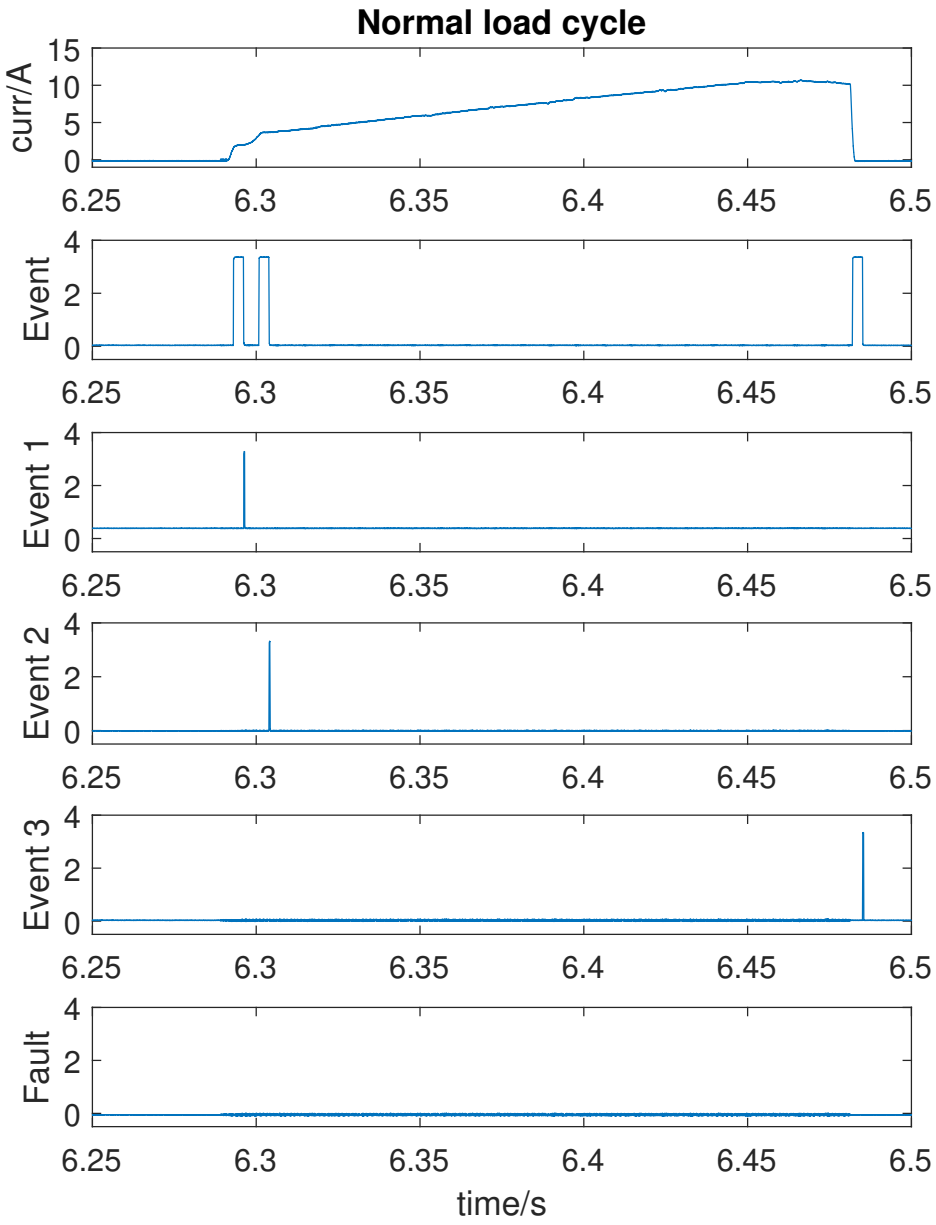

Figure 8.2: Coil gun load normal cycle

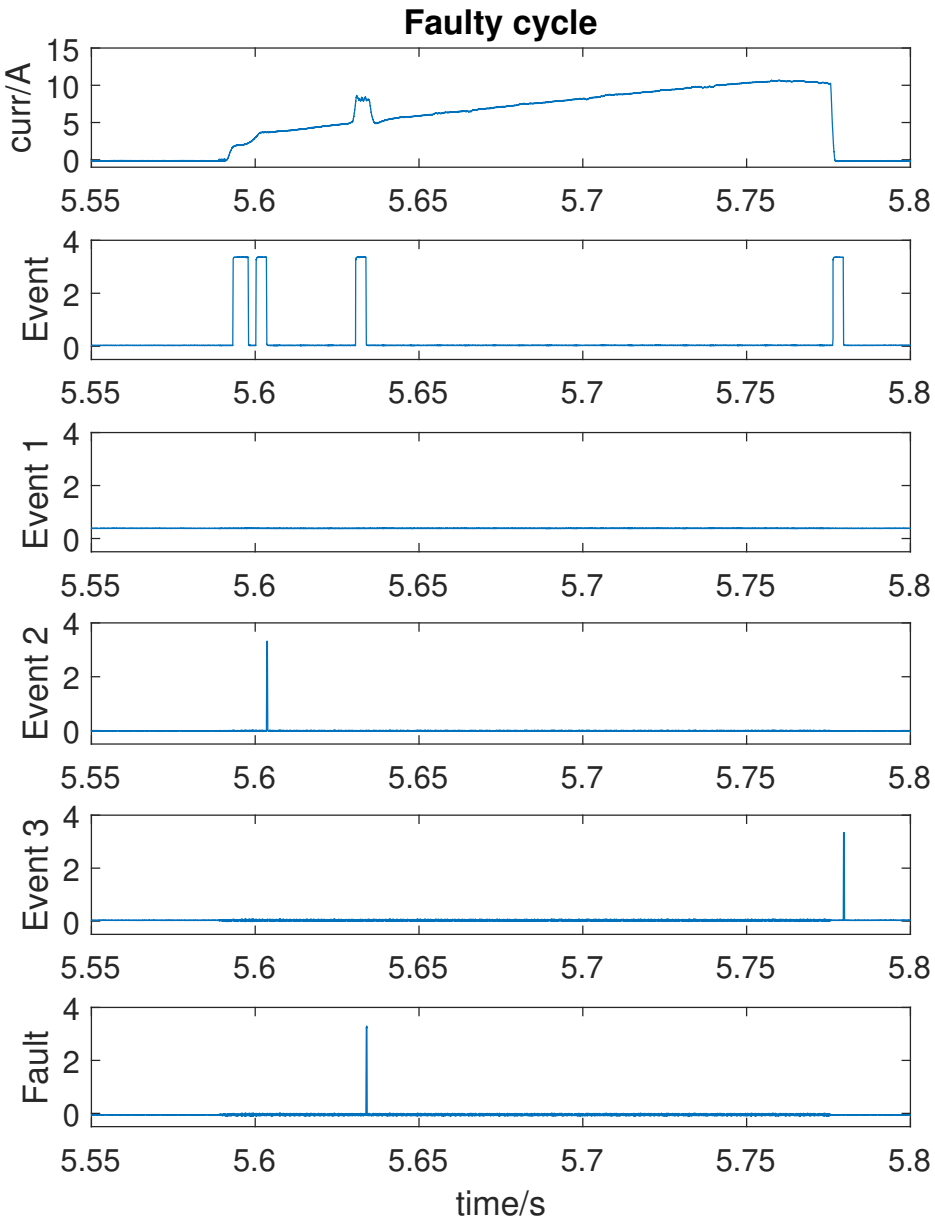

Figure 8.3: Coil gun load faulty cycle with shunt fault

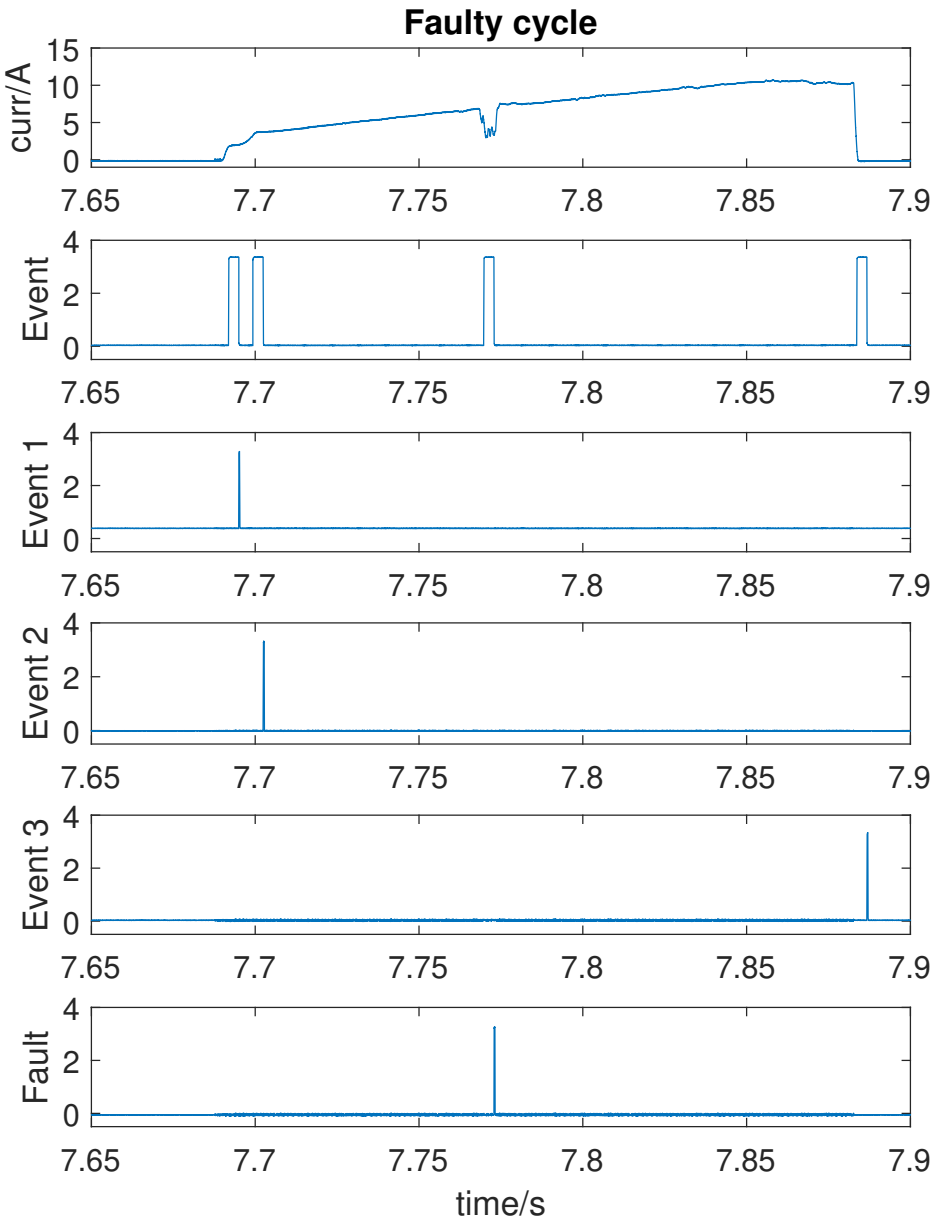

Figure 8.4: Coil gun load faulty cycle with noisy IGBT gate driver signal fault

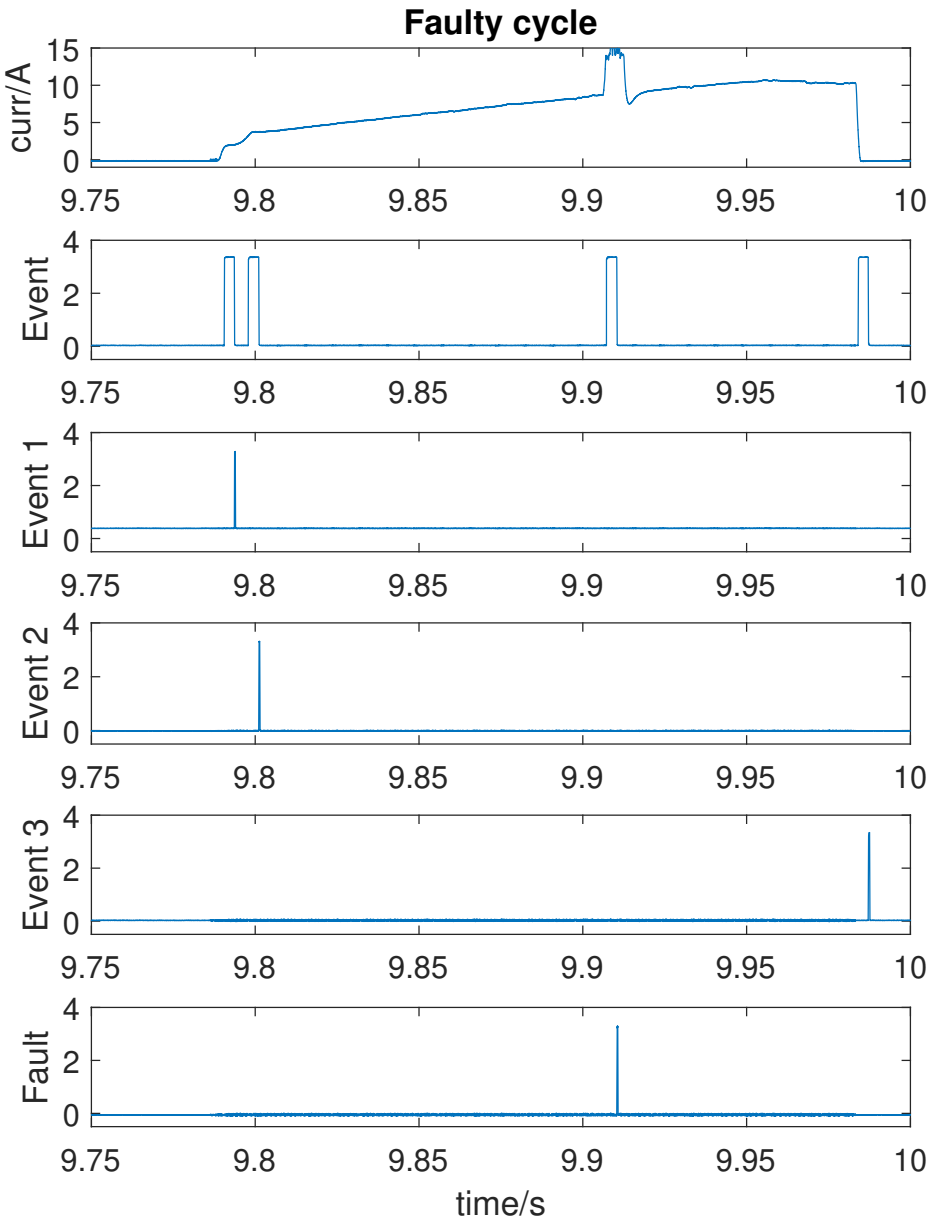

Figure 8.5: Coil gun load faulty cycle with large shunt fault

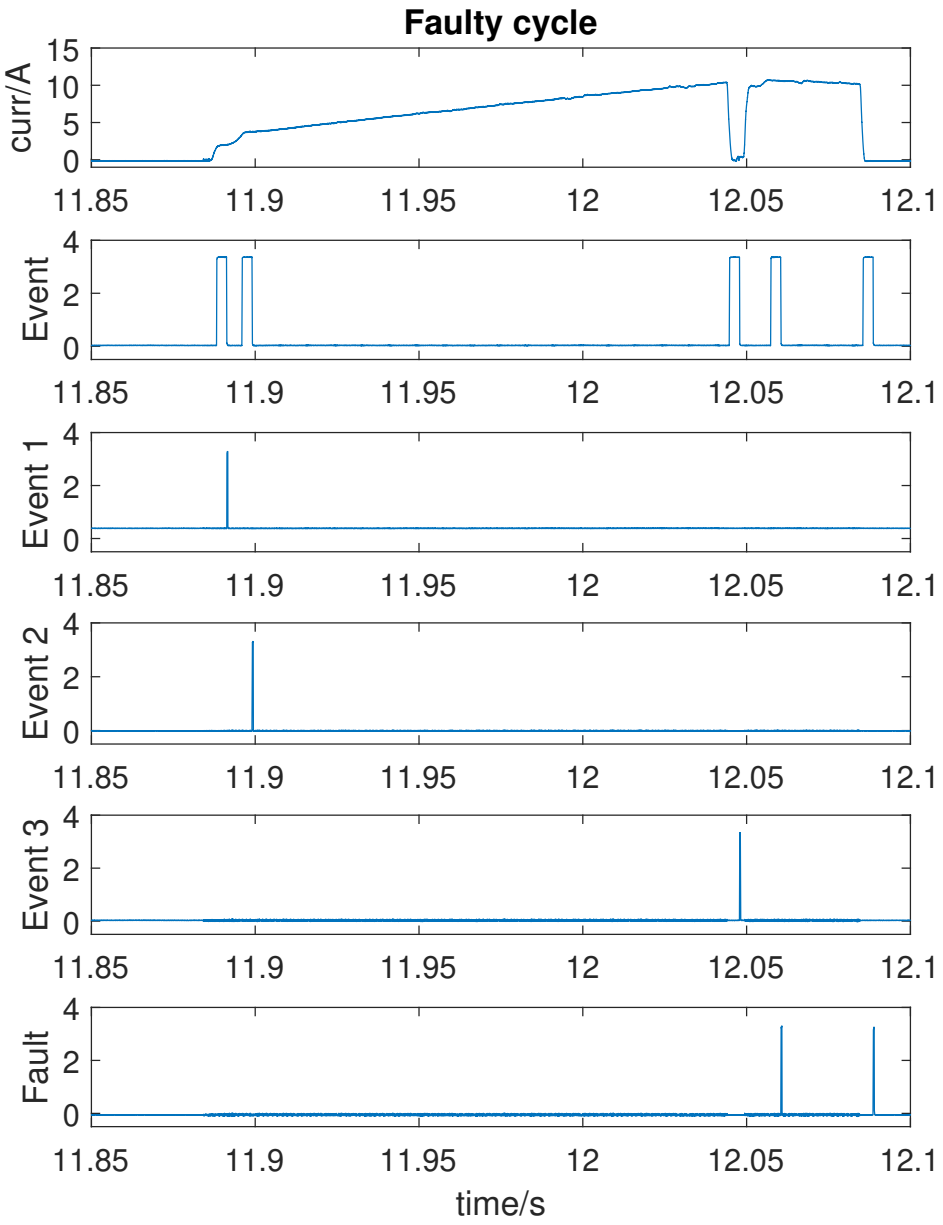

Figure 8.6: Coil gun load faulty cycle with a false negative and false positive

limitation it seems to give satisfactory results. The response for a normal load cycle during classifying mode is shown in Fig. 8.7. It can be seen that all the events are detected and labelled correctly and that there are no false positives. The width of the flag events have been increased to $1s$ for better visibility in run time. Also note that the dc value of the load profile is non-zero, this means that the initialization for recursive DFT algorithm must be adjusted otherwise an additional event would be seen at the start up during clustering mode.

Table 8.2: Parameters for monitoring load 2

F_S	N	Event Threshold	J	Length of ESA	Events per cycle	Arcing Threshold
$5kHz$	20	0.4	6	16	2	0.015

The setup for load 2 contains the series arc generation device. Figure 8.8 shows the response of the DSP when an arc is introduced for a few seconds. The disturbance created by the arc is not large enough to trigger an event but the DSP performing arc detection is able to identify it and raise flags continually during the duration of the arc at a designated GPIO.

8.4 Load 1 and 2 in Parallel

Load 1 has a load profile cycle of close to 200 ms while load 2 has a 10s cycle. For this section the cycle of load 2 is reduced to 1s in order for the two loads to have more overlap while operating in parallel. The updated load profile for load 2 has a step increase in current every 1s for a duration of 0.18s. The transients for both loads have identical duration so it is possible to use a single load monitoring solution for both these loads. Based on the window size previously

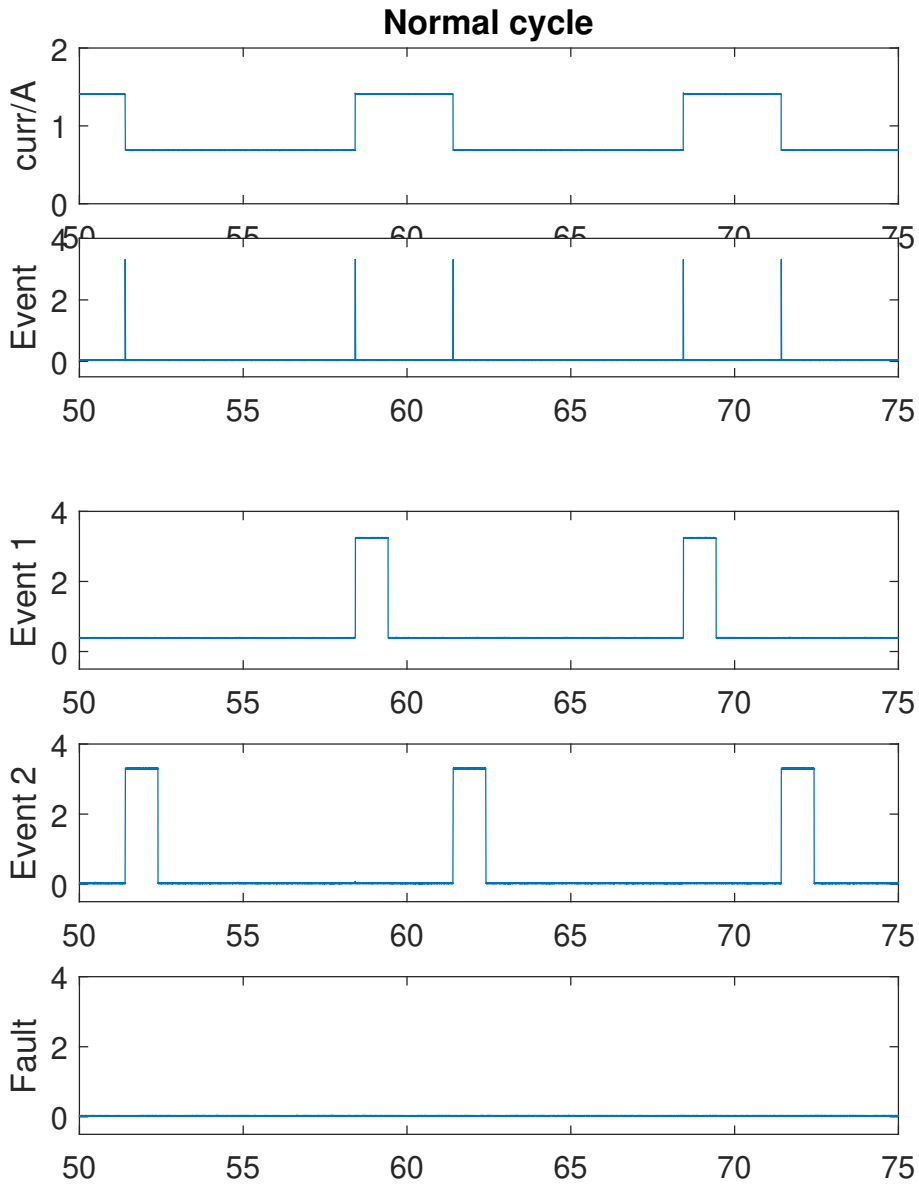

Figure 8.7: Fixed load normal cycle

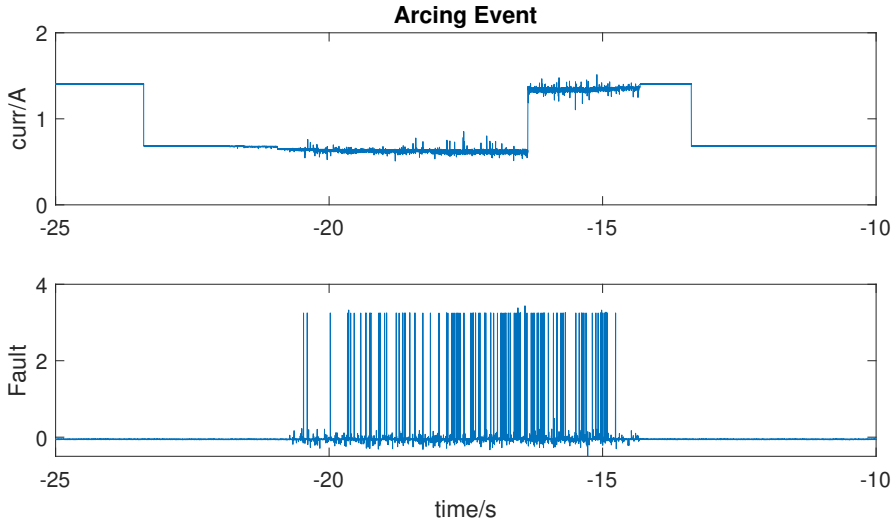

Figure 8.8: Fixed load with arcing

selected, Load 1 has 3 distinct events while load 2 has 2. This leads to a total of 5 unique events. In order to differentiate between 5 events the processing time is longer than what has been allowed previously. It is therefore decided to increase the window size and combine the first two events of load 1 into a single event. This has the effect of reducing the unique events to 4 and also allow for a smaller sampling frequency. As a result, the DSP can have enough processing time to successfully implement the monitoring algorithm. The new event labels are assigned as follows: Event 1 and 2 represent the charging and end of charging transient for the coil gun profile respectively, while event 3 and event 4 are the labels assigned to step increase and step decrease of current for the fixed load respectively.

This implementation is also challenging due to the difficulty of synchronizing the two loads such that the events do not happen simultaneously during the clustering mode. If multiple events happen within the same window during clustering mode it will distort the data

and the performance of the monitoring during classifying mode will fail. It is therefore decided to operate the two loads in sequence during the clustering mode and during classifying mode they are allowed to run independently of one another. One disadvantage of sequential operation during clustering mode is that it limits the database to the load profiles of the two loads with no overlap. This becomes a problem when the DSP encounters events during classifying mode that actually contain overlap between the two load profiles. The performance of the load monitoring algorithm for this case was not as consistent as the other cases due to these challenges. A more reliable method would involve some sort of synchronized action for the two loads at least during the clustering mode to better train the DSP. The parameters selected for this section are listed in table 8.3

Table 8.3: Parameters for monitoring load 1 and 2 in parallel

F_S	N	Event Threshold	J	Length of ESA	Events per cycle	Arcing Threshold
$1kHz$	20	0.8	6	120	4	0.015

Figure 8.9 shows one cycle of each load overlapped with one another during classifying mode. There is also a shunt fault being introduced near the 21.27 second mark. In this instance the load monitoring performs accurately. The first event being detected right after the 21.1 second mark is the step change in current for the fixed load, which correctly results in a flag for event 3. This is followed by the charging transient of the coil gun, identified as event 1. The shunt fault after that triggers a fault event. Once the fault is removed the next event is identified correctly as well, which is the step decrease in current for fixed load. This event is

identified correctly despite being overlapped with ramping current profile of load 1. Finally the end of the charging event for load 1 is detected and correctly labelled as event 1 close to the 21.43 second mark.

8.5 Load 3: Radar Load

Due to slower transients on the radar load profile there are no processing time strains on the DSP. The sampling frequency and window size parameters are used the same as in chapter 7. In additional to that a set of experiments is performed to determine the effect of the length of ESA and tolerance parameter J on the performance of the load monitoring scheme for radar load in terms of false positives. Each iteration considers 66 cycles of radar load profile during classifying mode. The results are shown in Fig. 8.10. The trends do not show anything unexpected. Increasing the training size and tolerance parameter J results in fewer false positives. Based on the results of Fig. 8.10 the parameters in table 8.4 are selected.

Table 8.4: Parameters for monitoring Load 3

F_S	N	Event Threshold	J	Length of ESA	Events per cycle	Arcing Threshold
$500Hz$	40	0.06	6	50	2	0.015

The response of the DSP to a couple of normal load cycles during classifying mode is shown in Fig. 8.11. Each event in the load profile is detected successfully and labeled accurately. Flags are raised for 0.2 s at the designated GPIO corresponding to the respective event label. Furthermore there are no false positives. Compare the top subplot of Fig. 8.11 to

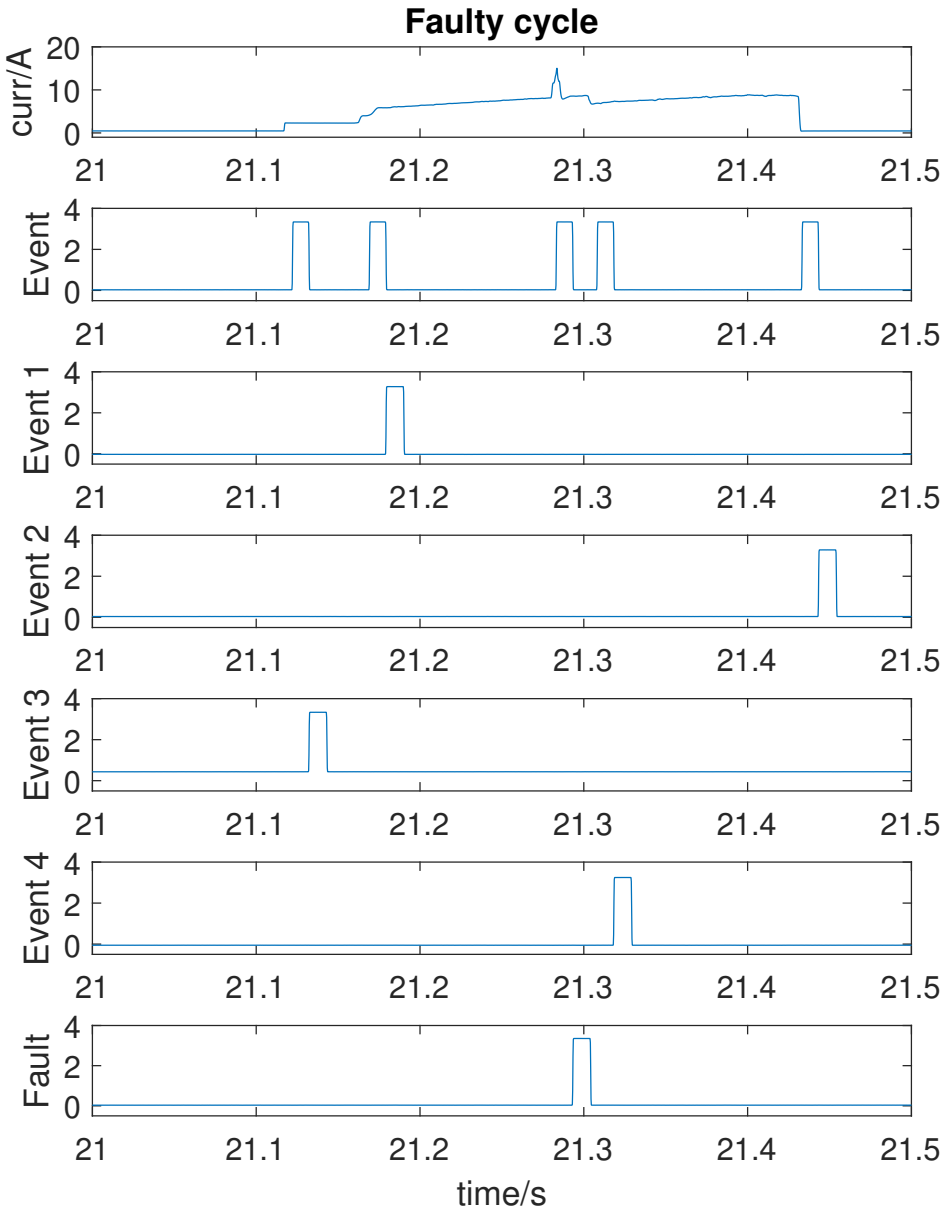

Figure 8.9: Coil gun and fixed load with a fault

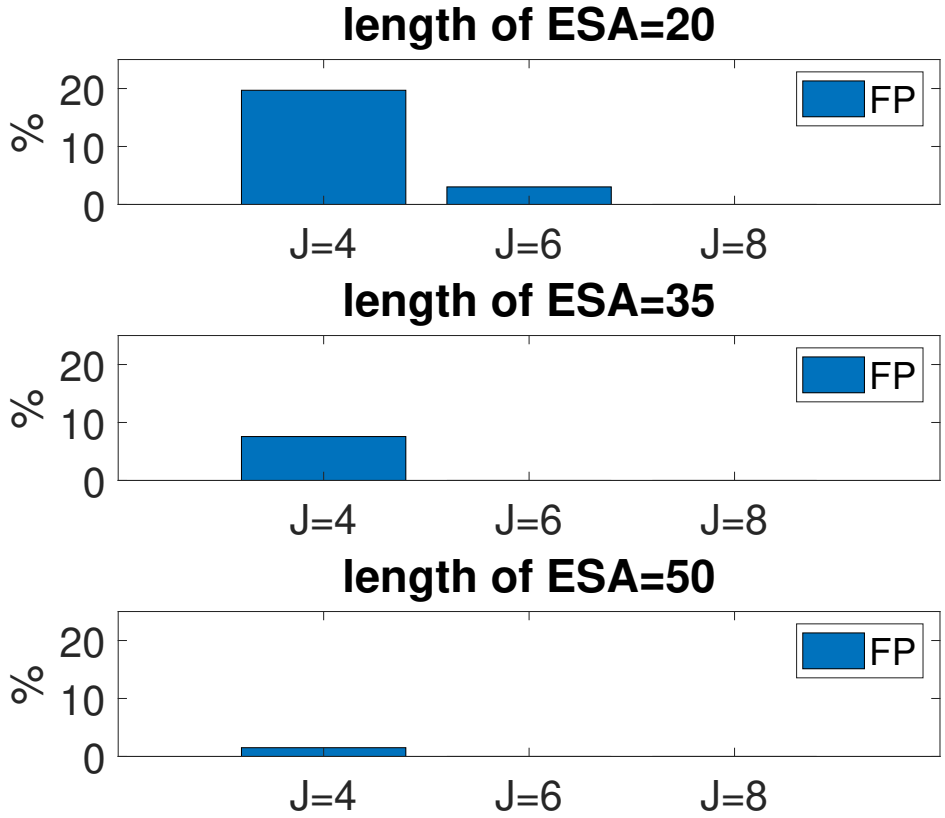

Figure 8.10: Effect of parameter selection on false positives for radar load

the top subplot of Fig. 8.12. It can be seen that significant 60Hz noise has been added to the system. For this experiment the noise is adding by loading it to the programmable load but in real scenarios interference from ac distribution cables is a common source of such noise. Based on the arcing threshold set in table 8.4 this noise is significant enough to raise a flag for fault. The tolerance of the algorithm to noise can easily be adjusted through a single parameter but for this application it is assumed that fault flag for noise interference is the desired response. Additionally it can be seen in Fig.8.12 that during the transient event the fault flag is cleared. This is consistent with the arc detection algorithm where the any change in current large enough to trigger an event overrides the arc detection command.

8.6 Load 4: Motor Load

The final load being tested with real-time implementation is the motor load. It has very slow transients so the sampling frequency and window size does not need to be adjusted for processing strain on the DSP. However, the load cycle of the motor load is close to 1 min and therefore it is not practical to use a large ESA as was done in chapter 7. Th relation between ESA and the tolerance variable J has been demonstrated several times so the variable J is increased in this application to compensate for smaller ESA. The final parameters being used are summarized in table 8.5.

The response of the DSP to a couple of normal load cycles during classifying mode is shown in Fig. 8.13. Each event in the load profile is detected successfully and labeled accurately. Flags are raised for 1s at the designated GPIO corresponding to the respective event

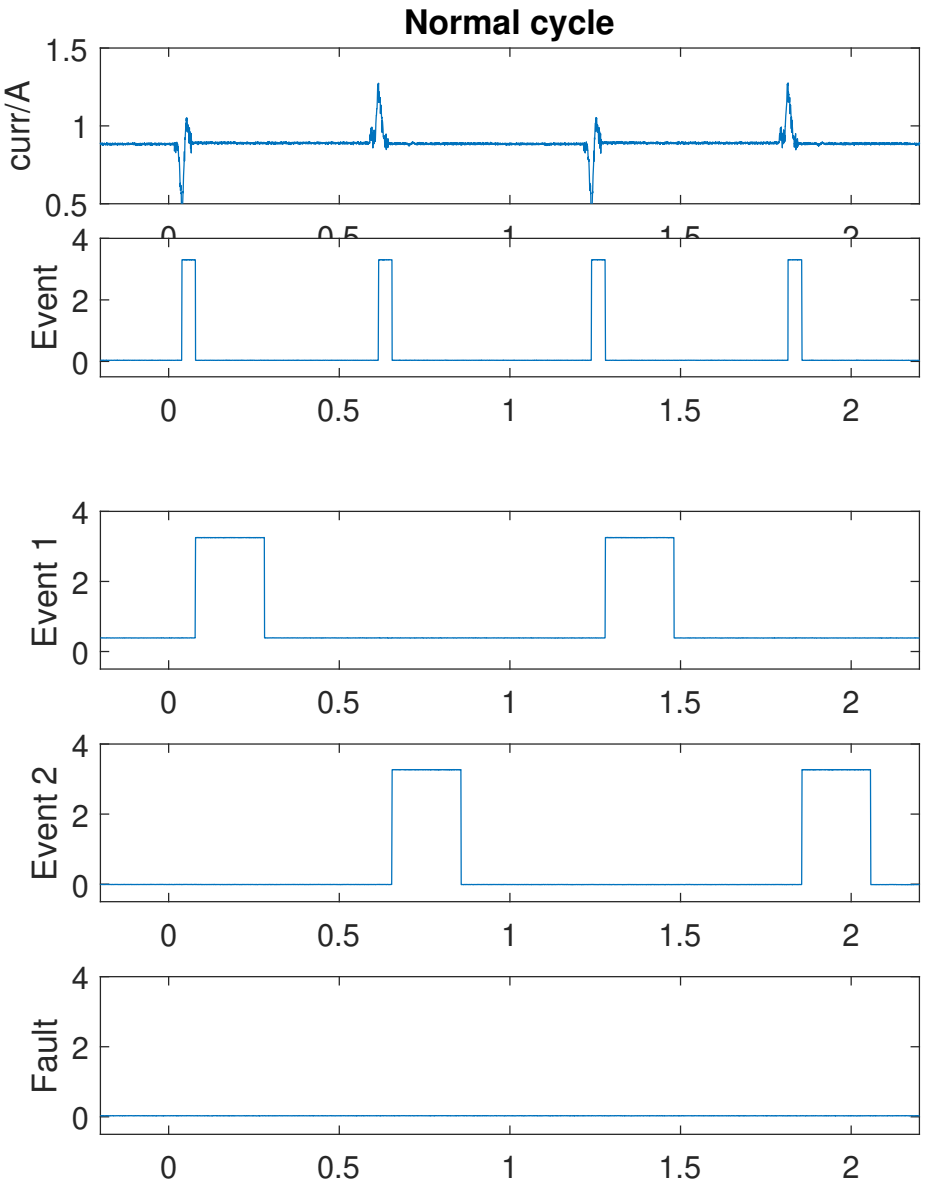

Figure 8.11: Radar load normal cycle

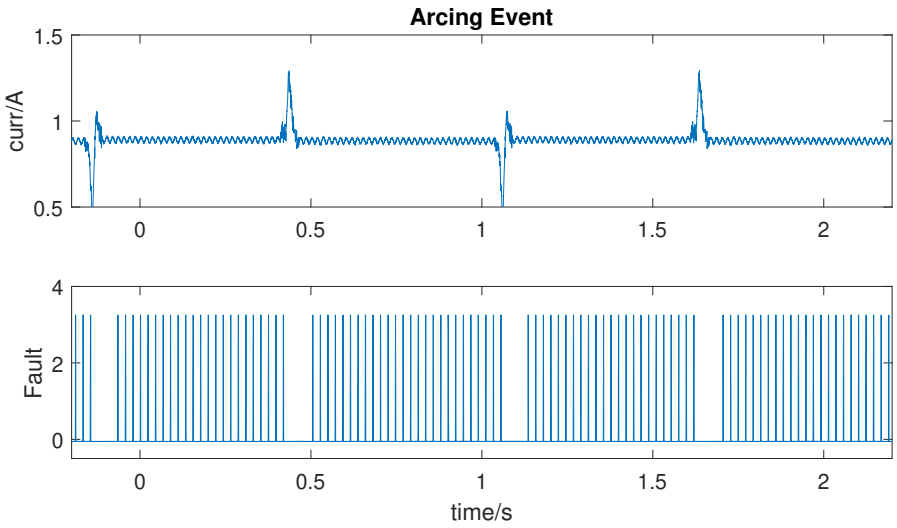

Figure 8.12: Radar load with additional noise

Table 8.5: Parameters for Monitoring Load 4

F_S	N	Event Threshold	J	Length of ESA	Events per cycle	Arcing Threshold
$10Hz$	80	0.031	15	20	2	0.015

label. Furthermore there are no false positives.

Two unique fault scenarios are shown in Fig. 8.14. The first one depicted in the first cycle of top subplot in Fig. 8.14 is created by adding mechanical friction to the flywheel during motor acceleration. The resulting spike in load current triggers an event in addition to the two normal events of the load profile. It can be seen that the additional event is flagged as a fault while the following two events are correctly labeled as event 1 and event 2. During the next cycle a fault is created by spinning the flywheel after the motor has come to a rest. This fault scenario is different from the first scenario in that it does not create an additional event, however it disturbs the profile during the second event. This deviation or disturbance results in that second event being correctly identified as a fault instead of being labeled as event 2.

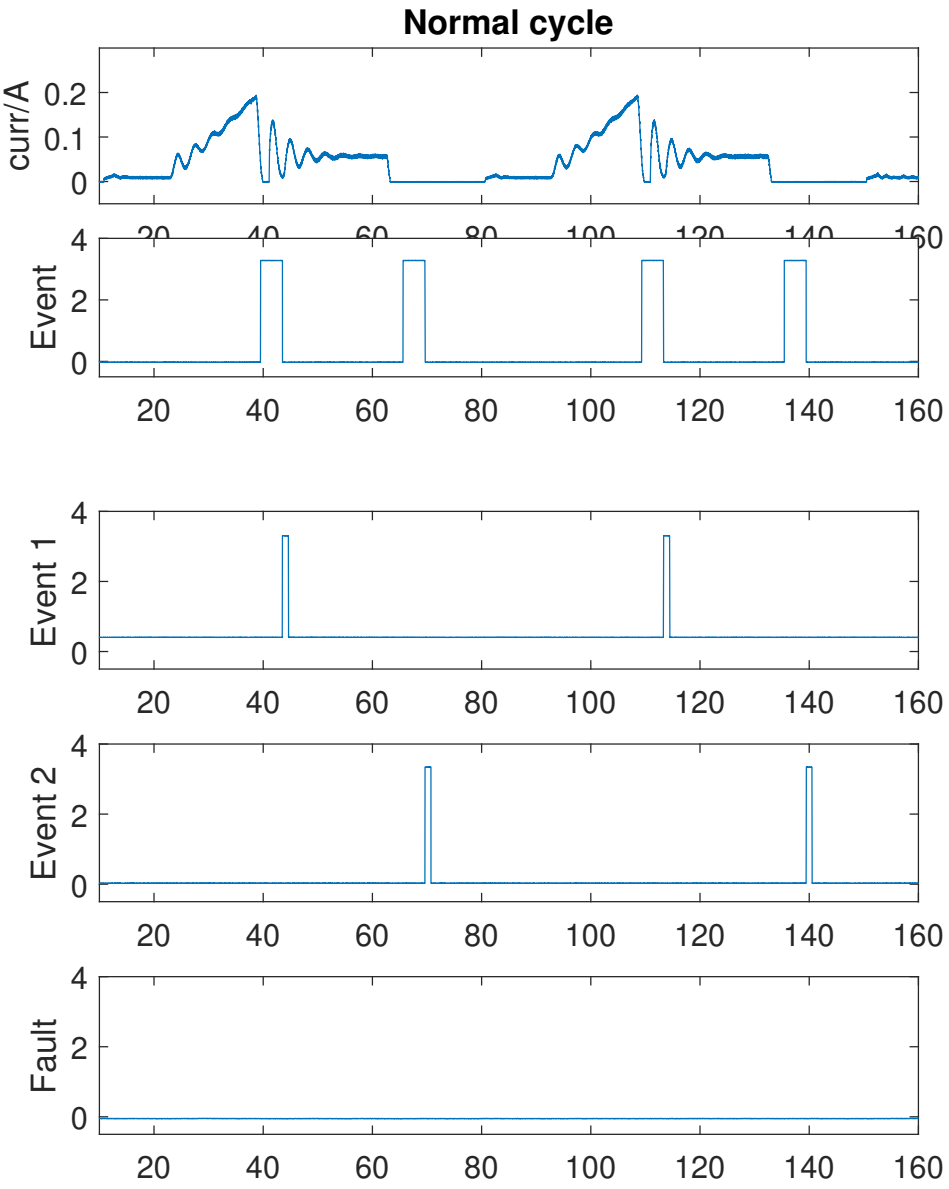

Figure 8.13: Motor load normal cycle

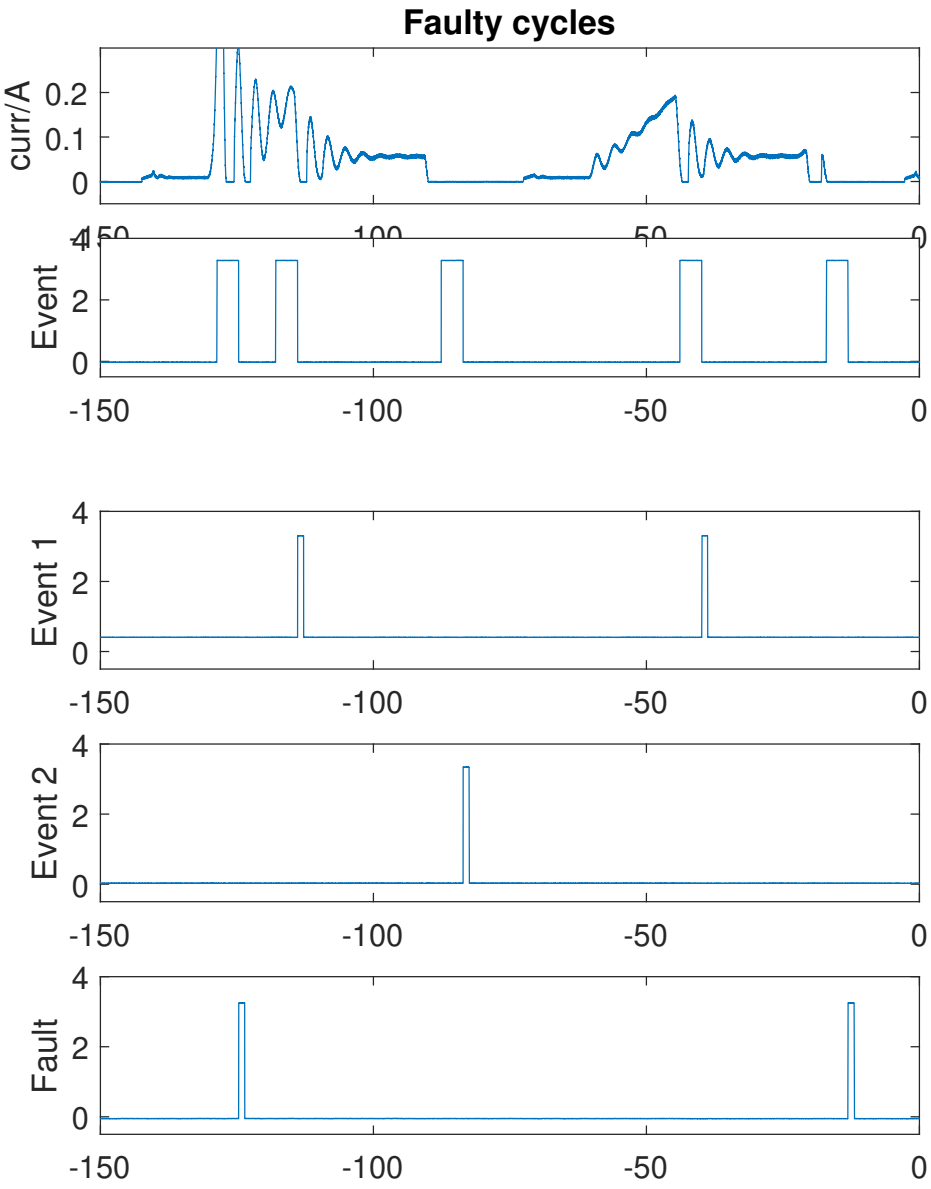

Figure 8.14: Motor load with faults

Chapter 9

Summary of Contributions

- The most significant contribution of the work completed and presented in this dissertation is a proposed load monitoring and fault detection algorithm to offer comprehensive solution for shunt transient faults as well as arcing faults specifically for pulsed power loads on dc grids. The mechanics of the proposed scheme have been explained in great detail and has been demonstrated to work on a wide range of loads.
- A low voltage dc setup has been assembled to model an electric ship load and collect data for the algorithm verification and protection schemes.
- Detailed system simulation created to assist with component design and control strategies
- Assembly of coil gun load
  - Current feedback control of H-bridge on DSP for coil gun charging
  - Program electrical faults

  - Synchronize multiple iterations of normal and faulty operation of by creating internal timer on DSP

- Fixed power load with step changes
  - Study of series arcing fault
  - Design of arcing generator
- Radar load profile
  - Buck converter design and control
  - Interface with Chroma Programmable load
- Assembly of motor load
  - Buck converter design and control
  - Braking circuit design and control
  - Program load profile on TI inverter driving a PMSM motor
- Demonstrate the effectiveness of the proposed solution on various load profiles including a notional pulsed-energy mission load.
- Low voltage hardware data collected for hundreds of iterations of:
  - Coil gun Load
  - Fixed power load with step changes
  - Radar load profile

  - Motor load profile
  - Coil gun and fixed power load combined

- Wrote the program for proposed scheme on MATLAB Simulink
  - Matlab Simulink program for recursive DFT
  - Matlab code for event detection, clustering, statistical matrix calculation, classification
  - Easy to reconfigure initialization file with different parameters for pre-processing
  - Study performance metrics with respect to algorithm parameters

- Programmed DSP and verified the scheme through real-time analysis of load current
  - Pre-sampling signal conditioning
  - Recursive DFT
  - Create dynamic database from extracted features
  - Single program file with re-configurable initialization file to use for multiple load profiles

- Publications on this project as first author:
  - STFT Cluster Analysis For Dc Pulsed Load Monitoring and Fault Detection. *IEEE Transactions on Transportation Electrification*. Decision pending after Major revisions

  - STFT Based Event Detection and Classification for a DC Pulsed Load. *2019 IEEE Electric Ship Technologies Symposium.* Published and presented
  - A Coupled-Inductor Dc Breaker with STFT-Based Arc Detection. *2020 IEEE Applied Power Electronics Conference and Exposition*. Approved, Presenting March 2020.
  - STFT based load monitoring and fault detection for a pulsed-energy mission load. *2020 Advanced Machinery Technology Symposium*. Approved pending public release
  - Real-time fault detection for a pulsed power load using STFT based feature vectors. Manuscript ready for IEEE conference submission.

- As contributing author:
  - 4 conference papers published
  - 1 Journal and 1 conference paper awaiting review.

Bibliography

[1] G. F. Reed, B. M. Grainger, A. R. Sparacino and Z. Mao, "Ship to Grid: Medium-Voltage DC Concepts in Theory and Practice," in IEEE Power and Energy Magazine, vol. 10, no. 6, pp. 70-79, Nov.-Dec. 2012.

[2] Z. Jin, G. Sulligoi, R. Cuzner, L. Meng, J. C. Vasquez and J. M. Guerrero, "Next-Generation Shipboard DC Power System: Introduction Smart Grid and dc Microgrid Technologies into Maritime Electrical Netowrks," in IEEE Electrification Magazine, vol. 4, no. 2, pp. 45-57, June 2016.

[3] M. Saeedifard, M. Graovac, R. F. Dias and R. Iravani, "DC power systems: Challenges and opportunities," IEEE PES General Meeting, Providence, RI, 2010, pp. 1-7.

[4] R. M. Cuzner and G. Venkataramanan, "The Status of DC Micro-Grid Protection," 2008 IEEE Industry Applications Society Annual Meeting, Edmonton, AB, 2008, pp. 1-8.

[5] R. Cuzner and A. Jeutter, "DC zonal electrical system fault isolation and reconfiguration," 2009 IEEE Electric Ship Technologies Symposium, Baltimore, MD, 2009, pp. 227-234.

[6] J. G. Ciezki and R. W. Ashton, "Selection and stability issues associated with a navy ship-

board DC zonal electric distribution system," in IEEE Transactions on Power Delivery, vol. 15, no. 2, pp. 665-669, April 2000.

[7] E. Johansson, A. Andersson, G. Johansson and M. Johansson, "Breaking Performance of a Novel DC Contactor Concept," 2018 IEEE Holm Conference on Electrical Contacts, Albuquerque, NM, 2018, pp. 483-487.

[8] M. E. Baran, S. Teleke and S. Bhattacharya, "Overcurrent Protection in DC Zonal Shipboard Power Systems using Solid State Protection Devices," 2007 IEEE Electric Ship Technologies Symposium, Arlington, VA, 2007, pp. 221-224.

[9] Zhenxue Xu, Bin Zhang, S. Sirisukprasert, Xigen Zhou and A. Q. Huang, "The emitter turn-off thyristor-based DC circuit breaker," 2002 IEEE Power Engineering Society Winter Meeting. Conference Proceedings (Cat. No.02CH37309), New York, NY, USA, 2002, pp. 288-293 vol.1.

[10] X. Song, C. Peng and A. Q. Huang, "A Medium-Voltage Hybrid DC Circuit Breaker, Part I: Solid-State Main Breaker Based on 15 kV SiC Emitter Turn-OFF Thyristor," in IEEE Journal of Emerging and Selected Topics in Power Electronics, vol. 5, no. 1, pp. 278-288, March 2017.

[11] R. Schmerda, R. Cuzner, R. Clark, D. Nowak and S. Bunzel, "Shipboard Solid-State Protection: Overview and Applications," in IEEE Electrification Magazine, vol. 1, no. 1, pp. 32-39, Sept. 2013.

[12] M. Hajian, D. Jovcic and B. Wu, "Evaluation of Semiconductor Based Methods for Fault

Isolation on High Voltage DC Grids," in IEEE Transactions on Smart Grid, vol. 4, no. 2, pp. 1171-1179, June 2013.

[13] P. M. McEwan and S. B. Tennakoon, "A two-stage DC thyristor circuit breaker," in IEEE Transactions on Power Electronics, vol. 12, no. 4, pp. 597-607, July 1997.

[14] R. Graves, A. Lemmon, L. Gant, "Fast configurable over-current protection for high power modules", Proc. IEEE Electr. Ship Technol. Symp. (ESTS), pp. 332-336, Jun. 2015.

[15] M. Andrus, H. Ravindra, J. Hauer, M. Steurer, M. Bosworth, R. Soman, "PHIL implementation of a MVDC fault management test bed for ship power systems based on megawatt-scale modular multilevel converters", Proc. IEEE Electr. Ship Technol. Symp. (ESTS), pp. 337-342, Jun. 2015.

[16] P. Cairoli, I. Kondratiev, R. A. Dougal, "Coordinated control of the bus tie switches and power supply converters for fault protection in DC microgrids", IEEE Trans. Power Electron., vol. 28, no. 4, pp. 2037-2047, Apr. 2013.

[17] R. Powers, "Automation as a manpower reduction strategy in navy ships", 2016.

[18] A. S. Eruguz, T. Tan, G.-J. van Houtum, "A survey of maintenance and service logistics management: Classification and research agenda from a maritime sector perspective", Comput. Oper. Res., vol. 85, pp. 184-205, Sep. 2017.

[19] Technology, Sense. "Technology." Sense Home Energy Monitor, 2019, sense.com/technology.

[20] S. Leeb, A Conjoint Pattern Recognition Approach to Nonintrusive Load Monitoring, February 1993.

[21] J. Gillis and W.G. Morsi, "Non-Intrusive Load Monitoring Using Orthogonal Wavelet Analysis," IEEE Canadian Conference on Electrical and Computer Engineering, 2016.

[22] N. Henao, S. Kelouwani, K. Agbossou, and Y. Dub, "Active Power Load Modeling Based on Uncertainties for Non Intrusive Load Monitoring," IEEE International Symposium on Industrial Electronics, pages 684-689, 2016.

[23] R. Bonfigli, M. Severini, S. Squartini, M. Fagiani, and F. Piazza, "Improving the Performance of the AFAMAP Algorithm for Non-Intrusive Load Monitoring," IEEE Congress on Evolutionary Computation, pages 303-310, 2016.

[24] T. DeNucci, R. Cox, S.B. Leeb, J. Paris, T.J. McCoy, C. Laughman, and W. C. Greene, "Diagnostic Indicators for Shipboard Systems Using Non-Intrusive Load Monitoring," IEEE Electric Ship Technologies Symposium, pages 413-420, 2005.

[25] R.W. Cox, LCDR P.L. Bennett, LCDR T.D. McKay, J. Paris, and S.B. Leeb, "Using the Non-Intrusive Load Monitor for Shipboard Supervisory Control," IEEE Electric Ship Technologies Symposium, pages 523-530, 2007.

[26] P.A. Lindahl, S.B. Leeb, J.S. Donnal, and G. Bredariol, "Noncontact Sensors and Nonintrusive Load Monitoring (NILM) aboard the USCGC Spencer," IEEE AUTOTESTCON, September 2016.

[27] P.A. Lindahl, D.H. Green, G. Bredariol, A. Aboulian, J.S. Donnal, and S.B. Leeb, "Shipboard Fault Detection Through Nonintrusive Load Monitoring: A Case Study," IEEE Sensors Journal, volume 18, number 21, pages 8986-8995, November 2018.

[28] M. Zeifman, K. Roth, Nonintrusive appliance load monitoring: review and outlook, IEEE Trans. Consumer Electron. 57 (1) (2011) 76–84

[29] G.W. Hart, Nonintrusive appliance load monitoring, Proc. IEEE 80 (12) (1992)1870–1891

[30] A.I. Cole, A. Albicki, Data extraction for effective non-intrusive identification of residential power loads, IMTC/98 Conference Proceedings. IEEE Instrumentation and Measurement Technology Conference. Where Instrumentation is Going (Cat. No. 98CH36222) vol. 2 (1998) 812–815

[31] A.I. Cole, A. Albicki, Algorithm for nonintrusive identification of residential appliances, Proceedings of the 1998 IEEE International Symposium on Circuits and Systems, 1998, ISCAS'98 vol. 3 (1998) 338–341

[32] L. Farinaccio, R. Zmeureanu, Using a pattern recognition approach to disaggregate the total electricity consumption in a house into the major end-uses, Energy Build. 30 (3) (1999) 245–259,

[33] M. Marceau, R. Zmeureanu, Nonintrusive load disaggregation computer program to estimate the energy consumption of major end uses in residential buildings, Energy Convers. Manag. 41 (13) (2000) 1389–1403,

[34] J.T. Powers, B. Margossian, B.A. Smith, Using a rule-based algorithm to disaggregate end-use load profiles from premise-level data, IEEE Comput.Appl. Power 4 (2) (1991) 42–47

[35] M. Baranski, J. Voss, Nonintrusive appliance load monitoring based on an optical sensor, 2003 IEEE Bologna Power Tech Conference Proceedings vol. 4(2003)

[36] M. Baranski, J. Voss, Detecting patterns of appliances from total load data using a dynamic programming approach, Fourth IEEE International Conference on Data Mining, 2004, ICDM'04 (2004) 327–330

[37] M. Baranski, J. Voss, Genetic algorithm for pattern detection in nialm systems,in: IEEE International Conference on Systems, Man and Cybernetics, 2004, vol.4, IEEE, 2004, pp. 3462–3468.

[38] A.G. Ruzzelli, C. Nicolas, A. Schoofs, G.M.P. O'Hare, Real-time recognition and profiling of appliances through a single electricity sensor, 2010 7th Annual IEEE Communications Society Conference on Sensor, Mesh and Ad Hoc Communications and Networks (SECON) (2010) 1–9

[39] M.B. Figueiredo, A. de Almeida, B. Ribeiro, An Experimental Study on Electrical Signature Identification of Non-Intrusive Load Monitoring (NILM) Systems,Springer, Berlin Heidelberg, 2011, pp. 31–40,

[40] F. Sultanem, Using appliance signatures for monitoring residential loads atmeter panel level, IEEE Trans. Power Deliv. 6 (4) (1991) 1380–1385

[41] L.K. Norford, S.B. Leeb, Non-intrusive electrical load monitoring in commercial buildings

based on steady-state and transient load-detectionalgorithms, Energy Build. 24 (1) (1996) 51–64,

[42] S.B. Leeb, S.R. Shaw, J.L. Kirtley, Transient event detection in spectral envelope estimates for nonintrusive load monitoring, IEEE Trans. Power Deliv. 10 (3)(1995) 1200–1210

[43] S.R. Shaw, S.B. Leeb, L.K. Norford, R.W. Cox, Nonintrusive load monitoring and diagnostics in power systems, IEEE Trans. Instrum. Meas. 57 (7) (2008)1445–1454

[44] K.D. Lee, S.B. Leeb, L.K. Norford, P.R. Armstrong, J. Holloway, S.R. Shaw,Estimation of variable-speed-drive power consumption from harmonic content, IEEE Trans. Energy Convers. 20 (3) (2005) 566–574

[45] P. A. Lindahl, D. H. Green, G. Bredariol, A. Aboulian, J. S. Donnal and S. B. Leeb, "Shipboard Fault Detection Through Nonintrusive Load Monitoring: A Case Study," in IEEE Sensors Journal, vol. 18, no. 21, pp. 8986-8995, 1 Nov.1, 2018.

[46] S. R. Shaw, System identification techniques and modeling for nonintrusive load diagnostics, Feb. 2000.

[47] S. R. Shaw, C. B. Abler, R. F. Lepard, D. Luo, S. B. Leeb, L. K. Norford, "Instrumentation for high performance nonintrusive electrical load monitoring", ASME J. Solar Energy Eng., vol. 120, no. 3, pp. 224-229, Aug. 1998.

[48] U. A. Khan, S. B. Leeb, M. C. Lee, "A multiprocessor for transient event detection", IEEE Trans. Power Del., vol. 12, no. 1, pp. 51-60, Jan. 1997.

[49] J. Paris, J. S. Donnal, and S. B. Leeb, “NilmDB: The non-intrusive load monitor database,” IEEE Trans. Smart Grids, vol. 5, no. 5, pp. 2459–2467, Sep. 2014.

[50] C. Laughman, K. Lee, R. Cox, S. Shaw, S. Leeb, L. Norford, P. Armstrong, Power signature analysis, IEEE Power Energy Mag. 1 (2) (2003) 56–63

[51] D. Srinivasan, W.S. Ng, A.C. Liew, Neural-network-based signature recognition for harmonic source identification, IEEE Trans. Power Deliv. 21 (1) (2006)398–405

[52] M. Berges, E. Goldman, H.S. Matthews, L. Soibelman, Learning systems for electric consumption of buildings, in: ASCE International Workshop onComputing in Civil Engineering, ASCE, Austin, TX, USA, 2009.

[53] M.E. Berges, E. Goldman, H.S. Matthews, L. Soibelman, Enhancing electricity audits in residential buildings with nonintrusive load monitoring, J. Ind. Ecol.14 (5) (2010) 844–858

[54] M. V. Ribeiro, C. A. Marques, C. A. Duque, A. S. Cerqueira and J. L. R. Pereira, ”Power quality disturbances detection using HOS,” 2006 IEEE Power Engineering Society General Meeting, Montreal, Que., 2006, pp. 6 pp.-

[55] Y.C. Su, K.L. Lian, H.H. Chang, Feature selection of non-intrusive load monitoring system using stft and wavelet transform, 2011 IEEE 8th International Conference on e-Business Engineering (2011) 293–298

[56] W.L. Chan, A.T.P. So, L.L. Lai, Harmonics load signature recognition by wavelets transforms, DRPT2000. International Conference on Electric Utility Deregulation and Restructuring and Power Technologies. Proceedings (Cat.No.00EX382) (2000) 666–671

[57] C. Duarte, P. Delmar, K.W. Goossen, K. Barner, E. Gomez-Luna, Non-intrusive load monitoring based on switching voltage transients and wavelet transforms, 2012 Future of Instrumentation International Workshop (FIIW)Proceedings (2012) 1–4

[58] H.-H. Chang, Non-intrusive demand monitoring and load identification for energy management systems based on transient feature analyses, Energies 5(11) (2012) 4569–4589

[59] H.H. Chang, K.L. Chen, Y.P. Tsai, W.J. Lee, A new measurement method for power signatures of nonintrusive demand monitoring and load identification,IEEE Trans. Ind. Appl. 48 (2) (2012) 764–771,

[60] M. Gray, W.G. Morsi, Application of wavelet-based classification in non-intrusive load monitoring, 2015 IEEE 28th Canadian Conference on 565Electrical and Computer Engineering (CCECE) (2015) 41–45

[61] S.M. Tabatabaei, S. Dick, W. Xu, Toward non-intrusive load monitoring via multi-label classification, IEEE Trans. Smart Grid 8 (1) (2017) 26–40

[62] J.M. Gillis, S.M. Alshareef, W.G. Morsi, Nonintrusive load monitoring using wavelet design and machine learning, IEEE Trans. Smart Grid 7 (1) (2016)320–328

[63] J.M. Gillis, W.G. Morsi, Non-intrusive load monitoring using semi-supervisedmachine learning and wavelet design, IEEE Trans. Smart Grid PP (99) (2016)1–8

[64] H.Y. Lam, G.S.K. Fung, W.K. Lee, A novel method to construct taxonomy electrical appliances based on load signatures, IEEE Trans. Consumer Electron.53 (2) (2007) 653–660

[65] K. Suzuki, S. Inagaki, T. Suzuki, H. Nakamura, K. Ito, Nonintrusive applianceload monitoring based on integer programming, 2008 SICE AnnualConference (2008) 2742–2747

[66] T. Hassan, F. Javed, N. Arshad, An empirical investigation of V-I trajectory based load signatures for non-intrusive load monitoring, IEEE Trans. SmartGrid 5 (2) (2014) 870–878

[67] L. Du, D. He, R.G. Harley, T.G. Habetler, Electric load classification by binary voltage current trajectory mapping, IEEE Trans. Smart Grid 7 (1) (2016)358–365

[68] T.D. Huang, W.S. Wang, K.L. Lian, A new power signature for nonintrusive appliance load monitoring, IEEE Trans. Smart Grid 6 (4) (2015) 1994–1995

[69] D.F. Teshome, T.D. Huang, K.L. Lian, Distinctive load feature extraction basedon fryzes time-domain power theory, IEEE Power Energy Technol. Syst. J. 3 (2)(2016) 60–70

[70] J. Gao, E.C. Kara, S. Giri, M. Bergés, A feasibility study of automated plug-load identification from high-frequency measurements, 2015 IEEE Global Conference on Signal and Information Processing (GlobalSIP) (2015) 220–224

[71] J. Liang, S.K. Ng, G. Kendall, J.W. Cheng, Load signature study. Part I. Basic concept, structure, and methodology, IEEE Trans. Power Deliv. 25 (2)

[72] S. Lin, L. Zhao, F. Li, Q. Liu, D. Li, Y. Fu, A nonintrusive load identificationmethod for residential applications based on quadratic programming, Electr.Power Syst. Res. 133 (2016) 241–248

[73] N. Sadeghianpourhamami, J. Ruyssinck, D. Deschrijver, T. Dhaene, and C. Develder,

"Comprehensive feature selection for appliance classification in NILM," Energy Buildings, vol. 151, pp. 98–106, Sep. 2017.

[74] M. Z A Bhotto, S. Makonin, and I. V. Bajic, "Load disaggregation based on aided linear integer programming," IEEE Trans. Circuits Syst. II, Exp. Briefs, vol. 64, no. 7, pp. 792–796, Jul. 2017.

[75] J. Z. Kolter and M. J. Johnson, "REDD: A public data set for energy disaggregation research," in Proc. Workshop Data Mining Appl. Sustainability (SIGKDD), San Diego, CA, USA, vol. 25, 2011, pp. 59–62.

[76] M. Aiad and P. H. Lee, "Unsupervised approach for load disaggregation with devices interactions," Energy Buildings, vol. 116, pp. 96–103, Mar. 2016.

[77] G. C. Koutitas and L. Tassiulas, "Low cost disaggregation of smart meter sensor data," IEEE Sensors J., vol. 16, no. 6, pp. 1665–1673, Mar. 2016.

[78] M. R. Durling, Z. Ren, N. Visnevski, L. E. Ray, "Cognitive electric power meter," US patent 7,693,670, 2010.

[79] Makonin, Stephen & Popowich, Fred & Gill, Bob. (2013). The Cognitive Power Meter: Looking Beyond the Smart Meter. Canadian Conference on Electrical and Computer Engineering. 1-5.

[80] Ribeiro, Paulo F. Power Systems Signal Processing for Smart Grids. Wiley, 2014.

[81] S. Gupta, M. S. Reynolds, S. N. Patel, "ElectriSense: Single-Point Sensing Using EMI

for Electrical Event Detection and Classification in the Home," Conference on Ubiquitous Computing, pp. 139-148, 2010.

[82] P.K. Murthy, J. Amarnath, S. Kamakshiah, and B.P. Singh, "Wavelet Transform Approach for Detection and Location of Faults in HVDC System," IEEE Region 10 International Conference on Industrial and Information Systems, 2008.

[83] A. Abdollahi and S. Seyedtabaii, "Comparison of Fourier & Wavelet Transform Methods for Transmission Line Fault Classification," IEEE International Power Engineering and Optimization Conference, pages 579-584, 2010.

[84] J. Ning and W. Gao, "A Wavelet-Based Method to Extract Frequency Feature for Power System Fault/Event Analysis," IEEE Power & Energy Society General Meeting, 2009.

[85] W. Li, A. Monti, and F. Ponci, "Fault Detection and Classification in Medium Voltage DC Shipboard Power Systems With Wavelets and Artificial Neural Networks," IEEE Transactions on Instrumentation and Measurement, volume 63, number 11, pages 2651-2665, November 2014.

[86] R. Nandi and B.K. Panigrahi, "Detection of Fault in a Hybrid Power System Using Wavelet Transform," Michael Faraday IET International Summit, 2015.

[87] Q. Xiong, X. Liu, X. Feng, A.L. Gattozzi, Y. Shi, L. Zhu, S. Ji, and R.E. Hebner, "Arc Fault Detection and Localization in Photovoltaic Systems Using Feature Distribution Maps of Parallel Capacitor Currents," IEEE Journal of Photovoltaics, volume 8, number 4, pages 1090-1097, July 2018.

[88] Q. Xiong, X. Feng, A.L. Gattozzi, X. Liu, L. Zheng, L. Zhu, S. Ji, and R.E. Hebner, "Series Arc Fault Detection and Localization in DC Distribution System," IEEE Transactions on Instrumentation and Measurement, 2019.

[89] L. Herrera and X. Yao, "Parameter Identification Approach to Series DC Arc Fault Detection and Localization," 2018 IEEE Energy Conversion Congress and Exposition (ECCE), Portland, OR, 2018, pp. 497-501.

[90] L. Yue, V. Le, Z. Yang and X. Yao, "A Novel Series Arc Fault Detection Method using Sparks in DC Microgrids with Buck Converter Interface," 2018 IEEE Energy Conversion Congress and Exposition (ECCE), Portland, OR, 2018, pp. 492-496.

[91] Y. Pan, M. Steurer and T. L. Baldwin, "Ground Fault Location Testing of a Noise-Pattern-Based Approach on an Ungrounded DC System," in IEEE Transactions on Industry Applications, vol. 47, no. 2, pp. 996-1002, March-April 2011.

[92] K. A. Corzine and R. W. Ashton, "A New Z-Source DC Circuit Breaker," in IEEE Transactions on Power Electronics, vol. 27, no. 6, pp. 2796-2804, June 2012.

[93] D. J. Ryan, H. D. Torresan and B. Bahrani, "A Bidirectional Series Z-Source Circuit Breaker," in IEEE Transactions on Power Electronics, vol. 33, no. 9, pp. 7609-7621, Sept. 2018.

[94] A. Maqsood and K. A. Corzine, "Integration of Z-Source Breakers Into Zonal DC Ship Power System Microgrids," in IEEE Journal of Emerging and Selected Topics in Power Electronics, vol. 5, no. 1, pp. 269-277, March 2017.

[95] K. A. Corzine, "A New-Coupled-Inductor Circuit Breaker for DC Applications," in IEEE Transactions on Power Electronics, vol. 32, no. 2, pp. 1411-1418, Feb. 2017.

[96] A. Maqsood and K. Corzine, "Z-source Dc circuit breakers with coupled inductors," 2015 IEEE Energy Conversion Congress and Exposition (ECCE), Montreal, QC, 2015, pp. 1905-1909.

[97] T. Thiruvaran, T. Phung and E. Ambikairajah, "Automatic detection and identification of electric loads at the event of switching-on that load," 2013 IEEE 8th International Conference on Industrial and Information Systems, Peradeniya, 2013, pp. 682-687.

[98] G. Devadasu and M. Sushama, "A novel multiple fault identification with fast fourier transform analysis," 2016 International Conference on Emerging Trends in Engineering, Technology and Science (ICETETS), Pudukkottai, 2016, pp. 1-5.

[99] H. Arabaci and O. Bilgin, "The Detection of Rotor Faults By Using Short Time Fourier Transform," 2007 IEEE 15th Signal Processing and Communications Applications, Eskisehir, 2007, pp. 1-4.

[100] Y. H. M. Thayoob, A. B. A. Ghani and P. S. Ghosh, "A new approach to identify electrical PD signal patterns using frequency spectral analysis," Annual Report Conference on Electrical Insulation and Dielectric Phenomena, Cancun, Quintana Roo, Mexico, 2002, pp. 716-719.

[101] H. V. Khang, H. R. Karimi and K. G. Robbersmyr, "Bearing fault detection based on

time-frequency representations of vibration signals," 2015 18th International Conference on Electrical Machines and Systems (ICEMS), Pattaya, 2015, pp. 1970-1975.

[102] K. Satpathi, Y. M. Yeap, A. Ukil and N. Geddada, "Short-Time Fourier Transform Based Transient Analysis of VSC Interfaced Point-to-Point DC System," in IEEE Transactions on Industrial Electronics, vol. 65, no. 5, pp. 4080-4091, May 2018.

[103] S. Agarwal, A. Swetapadma, C. Panigrahi and A. Dasgupta, "Fault detection in direct current transmission lines using discrete fourier transform from single terminal current signals," 2017 1st International Conference on Electronics, Materials Engineering and Nano-Technology (IEMENTech), Kolkata, 2017, pp. 1-5.

[104] Electric Ship Program Office (PMS-320), "Naval power and energy systems: Technology development roadmap," Washington DC, 2019.

[105] S. Hundertmark and O. Liebfried , "Railgun, Power Supply Options for a Naval," IEEE Transactions on Plasma Science, vol. 46, no. 10, pp. 3599-3605, 2018.